Understanding the Role of Comparative Clinical Studies in the Development of Oncology Biosimilars

Justin Stebbing, MA, PhD[1]; Paul N. Mainwaring, MBBS, MD[2]; Giuseppe Curigliano, MD, PhD[3,4]; Mark Pegram, MD[5]; Mark Latymer, BSc[6]; Angel H. Bair, PhD[7]; and Hope S. Rugo, MD[8]

abstract

Biosimilars have the potential to broaden patient access to biologics and provide cost savings for health care systems. During the development of a biosimilar, data that directly compare the proposed biosimilar with the reference product are required. Such comparative data are generated in a stepwise hierarchical process that begins with extensive laboratory-based structural analyses and functional assays. This initial analytical phase serves as the foundation for the demonstration of biosimilarity and is followed by nonclinical in vivo testing (if required) and then clinical evaluation, including a comparative pharmacokinetics/pharmacodynamics study that is usually conducted in healthy volunteers. The development program typically culminates with a comparative clinical efficacy study. The aim of this study is to confirm clinical equivalence of the potential biosimilar and reference product on the basis of prespecified margins, using a study population and efficacy end point that are sufficiently sensitive for detecting potential product-related differences. Such studies also include detailed analyses of safety as well as evaluation of immunogenicity. As biosimilars become more widely available in oncology, especially with recent regulatory approvals of rituximab, trastuzumab, and bevacizumab biosimilars, it is critically important that clinicians understand how the comparative clinical study differs from a traditional phase III efficacy and safety study in the development of a novel biologic originator product. Here, we review the role of comparative clinical studies in biosimilar development, with a focus on trials conducted to support approved trastuzumab biosimilars. We discuss the study populations and end points used, extrapolation of indications, and the confirmatory nature of these studies within the totality of evidence supporting biosimilarity.

J Clin Oncol 38. © 2020 by American Society of Clinical Oncology

INTRODUCTION

Biologic products (biologics) contain an active substance from a biologic source and are manufactured by complex processes using living systems.[1] They have a significant role in the clinical management of a range of medical conditions, including cancer. At a time when there is an increasing need to address the sustainability of cancer care, biosimilars have the potential to widen patient access to biologics and provide cost savings for health care systems,[2-4] and detailed regulatory guidance has been created to guide their development. From a regulatory perspective, a biosimilar is a biologic that has been shown to be highly similar to an approved reference biologic product in terms of structure, biologic activity, safety, and efficacy.[1,5,6] To gain regulatory approval in the United States, for example, it must be demonstrated that a proposed biosimilar is "highly similar to the reference product notwithstanding minor differences in clinically inactive components" and that "there are no clinically meaningful differences between the [biosimilar] and the reference product in terms [of] safety, purity, and potency."[6(p3)] The term biosimilar

reflects the fact that because of the inherent degree of natural minor variability exhibited by all biologic products, it is not possible to create a structurally identical copy of a reference product.[1,6] In practice, however, biosimilars approved through a robust regulatory pathway may be considered clinically equivalent to the relevant reference product. Reflecting this, in regions such as the European Union (EU) and United States, biosimilar product labeling is aligned closely with that of the reference product.[1,7] Furthermore, patient materials recently issued by the US Food and Drug Administration (FDA) describe biosimilars as having the same expected benefits and risks as their respective reference products.[8]

During the development of a biosimilar, an array of data that directly compare the candidate biosimilar with the reference product is required.[5,6,9] This is generated in a stepwise hierarchical process, which begins with extensive characterization of the proposed biosimilar and the reference product, using a range of laboratory-based comparative structural analyses and functional assays, such as assessment of antibody-dependent cellular cytotoxicity (ADCC).[5,6,10] This initial

ASCO

Journal of Clinical Oncology®

step serves as the foundation for a demonstration of biosimilarity, and the more rigorous this assessment in showing similar structure and function, the greater the justification for a selective, tailored program of nonclinical in vivo testing (if required) and clinical studies.[6] The determination of biosimilarity is based on the totality of the evidence from all stages of development.[5,6,9,10]

With respect to the underlying scientific principles, regulatory requirements for demonstrating biosimilarity are generally consistent among stringently regulated regions, such as Australia, Canada, the EU, Japan, and the United States.[11] Although biosimilar supportive care agents have been available for use in oncology for a number of years in several of these regions,[12,13] it is only more recently that biosimilar monoclonal antibodies (mAbs) for the treatment of cancer, including rituximab, trastuzumab, and bevacizumab biosimilars, have received regulatory approval.[14-17] Indeed, in the United States, the first bevacizumab and trastuzumab biosimilars became available for commercial sale in July 2019.[18] While representing a new development in oncology, biosimilar mAbs have been used successfully for several years in the treatment of chronic inflammatory diseases,[4] including conditions that were not initially studied in comparative trials as part of the biosimilarity assessment. Although oncologists may be accepting of biosimilar supportive care agents, it has been suggested that they could be less comfortable with anticancer biosimilars.[19] A recent survey of US community oncologists identified educational gaps with respect to the regulatory approval framework for biosimilars, with some respondents reporting that they were uncomfortable or unfamiliar with the current process.[20] A separate survey by the European Society for Medical Oncology among oncology prescribers identified gaps in knowledge related to biosimilar development, clinical trial design, and selection of end points.[21] To maximize the potential of biosimilars, such knowledge gaps must be addressed.[22] With the introduction of biosimilar mAbs into clinical practice, it is critically important that oncologists understand how the comparative clinical efficacy and safety study, which typically serves as the final step in the biosimilarity exercise, differs from the traditional phase III study in the development of a novel biologic originator product. In this review, we consider the role of comparative clinical studies in biosimilar development, with reference to approved trastuzumab biosimilars as an illustrative example.

COMPARATIVE CLINICAL STUDIES IN THE DEVELOPMENT OF BIOSIMILARS

The main aim of a biosimilar clinical development program is to confirm that any differences between a potential biosimilar and the reference product are not clinically meaningful.[1,5,6,10] Thus, the number and scope of clinical studies performed for a potential biosimilar depend on the degree of residual uncertainty with regard to biosimilarity

following the earlier analytical assessment (and nonclinical in vivo testing, if performed).[6] The clinical program includes a comparative pharmacokinetics (PK) study (with a pharmacodynamics [PD] comparison where suitable biomarkers exist), which is commonly conducted in healthy volunteers.[6,23,24] This is typically followed by a comparative clinical study that assesses efficacy and safety in at least one relevant indication.[6,23]

The aim of the comparative clinical efficacy study is not to demonstrate clinical benefit, as this has already been established independently for the reference product.[23,25] Rather, the aim is to confirm clinical equivalence of the potential biosimilar and reference product on the basis of prespecified margins, using a study population and efficacy end point that are sufficiently sensitive for detecting potential product-related differences while at the same time minimizing the influence of patient- or disease-related factors.[23,25] A sensitive study population would typically be one for which the treatment effect of the reference product has been shown to be robust in prior trials, which thus enhances the ability to detect small differences in efficacy.[26] Factors such as prior lines of therapy and the effect of concomitant medications are also relevant to sensitivity.[10] Ideally, a first-line study conducted in a homogeneous patient population (eg, in terms of disease severity) with a short-term clinical efficacy end point that measures pharmacologic activity would be recommended.[1,10,25] These studies should also include a detailed analysis of safety as well as an evaluation of immunogenicity. The end point chosen may differ from that used to demonstrate the efficacy of the reference product in pivotal studies. For example, although disease-free survival (DFS), progression-free survival (PFS), or overall survival (OS) end points are often required for demonstrating clinical benefit in registration trials of novel anticancer therapeutics, short-term surrogate end points, such as overall response rate (ORR) measured at a certain time point or pathologic complete response (pCR), are considered both adequate and more appropriate for detecting potential product-related differences in a comparative clinical study of a potential anticancer biosimilar.[25]

To statistically test whether a biosimilar is inferior or superior to the reference product in terms of the primary efficacy end point, an equivalence study design is preferred.[6,23] Equivalence is established if the CI for the selected parameter for treatment effect (eg, the difference or ratio between treatments) is completely contained within upper and lower equivalence margins; this is tantamount to performing two one-sided tests, simultaneously testing the null hypotheses of inferiority and superiority.[10,27] Such margins are derived specifically for the indication and end point studied and are based on historical data that concern the efficacy of the reference product as well as on clinical judgment.[1] In contrast to equivalence studies, noninferiority studies are one-sided and, hence, do not exclude the possibility that

a potential biosimilar may be superior in efficacy to the reference product.[10] If such superiority was considered clinically relevant, this might contradict the principle of similarity.[9] Guidelines from the European Medicines Agency (EMA), FDA, and WHO state that a noninferiority design for comparative clinical studies may be appropriate and acceptable in certain circumstances,[6,9,23] although a strong scientific rationale would be required.[23]

If biosimilarity has been successfully demonstrated on the basis of a comparative development program that includes data derived from a clinical study in one therapeutic indication, regulatory guidelines allow for the possibility of the biosimilar being approved for additional indications held by the reference product without conducting additional clinical studies (termed extrapolation).[6,23,28] From scientific, cost, and ethical perspectives, biosimilar studies should not seek to replicate the efficacy and safety data of the reference product across all indications.[28] However, extrapolation must be scientifically justified and considered within the context of the totality of the analytical, nonclinical, and clinical evidence supporting biosimilarity.[6,23] For example, extrapolation may be challenging if the mechanism of action (MOA) of the active substance involves several receptors or binding sites, the contribution of which may vary between the tested and extrapolated indications.[29]

Because prescribers and clinicians are familiar with evaluating novel drugs on the basis of clinical studies, it is important that they appreciate the distinct role of comparative clinical studies in the biosimilar development paradigm.[30] Although the paradigm for the development and approval of a novel biologic is that the positive benefit-risk profile is established mainly on the basis of controlled studies that demonstrate efficacy and safety in each indication approved, this is not the case for a biosimilar.[1] For biosimilars, the positive benefit-risk profile is established on the basis of the totality of the evidence that demonstrates biosimilarity to the reference product, with comparative clinical efficacy trials serving a confirmatory function, and highly sensitive analytical methods providing the foundation for the data[1,5,6,23] (Fig 1). Such analytical methods are generally much more sensitive than clinical studies for detecting potential differences.[1,30] Furthermore, significant differences observed in quality attributes cannot be justified using clinical data.[5]

COMPARATIVE CLINICAL STUDIES OF TRASTUZUMAB BIOSIMILARS IN BREAST CANCER

Which Study Settings and End Points Have Been Used?

Several of the points highlighted in the previous section can be illustrated by considering the example of recently approved biosimilars in reference to trastuzumab (Herceptin; Genentech, South San Francisco, CA; Roche Registration GmbH, Grenzach-Wyhlen, Germany). As of December 2019, five trastuzumab biosimilars have been approved in the EU and United States for intravenous use[31-40] (Table 1). During their respective clinical development programs, all five molecules were assessed in single-dose comparative PK similarity studies in healthy male volunteers,[41-45] and in comparative clinical efficacy and safety studies in women with human epidermal growth factor receptor 2 (HER2)–positive breast cancer.[46-50] There were differences in the designs of the comparative clinical efficacy studies that support biosimilarity, with the study setting (ie, patient population) representing one point of variation, although all
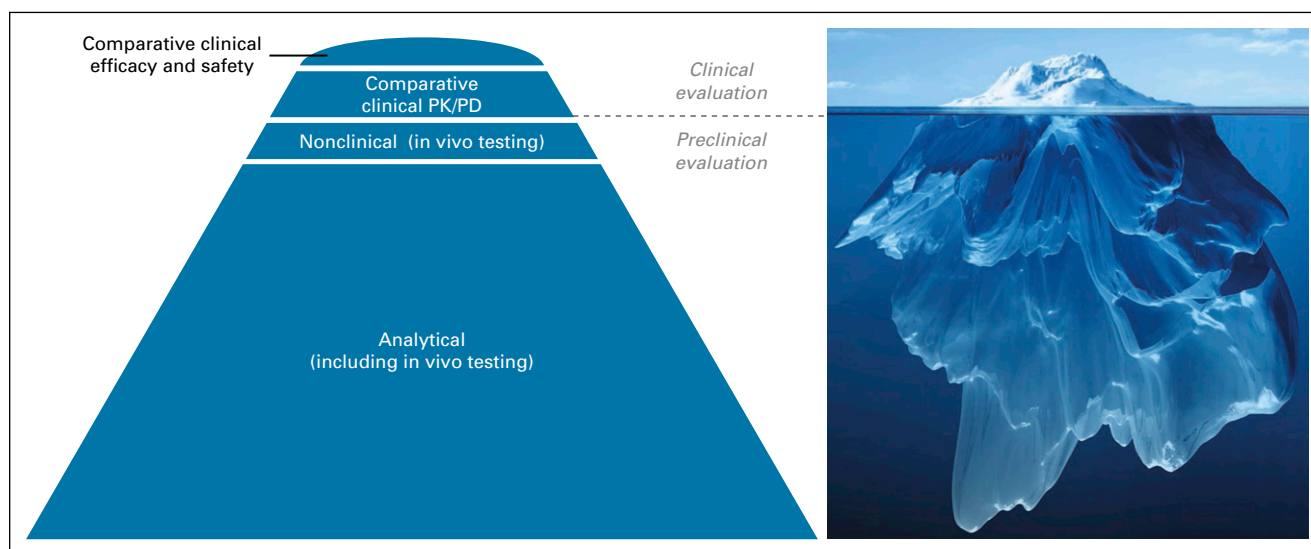

FIG 1. Totality of the evidence that supports biosimilarity. Extensive analytical characterization of a proposed biosimilar and the reference product, using an array of comparative structural analyses and functional assays, provides the foundation for a demonstration of biosimilarity. Data from comparative clinical efficacy and safety studies are confirmatory and are represented as the tip of the iceberg. PD, pharmacodynamics; PK, pharmacokinetics. Iceberg image copyright © Adike/Shutterstock.com.

studies used combinations with taxane-based chemotherapy[46-50] (see Table 2 for an overview of the studies, including primary results). For example, the approvals of ABP 980, CT-P6, and SB3 were supported by studies that compared each biosimilar with reference trastuzumab in the neoadjuvant and adjuvant treatment of early breast cancer (EBC).[46,47,50] In contrast, MYL-1401O and PF-05280014 were compared with reference trastuzumab in the first-line treatment of metastatic breast cancer (MBC).[48,49] In addition, PF-05280014 was compared with reference trastuzumab in a comparative PK noninferiority study in the neoadjuvant treatment of EBC.[51]

Study end points also differed across the development programs (Table 2). For example, although the EBC studies of ABP 980, CT-P6, and SB3 used a pCR primary end point, the definition of pCR varied. The studies of ABP 980 and CT-P6 assessed pCR defined as the absence of invasive tumor cells in the breast and axillary lymph nodes regardless of ductal carcinoma in situ (ie, ypT0/is ypN0, hereafter referred to as total pCR [tpCR]).[46,47] In contrast, the SB3 study used the primary end point of breast pCR (bpCR) defined as the absence of invasive tumor cells in the breast regardless of ductal carcinoma in situ (ie, ypT0/is).[50,52] Some experts have recommended standardizing the use of tpCR as the primary end point for evaluating neoadjuvant treatments (including biosimilars) on the grounds that tpCR is a stronger prognostic marker than bpCR.[53] Indeed, both the FDA and the EMA include absence of nodal involvement in their recommended definitions of pCR as an end point in neoadjuvant studies.[54,55] The investigators of the SB3 study stated that they selected bpCR to eliminate potential confounding factors related to tpCR determination that are not attributable to product-related differences, such as the extent of axillary dissection (tpCR was assessed as a secondary end point, however).[50] Longer-term survival-related end points included EFS and OS in the ABP 980 and SB3 studies and DFS, PFS, and OS in the CT-P6 study; planned follow-up durations differed across the trials[46,47,50,56-61] (see Table 2 for selected results available at the time of writing). The first-line MBC studies for MYL-1401O and PF-05280014 each used the primary end point of ORR on the basis of complete or partial responses achieved by week 24 and week 25, respectively.[48,49] In both MBC studies, secondary efficacy end points included assessment of PFS and OS.[48,49] The neoadjuvant study of PF-05280014 was a noninferiority trial that was considered supportive to the main MBC study and included a PK primary end point (the percentage of patients with trough plasma concentrations of the biosimilar or reference product > 20 μg/mL after five cycles of treatment).[51] Secondary end points included tpCR and ORR.[51,62]

Some experts have argued that a comparative study in the neoadjuvant EBC setting using a pCR end point could offer the greatest level of homogeneity and sensitivity for detecting potential differences between a potential trastuzumab biosimilar and the reference product because patients have received the same prior treatments, have lower disease burden, and may be less likely to be immunologically impaired, for example.[63,64] In addition, at the individual patient level, achieving pCR has been associated with longer EFS and OS compared with not achieving pCR.[65] However, the MBC setting is also appropriate for an assessment of biosimilarity, provided that effort is made to control and minimize heterogeneity sufficiently.[62] Indeed, biosimilar clinical trials conducted with MYL-1401O and PF-05280014 in the first-line MBC setting included relatively homogeneous populations. The MYL-1401O study excluded patients with prior exposure to chemotherapy or reference trastuzumab in the metastatic setting and required at least 1 year since adjuvant therapy with reference trastuzumab.[48] Similarly, the PF-05280014 study excluded patients with prior systemic therapy for MBC (except endocrine therapy) along with those who had relapsed within 1 year of the last dose of adjuvant or neoadjuvant treatment (again, except endocrine therapy).[49] In both studies, a low proportion of patients had prior exposure to reference trastuzumab (MYL-1401O study, 8%; PF-05280014 study, 10%).[48,49] Eligibility criteria for both studies also ensured proper identification of HER2-positive patients.[48,49] More generally, it is worth noting that potential heterogeneity in patient populations can be addressed by stratifying for important covariates during randomization, carefully selecting the prespecified equivalence margin, and/or increasing sample size, for example. With regard to their results, both first-line MBC studies robustly demonstrated similarity in ORR between the biosimilar and reference product[48,49] (Table 2). In both the MYL-1401O and the PF-05280014 studies, no clinically meaningful differences in PFS or OS were observed compared with reference trastuzumab[48,49,66,67] (selected results are listed in Table 2). An analysis of data from the MYL-1401O study also provided support for the use of ORR as a primary end point by showing a correlation between the responder/nonresponder category at week 24 and the probability of PFS (biserial correlation coefficient across all patients, 0.752).[68] An additional consideration with regard to study setting is that while neoadjuvant/adjuvant therapy is given for 1 year in an EBC study, patients in a first-line MBC trial continue trastuzumab until disease progression (or unacceptable toxicity); therefore, studies in the metastatic setting offer the possibility of assessing safety and immunogenicity outcomes associated with long-term treatment.[69]

From a regulatory perspective, there is no requirement for potential trastuzumab biosimilars to be assessed in a comparative clinical efficacy study in the neoadjuvant setting, and with the approval of MYL-1401O and PF-05280014, the EMA and FDA clearly consider the first-line MBC setting as acceptable and sufficiently sensitive for assessing similarity. In short, both neoadjuvant EBC and first-line MBC settings provide the data needed for confirming a lack of

TABLE 1. Trastuzumab Biosimilars Approved in the EU and United States

Biosimilar	EU Approval	US Approval	Approved for Same Indications as Reference Trastuzumab (Herceptin)?[a]
ABP 980			Yes
Name	Kanjinti (trastuzumab)	Kanjinti (trastuzumab-anns)	
Company	Amgen Europe B.V.	Amgen Inc	
Approval date	May 16, 2018	June 13, 2019	
CT-P6			Yes
Name	Herzuma (trastuzumab)	Herzuma (trastuzumab-pkrb)	
Company	Celltrion Healthcare Hungary Kft.	Celltrion Inc	
Approval date	February 8, 2018	December 14, 2018	
MYL-1401O			Yes
Name	Ogivri (trastuzumab)	Ogivri (trastuzumab-dkst)	
Company	Mylan S.A.S.	Mylan GmbH	
Approval date	December 12, 2018	December 1, 2017	
PF-05280014			Yes
Name	Trazimera (trastuzumab)	Trazimera (trastuzumab-qyyp)	
Company	Pfizer Europe MA EEIG	Pfizer Inc	
Approval date	July 26, 2018	March 11, 2019	
SB3			Yes
Name	Ontruzant (trastuzumab)	Ontruzant (trastuzumab-dttb)	
Company	Samsung Bioepis NL B.V.	Samsung Bioepis Co., Ltd.	
Approval date	November 15, 2017	January 18, 2019	

NOTE. Includes trastuzumab biosimilars approved in the EU and United States as of December 2019. Information in columns 2 and 3 was retrieved from web sites of the European Medicines Agency (www.ema.europa.eu/en/medicines) and US Food and Drug Administration (www.accessdata.fda.gov/scripts/cder/daf/index.cfm), respectively. Information in column 4 is based on EU summaries of product characteristics[31-35,70] and US prescribing information.[36-40,71]

Abbreviation: EU, European Union.

[a]The trastuzumab (Herceptin; Genentech) biosimilars included are for intravenous use only. Column refers to the indications of the intravenous formulation of reference trastuzumab.

clinically meaningful differences between a trastuzumab biosimilar and the reference product, and each has its own advantages and disadvantages.[69] All five trastuzumab biosimilars discussed here have been approved for the same indications as the intravenous formulation of reference trastuzumab (ie, HER2-positive EBC, MBC, and metastatic gastric cancer in the EU and HER2-positive adjuvant breast cancer, MBC, and metastatic gastric cancer in the United States).[31-40,70,71] Thus, both EBC and MBC have been considered as sufficiently sensitive settings to support extrapolation. For trastuzumab biosimilars, the scientific justification for extrapolation includes the fact that the MOA of trastuzumab is the same across indications, and the target receptor involved (HER2) is the same in each case.[57,72-78] Furthermore, on the basis of data available for the reference product, there are no significant differences in expected toxicities between patient populations or indications.[72,75]

How Have Regulatory Authorities Interpreted Comparative Clinical Study Data Within the Context of the Totality of the Evidence?

As described earlier, biosimilarity is determined on the basis of the totality of evidence. To illustrate how regulators interpret data from comparative clinical efficacy studies within the overall assessment of biosimilarity, it is helpful to consider the evaluation of SB3 and ABP 980 by the EMA's Committee for Medicinal Products for Human Use (CHMP) as described in European Public Assessment Reports (EPARs) and the subsequent EU approval of these biosimilars.[46,50,57,73]

In the SB3 study in EBC, equivalence was assessed on the basis of an analysis of the 95% CIs of both the ratio of bpCR rates and the difference in bpCR rates between arms.[50] The 95% CI for the adjusted ratio of bpCR rates was contained within the predefined equivalence margin, demonstrating equivalence (Table 2). In contrast, the upper limit of the 95% CI for the adjusted difference in bpCR rates was outside the predefined equivalence margin,[50] meaning that while noninferiority of SB3 was demonstrated, nonsuperiority was not. The CHMP primarily considered the difference in bpCR rates in its assessment of SB3.[73] Structural and functional analyses conducted by the sponsor of numerous lots of reference trastuzumab identified that certain lots exhibited a marked downward drift in glycosylation levels, FcγRIIIa binding, and ADCC.[50,79] ADCC is a known component of the trastuzumab MOA, and some of the affected

TABLE 2. Comparative Clinical Studies of Trastuzumab Biosimilars in Patients With HER2-Positive Breast Cancer

Biosimilar	Study Setting (No. of patients)	Treatment Regimen	Primary End Point	Primary End Point Result (BS v RP), %	Primary End Point Treatment Comparison, %			Selected Survival-Related End Point Data[a]
					Comparison	Equivalence Margin	Equivalence Shown?	
ABP 980	Neoadjuvant and adjuvant HER2-positive EBC (725)[46]	Neoadjuvant phase: EC → trastuzumab + P Adjuvant phase: trastuzumab (until 1 year from first dose of neoadjuvant trastuzumab; during adjuvant phase, patients either continued BS [BS/BS], continued RP [RP/RP], or switched from RP to BS [RP/BS])	tpCR (local assessment[b])	48 v 41	Difference, 7.3 (90% CI, 1.2 to 13.4)	−13-13	No (upper CI limit exceeded margin[b])	Study did not include long-term follow-up after adjuvant phase. As of final database lock, HR for on-study EFS was 0.9969 (90% CI, 0.5340 to 1.8612) for patients receiving BS/BS v RP/RP and 0.5414 (90% CI, 0.2207 to 1.3282) for RP/BS v RP/RP.[56,57] No HR for OS was identified.
					Ratio, 1.188 (90% CI, 1.033 to 1.366)	0.759-1.318	No (upper CI limit exceeded margin[b])	
CT-P6[c]	Neoadjuvant and adjuvant HER2-positive EBC (549)[47]	Neoadjuvant phase: trastuzumab + D → trastuzumab + FEC Adjuvant phase: trastuzumab (until 1 year of neoadjuvant and adjuvant treatment)	tpCR (local assessment[d])	46.8 v 50.4	Difference, −0.04 (95% CI, −0.12 to 0.05)	−0.15-0.15	Yes	At median follow-up of 39 months, HR for DFS was 1.23 (95% CI, 0.78 to 1.94; P = .3808), and HR for OS was 0.87 (95% CI, 0.42 to 1.82; P = .7181).[61] No HR for PFS was identified.
					Ratio, 0.93 (95% CI, 0.78 to 1.11)	0.74-1.35	Yes	
MYL-14010	First-line HER2-positive MBC (500)[48]	Trastuzumab (until disease progression) + taxane (D or P)	ORR (week 24; blinded central assessment)	69.6 v 64.0	Ratio, 1.09 (90% CI, 0.974 to 1.211)	0.81-1.24	Yes	Cumulative through 36 months from last patient in the study; HR for PFS was 0.98 (95% CI, 0.78 to 1.24); and HR for OS was 0.90 (95% CI, 0.69 to 1.17).[66]
					Difference, 5.53% (95% CI, −3.08 to 14.04)	−15-15	Yes	
PF-05280014	First-line HER2-positive MBC (707)[49]	Trastuzumab (until disease progression) + P	ORR (week 25; blinded central assessment)	62.5 v 66.5	Ratio,[e] 0.940 (95% CI, 0.842 to 1.049)	0.80-1.25	Yes	Using data up to 378 days post-random assignment, HR for PFS was 1.00 (95% CI, 0.80 to 1.26; P = .505).[49] Cumulative through 5 years from first patient screened, HR for OS was 0.888 (95% CI, 0.624 to 1.264; P = .254).[67]
	Neoadjuvant HER2-positive EBC (226)[51]	Trastuzumab + DC	Percentage of patients with cycle 5 C_{trough} > 20 µg/mL	92.1 v 93.3	Difference, −0.76 (95% CI, −8.02 to 6.49)	−12.5; (noninferiority margin)	Noninferiority shown (equivalence not assessed)	Not applicable (secondary efficacy end points included ORR and tpCR).[51,62]

(continued on following page)

TABLE 2. Comparative Clinical Studies of Trastuzumab Biosimilars in Patients With HER2-Positive Breast Cancer (continued)

Biosimilar	Study Setting (No. of patients)	Treatment Regimen	Primary End Point	Primary End Point Result (BS v RP), %	Primary End Point Treatment Comparison, %			Selected Survival-Related End Point Data[a]
					Comparison	Equivalence Margin	Equivalence Shown?	
SB3	Neoadjuvant and adjuvant HER2-positive EBC (875)[50]	Neoadjuvant phase: trastuzumab + D → trastuzumab + FEC	bpCR (local assessment[f])	51.7 v 42.0	Ratio, 1.259 (95% CI, 1.085 to 1.460)	0.785-1.546	Yes	At median follow-up of 437 days (BS) and 438 days (RP), HR for EFS was 0.94 (95% CI, 0.59 to 1.51), and HR for OS was 0.23 (95% CI, 0.03 to 1.97).[59] In an extension study that enrolled a subset of 367 patients, at median follow-up of 40.8 months (BS) and 40.5 months (RP) from enrollment in the main study, HR for EFS was 0.47 (95% CI, 0.26 to 0.87), and HR for OS was 0.37 (95% CI, 0.13 to 1.04).[60]
		Adjuvant phase: trastuzumab (until 1 year of neoadjuvant and adjuvant treatment)			Difference, 10.70 (95% CI, 4.13 to 17.26)	−13-13	No (upper CI limit exceeded margin)	

NOTE. Includes trastuzumab BSs approved in the European Union and United States as of December 2019. Studies included are those with primary publications available from PubMed. Comparative studies in healthy volunteers not included. Information in columns 1-8 is based on primary publications. In column 3, trastuzumab denotes either the BS or the trastuzumab RP. Consult cited references for information on dosing and treatment cycles and for additional details of the presented analyses (eg, analysis populations, statistical methods).

Abbreviations: bpCR, breast pathologic complete response; BS, biosimilar; C$_{trough}$, trough plasma concentration; D, docetaxel; DC, docetaxel and carboplatin; EBC, early breast cancer; EC, epirubicin and cyclophosphamide; EFS, event-free survival; FEC, fluorouracil, epirubicin, and cyclophosphamide; HER2, human epidermal growth factor receptor 2; HR, hazard ratio; MBC, metastatic breast cancer; ORR, objective response rate; OS, overall survival; P, paclitaxel; pCR, pathologic complete response; RP, reference product; tpCR, total pathologic complete response.

[a]Column reports HRs for treatment group comparisons (where available) for longest follow-up data identified for each study/end point as of December 2019. Consult cited references for additional results (eg, median values, event rates at specific time points).

[b]In sensitivity analyses that were based on central review of tumor samples, 90% CIs for the risk difference and risk ratio were contained within the predefined equivalence margins.[46]

[c]CT-P6 was also assessed in MBC[89]; however, these data were not part of submissions to regulators in the United States and European Union.[74,75]

[d]Histopathology reports were assessed centrally by a blinded reviewer.

[e]As noted in the European Medicines Agency assessment report for PF-05280014, equivalence was also assessed on the basis of ORR risk difference (−3.979%; 95% CI, −11.005 to 3.080). The 95% CI was contained within the equivalence margin of −13% to 13%.[62]

[f]For quality control, all bpCRs were reviewed by a study pathologist board

lots were used in the clinical study.[50,73] It was considered by the CHMP that this apparent shift in ADCC activity could have added variability to the estimation of the treatment difference, thereby contributing to the upper limit of the CI exceeding the margin.[73] As noted in the EPAR for SB3, "the magnitude of the differences observed can be in part attributed to other factors and the true difference is considered likely to fall within the equivalence margins and [be] of no clinical relevance."[73(p68)]

In the study of ABP 980 in EBC, equivalence was evaluated using the 90% CIs of both the risk difference and the risk ratio of locally assessed tpCR, using a sequential testing method.[46] In analyses that were based on both the risk difference and the risk ratio, the upper boundaries of the 90% CIs exceeded the predefined equivalence margins (Table 2). Thus, nonsuperiority of ABP 980 was not demonstrated. In a sensitivity analysis that was based on central review of tumor samples, 90% CIs of the risk difference and risk ratio were contained within the margins, however.[46] According to the EPAR for ABP 980, the CHMP seems to have considered 95% CIs (rather than 90% CIs) of the tpCR risk difference and risk ratio on the basis of local laboratory review.[57] Again, the upper limits of both 95% CIs exceeded the prespecified margins.[57] As with SB3, it was acknowledged in the EPAR for ABP 980 that the apparent difference between the groups was considered to be at least partly confounded by a shift in ADCC activity observed for certain lots of the trastuzumab reference product used in the study, which may have contributed to a more extreme location of the upper CI limit.[57] The CHMP noted that the observed difference in efficacy results was not considered clinically relevant.[57]

For both SB3 and ABP 980, considering the similarity data from across all stages of the respective comparison exercises, the CHMP determined that biosimilarity to reference trastuzumab had been sufficiently shown.[57,73] These examples help to illustrate that it is the totality of the evidence, with comprehensive and robust analytical data as the foundation, that is of crucial importance in a regulatory determination of biosimilarity. Data from comparative clinical studies, while clearly important, serve a confirmatory rather than a central function. As shown by the regulatory assessment of SB3 and ABP 980 in the EU, in certain circumstances, small apparent differences between a proposed biosimilar and reference product when using a sensitive clinical end point may be considered unlikely to be clinically meaningful and in view of the totality of data, may not preclude a determination of biosimilarity.

WHAT IS THE ROLE FOR COMPARATIVE CLINICAL STUDIES IN THE FUTURE DEVELOPMENT OF BIOSIMILARS?

Recently, some experts have argued that from a scientific, economic, and ethical perspective, comparative clinical efficacy studies may be unnecessary in the development of most biosimilars.[80-82] A recent opinion article proposed that

the current approach to biosimilar development should be replaced with a more efficient paradigm that "emphasizes analytical likeness between a biosimilar and its reference but does not generally require…in vivo nonclinical studies or clinical equivalence studies."[82(p604)] The authors of the article based their proposal on the observation that

> no biosimilar that has been found to be highly similar to its reference by both analytical and human pharmacokinetic studies has ever failed to be approved because it was found not to be clinically equivalent to its reference in a powered [efficacy] study.[82(p604)]

It should be noted that current regulatory guidelines do not mandate comparative clinical efficacy studies in all circumstances.[5,6] FDA guidance, for instance, states that a comparative clinical study will be necessary "if there is residual uncertainty about whether there are clinically meaningful differences between the proposed [biosimilar] product and the reference product based on structural and functional characterization, animal testing, human PK and PD data, and clinical immunogenicity assessment."[6(p18)] Factors that affect the type and extent of clinical data required include the complexity of the reference product, the magnitude of differences observed in comparative structural and functional assessment, the degree to which the MOA is understood, and the availability of a PD end point that correlates with efficacy.[1,6] In the EU, regulatory requirements with regard to clinical data have evolved since the biosimilar framework was first introduced, and although comparative PK/PD studies remain essential, the strict requirement for comparative efficacy studies has been waived (or is proposed to be waived) for certain product categories, along with comparative safety/immunogenicity studies in specific circumstances.[5,83,84] For granulocyte colony-stimulating factor, for example, structure, physicochemical characteristics, and biologic activity can be well characterized, and clinically relevant PD parameters are available.[85] Whereas the original version of the EMA guidance concerning biosimilar granulocyte colony-stimulating factor (published in 2006)[86] includes significant emphasis on comparative clinical efficacy and safety trials, a draft revision to the guideline (released in 2018 for consultation) stated that a dedicated comparative efficacy trial is "not considered necessary."[84(p7)] For many biosimilar mAbs, however, the absence of robust PD efficacy measures, as well as their importance to clinical outcome, means that comparative clinical trials will likely remain necessary.[87,88] In our view, the requirement for such studies is also particularly likely for oncology mAbs, where biosimilars may be used with curative intent, and prescribers will want to appraise comparative clinical data.

In summary, the paradigm for the development and approval of biosimilars differs markedly from that for novel biologics. For biosimilars, the positive benefit-risk profile is

based on the totality of the evidence that demonstrates biosimilarity to the reference product rather than on efficacy and safety studies in each approved indication. In biosimilar development, the comparative clinical efficacy study aims to confirm clinical equivalence between a proposed biosimilar and its reference product on the basis of prespecified margins, along with comparable safety and immunogenicity. Such studies do not aim to establish de novo efficacy and safety. Reflecting this difference, comparative clinical studies should be performed in a sensitive population using appropriate end points to allow detection of any clinically meaningful differences between the treatments, should they exist. As is evident from experience with recently approved trastuzumab biosimilars, for certain reference products, there may be more than one appropriate design for such studies in terms of the population studied and end point used. Furthermore, there may be more than one acceptable study setting to support extrapolation. As biosimilars become more widely available in oncology, it is important that clinicians appreciate the distinct confirmatory role of comparative clinical studies in the biosimilar paradigm.

AFFILIATIONS

[1]Division of Cancer, Department of Surgery and Cancer, Imperial College London, London, United Kingdom
[2]Center for Personalised Nanomedicine, University of Queensland, Brisbane, Queensland, Australia
[3]Division of Early Drug Development, European Institute of Oncology, IRCCS, Milan, Italy
[4]Department of Oncology and Hemato-Oncology, University of Milan, Milan, Italy
[5]Stanford Comprehensive Cancer Institute, Stanford University School of Medicine, Stanford, CA
[6]Pfizer, Sandwich, United Kingdom
[7]Pfizer, New York, NY
[8]University of California, San Francisco, Comprehensive Cancer Center, San Francisco, CA

CORRESPONDING AUTHOR

Justin Stebbing, MA, PhD, Imperial College/Imperial Healthcare NHS Trust, Charing Cross Hospital, First Floor, E Wing, Fulham Palace Rd, London W6 8RF, United Kingdom; e-mail: j.stebbing@imperial.ac.uk.

AUTHORS' DISCLOSURES OF POTENTIAL CONFLICTS OF INTEREST AND DATA AVAILABILITY STATEMENT

Disclosures provided by the authors and data availability statement (if applicable) are available with this article at DOI https://doi.org/10.1200/JCO.19.02953.

AUTHOR CONTRIBUTIONS

Conception and design: Justin Stebbing, Paul N. Mainwaring, Giuseppe Curigliano, Mark Latymer, Angel H. Bair, Hope S. Rugo
Administrative support: Mark Latymer
Collection and assembly of data: Justin Stebbing, Paul N. Mainwaring, Giuseppe Curigliano, Mark Latymer, Angel H. Bair
Data analysis and interpretation: All authors
Manuscript writing: All authors
Final approval of manuscript: All authors
Accountable for all aspects of the work: All authors

ACKNOWLEDGMENT

REFERENCES

1. European Medicines Agency; European Commission: Biosimilars in the EU: Information Guide for Healthcare Professionals, 2017. https://www.ema.europa.eu/en/documents/leaflet/biosimilars-eu-information-guide-healthcare-professionals_en.pdf

2. Tabernero J, Vyas M, Giuliani R, et al: Biosimilars: A position paper of the European Society for Medical Oncology, with particular reference to oncology prescribers. ESMO Open 1:e000142, 2017

3. Lyman GH, Balaban E, Diaz M, et al: American Society of Clinical Oncology statement: Biosimilars in oncology. J Clin Oncol 36:1260-1265, 2018

4. IQVIA: The Impact of Biosimilar Competition in Europe, 2018. https://ec.europa.eu/docsroom/documents/31642/attachments/1/translations/en/renditions/native

5. European Medicines Agency: Guideline on similar biological medicinal products, 2014. https://www.ema.europa.eu/documents/scientific-guideline/guideline-similar-biological-medicinal-products-rev1_en.pdf

6. US Food and Drug Administration: Scientific Considerations in Demonstrating Biosimilarity to a Reference Product: Guidance for Industry, 2015. https://www.fda.gov/media/82647/download

7. US Food and Drug Administration: Labeling for Biosimilar Products. Guidance for Industry, 2018. https://www.fda.gov/media/96894/download

8. US Food and Drug Administration: Patient materials, 2019. https://www.fda.gov/drugs/biosimilars/patient-materials

9. WHO: Guidelines on Evaluation of Similar Biotherapeutic Products (SBPs), 2009. http://www.who.int/biologicals/areas/biological_therapeutics/BIOTHERAPEUTICS_FOR_WEB_22APRIL2010.pdf

10. WHO: Guidelines on Evaluation of Monoclonal Antibodies as Similar Biotherapeutic Products (SBPs), 2017. https://www.who.int/biologicals/biotherapeutics/WHO_TRS_1004_web_Annex_2.pdf?ua=1

11. Cazap E, Jacobs I, McBride A, et al: Global acceptance of biosimilars: Importance of regulatory consistency, education, and trust. Oncologist 23:1188-1198, 2018

12. Aapro M, Krendyukov A, Schiestl M, et al: Epoetin biosimilars in the treatment of chemotherapy-induced anemia: 10 years' experience gained. BioDrugs 32:129-135, 2018 [Erratum: BioDrugs 32:137-138, 2018]

13. Gascón P, Tesch H, Verpoort K, et al: Clinical experience with Zarzio in Europe: What have we learned? Support Care Cancer 21:2925-2932, 2013

14. US Food and Drug Administration: Biosimilar product information, 2019. https://www.fda.gov/drugs/developmentapprovalprocess/howdrugsaredevelopedandapproved/approvalapplications/therapeuticbiologicapplications/biosimilars/ucm580432.htm

15. European Medicines Agency: Medicines, 2019. https://www.ema.europa.eu/en/medicines/search_api_aggregation_ema_medicine_types/field_ema_med_biosimilar

16. Genetics and Biosimilars Initiative: Biosimilars approved in Japan, 2019. http://gabionline.net/Biosimilars/General/Biosimilars-approved-in-Japan

17. Genetics and Biosimilars Initiative: Biosimilars approved in Australia, 2019. http://www.gabionline.net/Biosimilars/General/Biosimilars-approved-in-Australia

18. Amgen: Amgen and Allergan's MVASI™ (bevacizumab-awwb) and KANJINTI (trastuzumab-anns) Now Available in the United States, 2019. https://www.amgen.com/media/news-releases/2019/07/amgen-and-allergans-mvasi-bevacizumabawwb-and-kanjinti-trastuzumabanns-now-available-in-the-united-states

19. Nabhan C, Valley A, Feinberg BA: Barriers to oncology biosimilars uptake in the United States. Oncologist 23:1261-1265, 2018

20. Nabhan C, Jeune-Smith Y, Valley A, et al: Community oncologists' perception and acceptance of biosimilars in oncology. J Clin Pathways 4:43-47, 2018

21. Giuliani R, Tabernero J, Cardoso F, et al: Knowledge and use of biosimilars in oncology: A survey by the European Society for Medical Oncology. ESMO Open 4: e000460, 2019

22. Leonard E, Wascovich M, Oskouei S, et al: Factors affecting health care provider knowledge and acceptance of biosimilar medicines: A systematic review. J Manag Care Spec Pharm 25:102-112, 2019

23. European Medicines Agency: Guideline on similar Biological Medicinal Products Containing Biotechnology-Derived Proteins as Active Substance: Non-Clinical and Clinical Issues, 2014. https://www.ema.europa.eu/en/documents/scientific-guideline/guideline-similar-biological-medicinal-products-containing-biotechnology-derived-proteins-active_en-2.pdf

24. US Food and Drug Administration: Clinical Pharmacology Data to Support a Demonstration of Biosimilarity to a Reference Product: Guidance for Industry, 2016. https://www.fda.gov/media/88622/download

25. European Medicines Agency: Guideline on Similar Biological Medicinal Products Containing Monoclonal Antibodies—Non-Clinical and Clinical Issues, 2012. http://www.ema.europa.eu/docs/en_GB/document_library/Scientific_guideline/2012/06/WC500128686.pdf

26. Krendyukov A, Schiestl M: Extrapolation concept at work with biosimilar: A decade of experience in oncology. ESMO Open 3:e000319, 2018

27. Walker E, Nowacki AS: Understanding equivalence and noninferiority testing. J Gen Intern Med 26:192-196, 2011

28. Curigliano G, O'Connor DP, Rosenberg JA, et al: Biosimilars: Extrapolation for oncology. Crit Rev Oncol Hematol 104:131-137, 2016

29. Weise M, Kurki P, Wolff-Holz E, et al: Biosimilars: The science of extrapolation. Blood 124:3191-3196, 2014

30. Christl LA, Woodcock J, Kozlowski S: Biosimilars: The US regulatory framework. Annu Rev Med 68:243-254, 2017

31. Amgen Europe: Kanjinti summary of product characteristics, 2019. https://www.ema.europa.eu/documents/product-information/kanjinti-epar-product-information_en.pdf

32. Celltrion Healthcare Hungary: Herzuma summary of product characteristics, 2019. https://www.ema.europa.eu/documents/product-information/herzuma-epar-product-information_en.pdf

33. Mylan: Ogivri summary of product characteristics, 2019. https://www.ema.europa.eu/documents/product-information/ogivri-epar-product-information_en.pdf

34. Pfizer Europe: Trazimera summary of product characteristics, 2019. https://www.ema.europa.eu/en/documents/product-information/trazimera-epar-product-information_en.pdf

35. Samsung Bioepis: Ontruzant summary of product characteristics, 2019. https://www.ema.europa.eu/documents/product-information/ontruzant-epar-product-information_en.pdf

36. Amgen: Kanjinti prescribing information, 2019. https://www.accessdata.fda.gov/drugsatfda_docs/label/2019/761073Orig1s000lbl.pdf

37. Celltrion: Herzuma prescribing information, 2019. https://www.accessdata.fda.gov/drugsatfda_docs/label/2019/761091s001s002lbl.pdf

38. Mylan Pharmaceuticals: Ogivri prescribing information, 2019. https://www.accessdata.fda.gov/drugsatfda_docs/label/2019/761074s004lbl.pdf

39. Pfizer: Trazimera prescribing information, 2019. https://www.accessdata.fda.gov/drugsatfda_docs/label/2019/761081s000lbl.pdf

40. Samsung Bioepis: Ontruzant prescribing information, 2019. https://www.accessdata.fda.gov/drugsatfda_docs/label/2019/761100s000lbl.pdf

41. Hanes V, Chow V, Zhang N, et al: A randomized, single-blind, single-dose study evaluating the pharmacokinetic equivalence of proposed biosimilar ABP 980 and trastuzumab in healthy male subjects. Cancer Chemother Pharmacol 79:881-888, 2017

42. Esteva FJ, Stebbing J, Wood-Horrall RN, et al: A randomised trial comparing the pharmacokinetics and safety of the biosimilar CT-P6 with reference trastuzumab. Cancer Chemother Pharmacol 81:505-514, 2018

43. Waller CF, Vutikullird A, Lawrence TE, et al: A pharmacokinetics phase 1 bioequivalence study of the trastuzumab biosimilar MYL-1401O vs. EU-trastuzumab and US-trastuzumab. Br J Clin Pharmacol 84:2336-2343, 2018

44. Yin D, Barker KB, Li R, et al: A randomized phase 1 pharmacokinetic trial comparing the potential biosimilar PF-05280014 with trastuzumab in healthy volunteers (REFLECTIONS B327-01). Br J Clin Pharmacol 78:1281-1290, 2014

45. Pivot X, Curtit E, Lee YJ, et al: A randomized phase I pharmacokinetic study comparing biosimilar candidate SB3 and trastuzumab in healthy male subjects. Clin Ther 38:1665-1673.e3, 2016

46. von Minckwitz G, Colleoni M, Kolberg HC, et al: Efficacy and safety of ABP 980 compared with reference trastuzumab in women with HER2-positive early breast cancer (LILAC study): A randomised, double-blind, phase 3 trial. Lancet Oncol 19:987-998, 2018

47. Stebbing J, Baranau Y, Baryash V, et al: CT-P6 compared with reference trastuzumab for HER2-positive breast cancer: A randomised, double-blind, active-controlled, phase 3 equivalence trial. Lancet Oncol 18:917-928, 2017

48. Rugo HS, Barve A, Waller CF, et al: Effect of a proposed trastuzumab biosimilar compared with trastuzumab on overall response rate in patients with ERBB2 (HER2)-positive metastatic breast cancer: A randomized clinical trial. JAMA 317:37-47, 2017

49. Pegram MD, Bondarenko I, Zorzetto MMC, et al: PF-05280014 (a trastuzumab biosimilar) plus paclitaxel compared with reference trastuzumab plus paclitaxel for HER2-positive metastatic breast cancer: A randomised, double-blind study. Br J Cancer 120:172-182, 2019

50. Pivot X, Bondarenko I, Nowecki Z, et al: Phase III, randomized, double-blind study comparing the efficacy, safety, and immunogenicity of SB3 (trastuzumab biosimilar) and reference trastuzumab in patients treated with neoadjuvant therapy for human epidermal growth factor receptor 2-positive early breast cancer. J Clin Oncol 36:968-974, 2018

51. Lammers PE, Dank M, Masetti R, et al: Neoadjuvant PF-05280014 (a potential trastuzumab biosimilar) versus trastuzumab for operable HER2+ breast cancer. Br J Cancer 119:266-273, 2018

52. Center for Drug Evaluation and Research: Summary review: BLA 761100 (Ontruzant), 2019. https://www.accessdata.fda.gov/drugsatfda_docs/nda/2019/761100Orig1s000SumR.pdf

53. Stebbing J, Baranau Y, Manikhas A, et al: Total pathological complete response versus breast pathological complete response in clinical trials of reference and biosimilar trastuzumab in the neoadjuvant treatment of breast cancer. Expert Rev Anticancer Ther 18:531-541, 2018

54. US Food and Drug Administration: Guidance for industry. Pathological complete response in neoadjuvant treatment of high-risk early-stage breast cancer: Use as an endpoint to support accelerated approval, 2014. https://www.fda.gov/media/83507/download

55. European Medicines Agency: Appendix 4 to the guideline on the evaluation of anticancer medicinal products in man, 2015. https://www.ema.europa.eu/en/documents/scientific-guideline/evaluation-anticancer-medicinal-products-man-appendix-4-condition-specific-guidance-rev2_en.pdf

56. Amgen: ABP 980. Clinical Study Report: 20120283. Synopsis, 2017. http://filehosting.pharmacm.com/DownloadService.ashx?client=AMG&studyid=500&filename=20120283%2001.09.04.01%20Public%20Results%20Redacted%20CSR%20Synopsis%202017-01-27%20NA.pdf

57. European Medicines Agency: Assessment report: Kanjinti, 2018. https://www.ema.europa.eu/en/documents/assessment-report/kanjinti-epar-public-assessment-report_en.pdf

58. Pivot X, Bondarenko I, Nowecki Z, et al: A phase III study comparing SB3 (a proposed trastuzumab biosimilar) and trastuzumab reference product in HER2-positive early breast cancer treated with neoadjuvant-adjuvant treatment: Final safety, immunogenicity and survival results. Eur J Cancer 93:19-27, 2018

59. Pivot X, Bondarenko IM, Zbigniew N, et al: One-year safety, immunogenicity, and survival results from a phase III study comparing SB3 (a proposed trastuzumab biosimilar) and originator trastuzumab in HER2-positive early breast cancer treated with neoadjuvant-adjuvant treatment. Presented at the Eur Soc Med Oncol Congr 2017, Madrid, Spain, September 8-12, 2017

60. Pivot X, Pegram M, Cortes J, et al: Three-year follow-up from a phase 3 study of SB3 (a trastuzumab biosimilar) versus reference trastuzumab in the neoadjuvant setting for human epidermal growth factor receptor 2-positive breast cancer. Eur J Cancer 120:1-9, 2019

61. Stebbing J, Baranau Y, Baryash V, et al: 3-year follow-up of a phase III trial comparing the efficacy and safety of neoadjuvant and adjuvant trastuzumab and its biosimilar CT-P6 in HER2 positive early breast cancer (EBC). Ann Oncol 30, 2019 (suppl 5; abstr 190P)

62. European Medicines Agency: Assessment report: Trazimera, 2018. https://www.ema.europa.eu/documents/assessment-report/trazimera-epar-public-assessment-report_en.pdf

63. Cortés J, Curigliano G, Diéras V: Expert perspectives on biosimilar monoclonal antibodies in breast cancer. Breast Cancer Res Treat 144:233-239, 2014

64. Jackisch C, Scappaticci FA, Heinzmann D, et al: Neoadjuvant breast cancer treatment as a sensitive setting for trastuzumab biosimilar development and extrapolation. Future Oncol 11:61-71, 2015

65. Cortazar P, Zhang L, Untch M, et al: Pathological complete response and long-term clinical benefit in breast cancer: The CTNeoBC pooled analysis. Lancet 384:164-172, 2014

66. Waller CF, Manikhas A, Pennella EJ, et al: Biosimilar trastuzumab-dkst monotherapy versus trastuzumab monotherapy after combination therapy: Final overall survival (OS) from the phase III HERITAGE Trial. Presented at the Am Soc Clin Oncol Ann Meet, Chicago, IL, May 31-June 4, 2019

67. Li RK, Lipatov O, Adamchuk H, et al: Trazimera (a trastuzumab biosimilar) in HER2-positive metastatic breast cancer: Long-term safety and overall survival data. Presented at the San Antonio Breast Cancer Symp, San Antonio, TX, December 10-14, 2019

68. Rugo HS, Curigliano G, Cardoso F, et al: Settings-based efficacy comparison of trastuzumab biosimilars in breast cancer: A systematic literature review. Presented at the Eur Soc Med Oncol 2018 Congr, Munich, Germany, October 19-23, 2018

69. Rugo HS, Cortes J: The new world of biosimilars in oncology: Translation of data to the clinic. Eur J Cancer 96:125-127, 2018

70. Roche Registration: Herceptin summary of product characteristics, 2019. https://www.ema.europa.eu/en/documents/product-information/herceptin-epar-product-information_en.pdf

71. Genentech: Herceptin prescribing information, 2018. https://www.accessdata.fda.gov/drugsatfda_docs/label/2018/103792s5345lbl.pdf

72. European Medicines Agency: Assessment report: Ogivri, 2018. https://www.ema.europa.eu/en/documents/assessment-report/ogivri-epar-public-assessment-report_en.pdf

73. European Medicines Agency: Assessment report: Ontruzant, 2017. https://www.ema.europa.eu/en/documents/assessment-report/ontruzant-epar-public-assessment-report_en-0.pdf

74. European Medicines Agency: Assessment report: Herzuma, 2017. https://www.ema.europa.eu/en/documents/assessment-report/herzuma-epar-public-assessment-report_en.pdf

75. Center for Drug Evaluation and Research: Summary review: BLA 761091 (Herzuma), 2018. https://www.accessdata.fda.gov/drugsatfda_docs/nda/2018/761091Orig1s000SumR.pdf

76. Center for Drug Evaluation and Research: Clinical review(s): BLA 761073 (Kanjinti), 2019. https://www.accessdata.fda.gov/drugsatfda_docs/nda/2019/761073Orig1s000MedR.pdf

77. Center for Drug Evaluation and Research: Summary review: BLA 761074 (Ogivri), 2017. https://www.accessdata.fda.gov/drugsatfda_docs/nda/2017/761074Orig1s000SumR.pdf

78. Center for Drug Evaluation and Research: Summary review: BLA 761081 (Trazimera), 2019. https://www.accessdata.fda.gov/drugsatfda_docs/nda/2019/761081Orig1s000SumR.pdf

79. Kim S, Song J, Park S, et al: Drifts in ADCC-related quality attributes of Herceptin: Impact on development of a trastuzumab biosimilar. MAbs 9:704-714, 2017

80. Webster CJ, Woollett GR: Comment on "The End of Phase 3 Clinical Trials in Biosimilars Development?" BioDrugs 32:519-521, 2018

81. Frapaise FX: The end of phase 3 clinical trials in biosimilars development? BioDrugs 32:319-324, 2018

82. Webster CJ, Wong AC, Woollett GR: An efficient development paradigm for biosimilars. BioDrugs 33:603-611, 2019

83. Wolff-Holz E, Tiitso K, Vleminckx C, et al: Evolution of the EU biosimilar framework: Past and future. BioDrugs 33:621-634, 2019

84. European Medicines Agency: Guideline on similar biological medicinal products containing recombinant granulocyte-colony stimulating factor (rG-CSF). Draft, 2018. https://www.ema.europa.eu/en/documents/scientific-guideline/draft-guideline-similar-biological-medicinal-products-containing-recombinant-granulocyte-colony_en.pdf

85. European Medicines Agency: Concept paper on the revision of the guideline on non-clinical and clinical development of similar biological medicinal products containing recombinant granulocyte-colony stimulating factor, 2015. https://www.ema.europa.eu/en/documents/scientific-guideline/concept-paper-revision-guideline-non-clinical-clinical-development-similar-biological-medicinal_en.pdf

86. European Medicines Agency: Annex to guideline on similar biological medicinal products containing biotechnology-derived proteins as active substance: Non-clinical and clinical issues: Guidance on similar medicinal products containing recombinant granulocyte-colony stimulating factor, 2006. https://www.ema.europa.eu/documents/scientific-guideline/annex-guideline-similar-biological-medicinal-products-containing-biotechnology-derived-proteins_en.pdf

87. Markus R, Liu J, Ramchandani M, et al: Developing the totality of evidence for biosimilars: Regulatory considerations and building confidence for the healthcare community. BioDrugs 31:175-187, 2017

88. Zhu P, Ji P, Wang Y: Using clinical PK/PD studies to support no clinically meaningful differences between a proposed biosimilar and the reference product. AAPS J 20:89, 2018

89. Im YH, Odarchenko P, Grecea D, et al: Double-blind, randomized, parallel group, phase III study to demonstrate equivalent efficacy and comparable safety of CT-P6 and trastuzumab, both in combination with paclitaxel, in patients with metastatic breast cancer (MBC) as first-line treatment. J Clin Oncol 31, 2013 (suppl; abstr 629)

■ ■ ■

AUTHORS' DISCLOSURES OF POTENTIAL CONFLICTS OF INTEREST

Understanding the Role of Comparative Clinical Studies in the Development of Oncology Biosimilars

The following represents disclosure information provided by authors of this manuscript. All relationships are considered compensated unless otherwise noted. Relationships are self-held unless noted. I = Immediate Family Member, Inst = My Institution. Relationships may not relate to the subject matter of this manuscript. For more information about ASCO's conflict of interest policy, please refer to www.asco.org/rwc or ascopubs.org/journal/jco/site/ifc.

Open Payments is a public database containing information reported by companies about payments made to US-licensed physicians (Open Payments).

Justin Stebbing
Leadership: BB Healthcare Trust, Xerion Healthcare, Springer Nature
Consulting or Advisory Role: Celltrion, TLC Biopharmaceuticals, Vor Biopharma, Lansdowne, Vitruvian, Singapore Biotech, Benevolent AI, Vaccitech

Paul N. Mainwaring
Employment: Xing Technologies
Leadership: Xing Technologies
Stock and Other Ownership Interests: Xing Technologies
Honoraria: Ipsen, Roche, Genentech, Pfizer, Janssen Oncology, Medivation, Astellas Pharma, Merck, Novartis
Consulting or Advisory Role: Pfizer, Janssen Oncology
Speakers' Bureau: Ipsen, Roche, Genentech, Pfizer, Janssen Oncology, Medivation, Astellas Pharma, Merck, Novartis, AstraZeneca
Research Funding: Merck KGaA
Patents, Royalties, Other Intellectual Property: Four patents on nanotechnology
Travel, Accommodations, Expenses: Ipsen, Roche, Genentech, Pfizer, Janssen Oncology, Medivation, Astellas Pharma, Merck, Novartis, Xing Technologies

Giuseppe Curigliano
Honoraria: Ellipses Pharma
Consulting or Advisory Role: Roche, Genentech, Pfizer, Novartis, Eli Lilly, Foundation Medicine, Bristol-Myers Squibb, Samsung
Speakers' Bureau: Roche, Genentech, Novartis, Pfizer, Eli Lilly, Foundation Medicine, Samsung Bioepis
Travel, Accommodations, Expenses: Roche, Genentech, Pfizer

Mark Pegram
Honoraria: Genentech, Roche
Consulting or Advisory Role: Genentech, Roche

Mark Latymer
Employment: Pfizer
Leadership: Pfizer
Stock and Other Ownership Interests: Pfizer
Travel, Accommodations, Expenses: Pfizer

Angel H. Bair
Employment: Pfizer
Stock and Other Ownership Interests: Pfizer

Hope S. Rugo
Research Funding: Macrogenics (Inst), OBI Pharma (Inst), Eisai (Inst), Pfizer (Inst), Novartis (Inst), Eli Lilly (Inst), Genentech (Inst), Merck (Inst), Immunomedics (Inst), Odonate Therapeutics (Inst), Daiichi Sankyo (Inst), Seattle Genetics (Inst)
Travel, Accommodations, Expenses: Pfizer, Puma Biotechnology, Mylan, Amgen, AstraZeneca, Macrogenics, Daiichi Sankyo, Merck, Novartis, OBI Pharma

No other potential conflicts of interest were reported.

Baricitinib as potential treatment for 2019-nCoV acute respiratory disease

Given the scale and rapid spread of the 2019 novel coronavirus (2019-nCoV) acute respiratory disease, there is an immediate need for medicines that can help before a vaccine can be produced. Results of rapid sequencing of 2019-nCoV, coupled with molecular modelling based on the genomes of related virus proteins,[1] have suggested a few compounds that are likely to be effective, including the anti-HIV lopinavir plus ritonavir combination.

BenevolentAI's knowledge graph is a large repository of structured medical information, including numerous connections extracted from scientific literature by machine learning.[2] Together with customisations bespoke to 2019-nCoV, we used BenevolentAI to search for approved drugs that could help, focusing on those that might block the viral infection process. We identified baricitinib, which is predicted to reduce the ability of the virus to infect lung cells.

Most viruses enter cells through receptor-mediated endocytosis. The receptor that 2019-nCoV uses to infect lung cells might be ACE2, a cell-surface protein on cells in the kidney, blood vessels, heart, and, importantly, lung AT2 alveolar epithelial cells (figure). These AT2 cells are particularly prone to viral infection.[3] One of the known regulators of endocytosis is the AP2-associated protein kinase 1 (AAK1). Disruption of AAK1 might, in turn, interrupt the passage of the virus into cells and also the intracellular assembly of virus particles.[4]

Of 378 AAK1 inhibitors in the knowledge graph, 47 have been approved for medical use and six inhibited AAK1 with high affinity. These included a number of oncology drugs such as sunitinib and erlotinib, both of which have been shown to inhibit viral infection of cells through the inhibition of AAK1.[5] However, these compounds bring serious side-effects, and our data infer high doses to inhibit AAK1 effectively. We do not consider these drugs would be a safe therapy for a population of sick and infected people.

By contrast, one of the six high-affinity AAK1-binding drugs was the janus kinase inhibitor baricitinib, which also binds the cyclin G-associated kinase, another regulator of endocytosis. Because the plasma concentration of baricitinib on therapeutic dosing (either as 2 mg or 4 mg once daily) is sufficient to inhibit AAK1, we suggest it could be trialled, using an appropriate patient population with 2019-nCoV acute respiratory disease, to reduce both the viral entry and the inflammation in patients, using endpoints such as the MuLBSTA score, an early warning model for predicting mortality in viral pneumonia.[7]

*Peter Richardson, Ivan Griffin, Catherine Tucker, Dan Smith, Olly Oechsle, Anne Phelan, *Justin Stebbing*
j.stebbing@imperial.ac.uk

BenevolentAI, London, UK (PR, IG, CT, DS, OO, AP); and Department of Surgery and Cancer, Imperial College London, London SW7 2AZ, UK (JS)
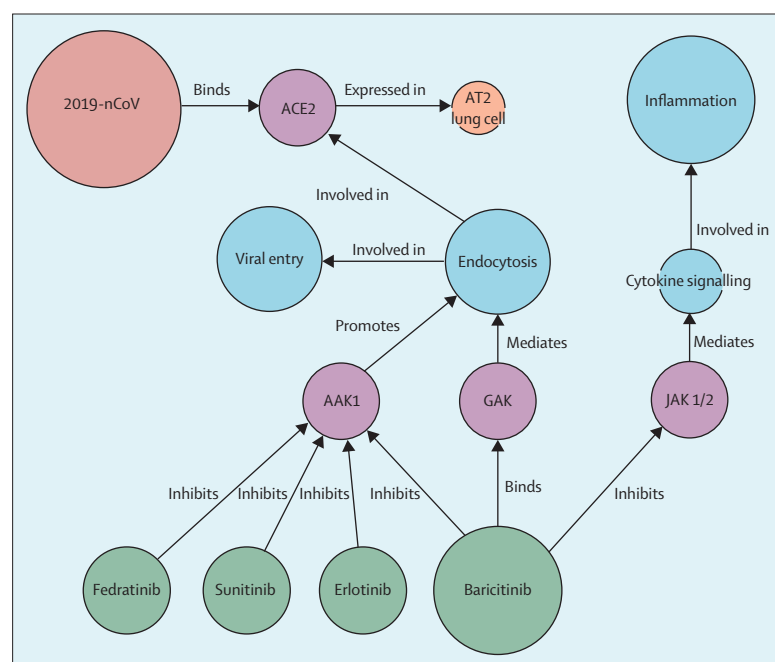
Figure: **The BenevolentAI knowledge graph**
The BenevolentAI knowledge graph integrates biomedical data from structured and unstructured sources. It is queried by a fleet of algorithms to identify new relationships to suggest new ways of tackling disease. 2019-nCoV=2019 novel coronavirus. AAK1=AP-2 associated kinase 1. GAK=cyclin g-associated kinase. JAK1/2=janus kinase 1/2.

1   Gruber CC, Steinkellner G. Wuhan coronavirus 2019-nCoV—what we can find out on a structural bioinformatics level. Jan 23, 2020. https://innophore.com/2019-ncov/ (accessed Feb 3, 2020).

2   Segler MHS, Preuss M, Waller P. Planning chemical syntheses with deep neural networks and symbolic AI. *Nature* 2018; **555**: 604–10.

3   Zhao Y Zhao Z Wang Y et al. Single-cell RNA expression profiling of ACE2, the putative receptor of Wuhan 2019-nCov. *BioRxiv* 2020; published online Jan 26. DOI:https://doi.19985.

4   Lu R, Zhao X, Li J, et al. Genomic characterisation and epidemiology of 2019 novel coronavirus: implications for virus origins and receptor binding. *Lancet* 2020; published online Jan 30. https://doi.org/10.1016/S0140-6736(20)30251-8.

5   Pu SY, Xiao F, Schor S, et al. Feasibility and biological rationale of repurposing sunitinib and erlotinib for dengue treatment. *Antiviral Res* 2018, **155:** 67–75.

6   Sorrell F, Szklarz M, Abdul Areez KR, et al. Family-wide structural analysis of human numb-associated protein kinases. *Structure* 2016; **24:** 401–11.

7   Chen N Zhou M Dong X et al. Epidemiological and clinical characteristics of 99 cases of 2019 novel coronavirus pneumonia in Wuhan, China: a descriptive study. *Lancet* 2020; published online Jan 29. https://doi.org/10.1016/S0140-6736(20)30211-7.

COVID-19: combining antiviral and anti-inflammatory treatments

Both coronavirus disease 2019 (COVID-19) and severe acute respiratory syndrome (SARS) are characterised by an overexuberant inflammatory response and, for SARS, viral load is not correlated with the worsening of symptoms.[1,2] In our previous Correspondence to *The Lancet*,[3] we described how BenevolentAI's proprietary artificial intelligence (AI)-derived knowledge graph,[4] queried by a suite of algorithms, enabled identification of a target and a potential therapeutic against SARS coronavirus 2 (SARS-CoV-2; the causative organism in COVID-19). We identified a group of approved drugs that could inhibit clathrin-mediated endocytosis and thereby inhibit viral infection of cells (appendix). The drug targets are members of the numb-associated kinase (NAK) family—including AAK1 and GAK—the inhibition of which has been shown to reduce viral infection in vitro.[5,6] Baricitinib was identified as a NAK inhibitor, with a particularly high affinity for AAK1, a pivotal regulator of clathrin-mediated endocytosis. We suggested that this drug could be of use in countering SARS-CoV-2 infections, subject to appropriate clinical testing.

To take this work further in a short timescale, a necessity when dealing with a new human pathogen, we re-examined the affinity and selectivity of all the approved drugs in our knowledge graph to identify those with both antiviral and anti-inflammatory properties. Such drugs are predicted to be of particular importance in the treatment of severe cases of COVID-19, when the host inflammatory response becomes a major cause of lung damage and subsequent mortality. Comparison of the properties of the three best candidates are shown in the table. Baricitinib, fedratinib, and ruxolitinib are potent and selective JAK inhibitors approved for indications such as rheumatoid arthritis and myelofibrosis. All three are powerful anti-inflammatories that, as JAK–STAT signalling inhibitors, are likely to be effective against the consequences of the elevated levels of cytokines (including interferon-γ) typically observed in people with COVID-19.[2] Although the three candidates have similar JAK inhibitor potencies, a high affinity for AAK1 suggests baricitinib is the best of the group, especially given its once-daily oral dosing and acceptable

side-effect profile.[7] The most significant side-effect seen over 4214 patient-years in the clinical trial programmes used for European Medicines Agency registration was a small increase in upper respiratory tract infections (similar to that observed with methotrexate), but the incidence of serious infections (eg, herpes zoster) over

See **Online** for appenidx

	Baricitinib	Ruxolitinib	Fedratinib
Daily dose, mg	2–10	25	400
Affinity and efficacy: K_d or IC_{50}, nM*			
AAK1†			
Cell free	17	100	32
Cell	34	700	960
GAK†			
Cell free	136	120	1
Cell	272	840	30
BIKE†			
Cell free	40	210	32
Cell	80	1470	960
JAK1			
Cell free	6	3	20
Cell	12	20	600
JAK2			
Cell free	6	3	3
Cell	11	21	100
JAK3			
Cell free	>400	2	79
Cell	>800	14	2370
TYK2			
Cell free	53	1	20
Cell	106	7	600
Pharmacokinetics			
Plasma protein binding	50%	97%	95%
C_{max} (unbound), nM	103‡	117	170
Safety: tolerated dose	≤10 mg/day	≤20 mg twice daily	≤400 mg/day

See regulatory approval documents for further information on these drugs. K_d=dissociation constant. IC_{50}=half-maximal inhibitory concentration. C_{max}=maximum serum concentration. *All values are IC_{50} except the cell free values for AAK1, GAK, and BIKE; "cell free" values indicate inhibitory activity against purified protein in biochemical assay; "cell" values indicate enzyme-inhibitory activity inside a cell. †In the absence of direct measurements of drug inhibition in cells, the predicted cell affinity and efficacy values are derived from the ratio of each compound for their primary target; for example, for baricitinib, IC_{50} AAK1[cell] = (IC_{50}AK1[cell] / IC_{50}AK1[cell free]) × IC_{50}AAK1[cell free]. ‡At a 10 mg dose.

Table: Properties of three antiviral and anti-inflammatory candidate drugs

52 weeks' dosing was small (3·2 per 100 patient-years), and similar to placebo.[7] Use of this agent in patients with COVID-19 over 7–14 days, for example, suggests side-effects would be trivial.

Other AI-algorithm-predicted NAK inhibitors include a combination of the oncology drugs sunitinib and erlotinib, shown to reduce the infectivity of a wide range of viruses, including hepatitis C virus, dengue virus, Ebola virus, and respiratory syncytial virus.[5,6] However, sunitinib and erlotinib would be difficult for patients to tolerate at the doses required to inhibit AAK1 and GAK. By contrast, at therapeutic doses used for the treatment of patients with rheumatoid arthritis, the free plasma concentrations of baricitinib are predicted to be sufficient to inhibit AAK1, and potentially GAK, in cell-based assays.

The predicted inhibition of clathrin-mediated endocytosis by baricitinib is unlikely to be observed with other anti-arthritic drugs or JAK inhibitors. Our analysis of the closely related JAK inhibitors ruxolitinib and fedratinib (table) illustrates that the predicted unbound plasma exposure required to inhibit the enzymes needed for clathrin-mediated endocytosis greatly exceeds the currently tolerated exposures used therapeutically. These drugs are, therefore, unlikely to reduce viral infectivity at tolerated doses, although they might reduce the host inflammatory response through JAK inhibition. Intriguingly, another JAK inhibitor, tofacitinib, shows no detectable inhibition of AAK1. The high affinity of baricitinib for NAKs, its anti-inflammatory properties, and its ability to ameliorate associated chronic inflammation in interferonopathies,[8] together with its advantageous pharmacokinetic properties, appear to make it a special case among the approved drugs.

In addition, the potential for combination therapy with baracitinib is high because of its low plasma protein binding and minimal interaction with CYP enzymes and drug transporters. Furthermore, there is the potential for combining baricitinib with the direct-acting antivirals (lopinavir or ritonavir and remdesivir) currently being used in the COVID-19 outbreak, since it has a minimal interaction with the relevant CYP drug-metabolising enzymes. Combinations of baricitinib with these direct-acting antivirals could reduce viral infectivity, viral replication, and the aberrant host inflammatory response. This work demonstrates that the use of an AI-driven knowledge graph can facilitate rapid drug development.

**Justin Stebbing, Anne Phelan, Ivan Griffin,
Catherine Tucker, Olly Oechsle, Dan Smith, Peter Richardson*
j.stebbing@imperial.ac.uk

Department of Surgery and Cancer, Imperial College London, London W12 0NN, UK (JS); and Benevolent AI, London, UK (AP, IG, CT, OO, DS, PR)

1   Peiris JSM, Chu CM, Cheng VCC, et al. Clinical progression and viral load in a community outbreak or coronavirus-associated SARS pneumonia: a prospective study. *Lancet* 2003; **361:** 1767–72.

2   Huang C, Wang Y, Li X, et al. Clinical features of patients infected with 2019 novel coronavirus in Wuhan, China. *Lancet* 2020; **395:** 497–506. https://doi.org/10.1016/S0140–6736(20)30183–5.

3   Richardson P, Griffin I, Tucker C, et al. Baricitinib as potential treatment for 2019-nCoV acute respiratory disease. *Lancet* 2020; **395:** 497–506.

4   Segler MHS, Preuss M, Waller P. Planning chemical syntheses with deep neural networks and symbolic AI. *Nature* 2018; **555:** 604–10.

5   Bekerman E, Neveu G, Shulla A, et al. Anticancer kinase inhibitors impair intracellular viral trafficking and exert broad-spectrum antiviral effects. *J Clin Invest* 2017; **127:** 1338–52.

6   Pu S-Y, Xiao F, Schor S, et al. Feasibility and biological rationale of repurposing sunitinib and erlotinib for dengue treatment. *Antiviral Res* 2018; **155:** 67–75.

7   European Medicines Agency. Olumiant: summary of product characteristics. https://www.ema.europa.eu/en/documents/product-information/olumiant-epar-product-information_en.pdf (accessed Feb 24, 2020).

8   Sanchez GAM, Reinhardt A, Ramsey S et al., JAK1/2 inhibition with baricitinib in the treatment of autoinflammatory interferonopathies. *J Clin Invest* 2018; **128:** 3041–52.

# THE LANCET Infectious Diseases

Supplementary webappendix

This webappendix formed part of the original submission and has been peer reviewed. We post it as supplied by the authors.

Figure: **Viral entry via clathrin-mediated endocytosis**

The virus binds through its spike protein to ACE2 on the surface of AT2 epithelial cells (1), which induces activation of clathrin-mediated endocytosis. AAK1- and GAK-mediated phosphorylation of clathrin adapter proteins (2) starts the assembly of the clathrin cage around the enclosed virus, before it is pinched off and trafficked to endosomes (3). Inhibition of AAK1 and GAK by baricitinib thereby inhibits virus entry. SARS-CoV-2=severe acute respiratory syndrome coronavirus 2.
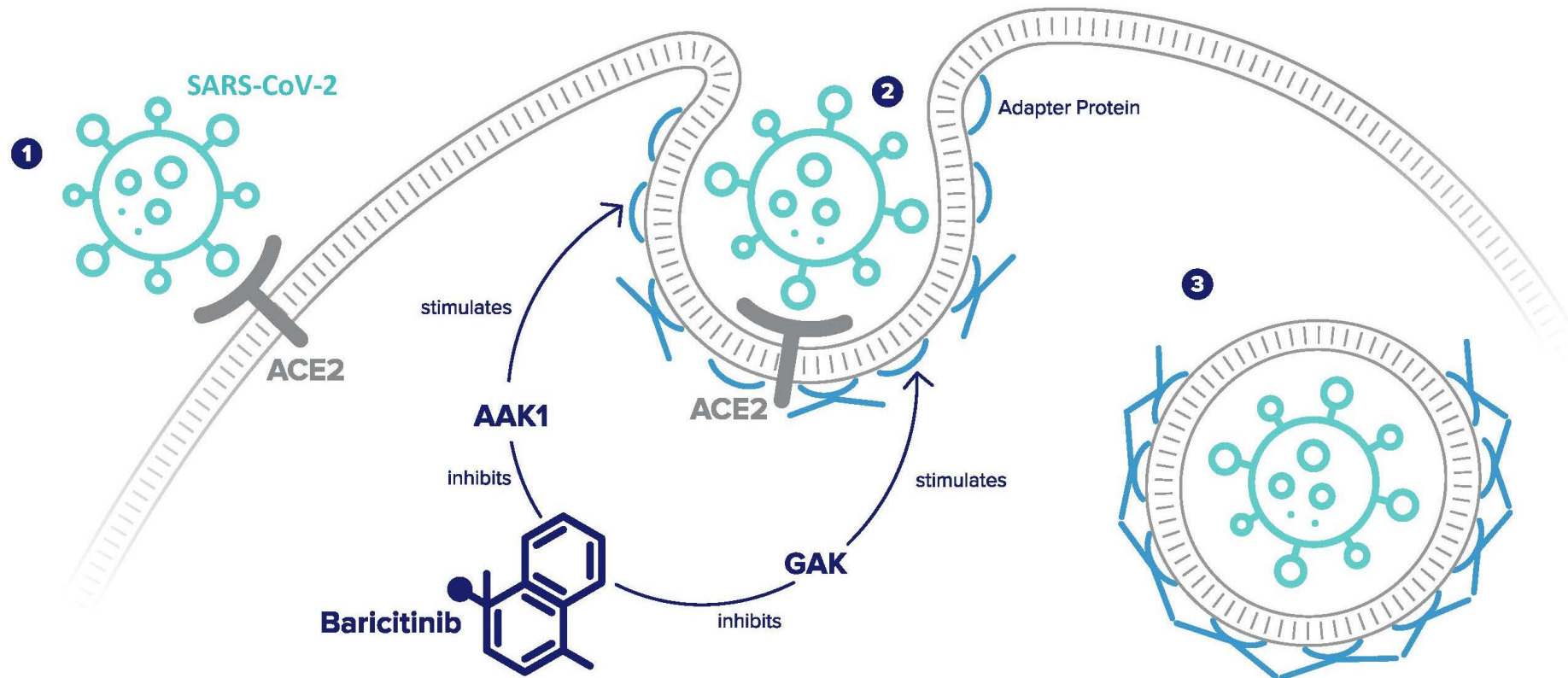
Cell-derived extracellular vesicles can be used as a biomarker reservoir for glioblastoma tumor subtyping

Rosemary Lane[1,6], Thomas Simon [1,6], Marian Vintu[1,6], Benjamin Solkin[1], Barbara Koch[1], Nicolas Stewart [2], Graeme Benstead-Hume [3], Frances M.G. Pearl [3], Giles Critchley[4], Justin Stebbing[5] & Georgios Giamas[1]

Glioblastoma (GBM) is one of the most aggressive solid tumors for which treatment options and biomarkers are limited. Small extracellular vesicles (sEVs) produced by both GBM and stromal cells are central in the inter-cellular communication that is taking place in the tumor bulk. As tumor sEVs are accessible in biofluids, recent reports have suggested that sEVs contain valuable biomarkers for GBM patient diagnosis and follow-up. The aim of the current study was to describe the protein content of sEVs produced by different GBM cell lines and patient-derived stem cells. Our results reveal that the content of the sEVs mirrors the phenotypic signature of the respective GBM cells, leading to the description of potential informative sEV-associated biomarkers for GBM subtyping, such as CD44. Overall, these data could assist future GBM in vitro studies and provide insights for the development of new diagnostic and therapeutic methods as well as personalized treatment strategies.

[1] Department of Biochemistry and Biomedicine, School of Life Sciences, University of Sussex, Brighton BN1 9QG, UK. [2] Pharmacy and Biomolecular Sciences, University of Brighton, Brighton BN2 4GJ, UK. [3] Bioinformatics Group, School of Life Sciences, University of Sussex, Falmer, Brighton BN1 9QG, UK. [4] Department of Neurosurgery, Hurstwood Park Neurosciences Centre, Brighton and Sussex University Hospitals, Brighton, UK. [5] Department of Surgery and Cancer, Division of Cancer, Imperial College London, Hammersmith Hospital Campus, Du Cane Road, London W12 ONN, UK. [6]These authors contributed equally: Rosemary Lane, Thomas Simon, Marian Vintu. Correspondence and requests for materials should be addressed to T.S. (email: t.simon@sussex.ac.uk) or to G.G. (email: g.giamas@sussex.ac.uk)

G lioblastoma multiforme (GBM) is amongst the most aggressive types of brain tumors for which current treatments are of limited benefit[1]. Verhaak et al. has previously described different clinical genetic GBM subtypes (proneural, neural, mesenchymal, and classical) based on the gene expression of different markers, such as platelet-derived growth factor-receptor alpha (PDGF-Rα), neurofilament light (NEFL), CD44, and epidermal growth factor-receptor (EGF-R), respectively[2]. This sub-classification might have diagnostic and prognostic applications as, for example, the mesenchymal subtype is acknowledged as the most aggressive one[3,4]. Nevertheless, all these subtypes can co-exist within the same tumor, making patients' sub-classification challenging[5]. In addition, according to recent reports, the neural subtype may simply represent normal brain contamination[6].

During GBM growth, the close crosstalk between the different components of the integrated GBM microenvironment, including the hyaluronic acid (HA)-rich extracellular matrix and stromal cells, such as endothelial cells or astrocytes, can support tumor invasiveness and resistance to therapy[7]. In addition, an important role in tumor recurrence and resistance to treatment is attributed to GBM stem cells present in the tumor bulk as they are less affected by radio-therapy and chemo-therapy[8–10]. Such resistance is further supported by GBM stem cells capabilities to generate different GBM cell sub-populations of various molecular signatures[11,12]. Intra-tumoral heterogeneity is therefore a central feature of GBM tumors, although it has not been fully described to date[13,14]. Nevertheless, a better understanding of GBM heterogeneous sub-populations/molecular signatures would be of great help for future in-depth studies and, eventually, novel therapeutic strategies.

Extracellular vesicles (EVs) represent one of the plausible ways through which tumor cells, including cancer stem cells, self-regulate and communicate with their stromal counterparts and hence maintain such high intra-tumoral heterogeneity[15]. EVs are membrane-enclosed vesicles that can carry proteins, lipids, metabolites, and nucleic acids from one cell to another, for short or long distances[16,17]. In GBM, EVs have been described to be involved in tumor invasion, neo-angiogenesis, modulation of the immune response and resistance to treatments such as temozolomide[18–20]. Recent reports have focused on the role of small EVs (sEVs, <200 nm diameter) in cancer progression, as opposed to medium/large EVs (m/lEVs, >200 nm)[15,21]. We have recently reported that shedding of bevacizumab, an antibody neutralizing VEGF-A, at the surface of GBM cell-derived sEVs might be involved in the tumor resistance to anti-angiogenic therapies[22]. Furthermore, recent reports suggested that GBM cells of distinct subtypes/molecular signatures accordingly produce EVs with different contents[3,23,24]. Indeed, Spinelli et al. showed that proneural and mesenchymal GBM stem cells produce different EVs in terms of proteomic content and pro-angiogenic effects[23]. By describing the proteomic cargo of GBM cell line-derived EVs, Mallawaaratchy et al. identified EV biomarkers that are potentially associated with higher GBM invasiveness, such as Annexin A1 and Integrin ß1. Interestingly, through a gene expression analysis of GBM specimens, authors reported that Annexin A1 expression is higher in the mesenchymal and classical subtypes, suggesting a survival/subtype prediction potential for EV-associated Annexin A1[3]. Similarly, blood-derived and cerebrospinal fluid (CSF)-derived EV cargos have been recently proposed as good biomarker candidates for diagnosing GBM and describing specific subtypes/molecular signatures, and also for assessing tumor resistance to existing therapies[18,25,26]. Indeed, the presence of EVs in biofluids along with their capability to cross the blood brain barrier, makes them very valuable carriers of potential GBM biomarkers, while current methods for the

purposes of diagnosis/prognosis are still painful and invasive[15,27,28]. Recently, Osti et al. reported higher levels of EVs in GBM patients compared to healthy controls, suggesting a new potential method to help GBM diagnosis[24]. Nevertheless, there is still a great need for identifying precise EV-associated biomarkers that could help determine specific GBM tumor subtype/molecular signatures in patients. In addition, as the EV field is constantly evolving and relies a lot on fast growing and highly EV-producing tumor cell lines, an extended description of available models for EV-related GBM research would be of great value.

For all these reasons, our aim was to describe the proteomic content of sEVs derived from GBM cells with various molecular signatures. We first grouped GBM cell lines and patient-derived stem cells according to the expression of specific key markers and their in vitro invasiveness potential. Interestingly, we were able to associate some of the cell sub-groups that we identified to GBM subtypes/molecular signatures that have already been described[2]. Ultimately, we observed that description of the proteomic content of the GBM cell-derived sEVs mirrored our original cell grouping. Consequently, this extensive study led to the identification of new potential sEV-associated protein biomarkers that can be used as indicators of GBM aggressiveness and assist in GBM subtype classification.

Results

In vitro invasion capabilities of astrocytes and GBM cells. Invasion assays in 3D HA-hydrogels were undertaken to determine the colony forming abilities of astrocytes and GBM cells (Fig. 1a and Supplementary Data 1). LN18, LN229, and U87 cells formed the highest number of colonies with an average of 52, 48, and 64 colonies per well, respectively ($p = 0.0003$, $p = 0.0008$, and $p = 0.0001$ compared to astrocytes, respectively), while U118, U138, and GS090 cells had 31, 32, 19, and 31 colonies, respectively ($p = 0.0407$, $p = 0.0283$, and $p = 0.0417$ compared to astrocytes, respectively). T98, G166 cells, and astrocytes' number of colonies were significantly lower (13 and 2 per well, respectively, *$p < 0.05$, **$p < 0.01$, ***$p < 0.001$, ****$p < 0.0001$, ordinary one-way ANOVA) (Fig. 1a and Supplementary Data 1). To further describe the GBM cells' behavior when growing in the HA hydrogels, we then performed a cell viability assay (Fig. 1b and Supplementary Data 1). The relative viability, expressed here in Relative Light Units (RLU), was 4.2, 3.5, 4.95, 2.4, and 4.2 fold higher in LN18, LN229, U87, U138, and GS090 cells, respectively, when compared to astrocytes ($p = 0.0033$, $p = 0.0251$, $p = 0.0004$, $p = 0.0323$, and $p = 0.0034$ compared to astrocytes, respectively). The viability of T98, U118, and G166 cells was not significantly different to the astrocytes' (*$p < 0.05$, **$p < 0.01$, ***$p < 0.001$, ****$p < 0.0001$, ordinary one-way ANOVA) (Fig. 1b and Supplementary Data 1).

Further assays were implemented to complete our understanding of the migration, proliferation, and invasion capabilities of the studied cells. As presented in Fig. 1c, U87 cells were able to invade through a basement membrane matrix-coated insert more than any of the other cell lines. Indeed, when compared to the control (no FCS), U87 cells migrated 66% more into the matrix in the presence of FCS in the lower chamber (Fig. 1c and Supplementary Data 1). In addition, as shown in Supplementary Fig. 1A, AS, U118 and U138 showed the highest migration potential with 77%, 76%, and 72% wound healing, while LN229 and U87 cells had a 43% and 53% closure, respectively (Supplementary Data 2). LN18 and T98 cells' wound healing abilities were significantly lower than the one observed in AS (40%, $p = 0.0441$ and 7%, $p = 0.0003$ respectively, *$p < 0.05$, **$p < 0.01$, ***$p < 0.001$, ****$p < 0.0001$, ordinary one-way ANOVA). Furthermore, U87 cells presented the shortest population
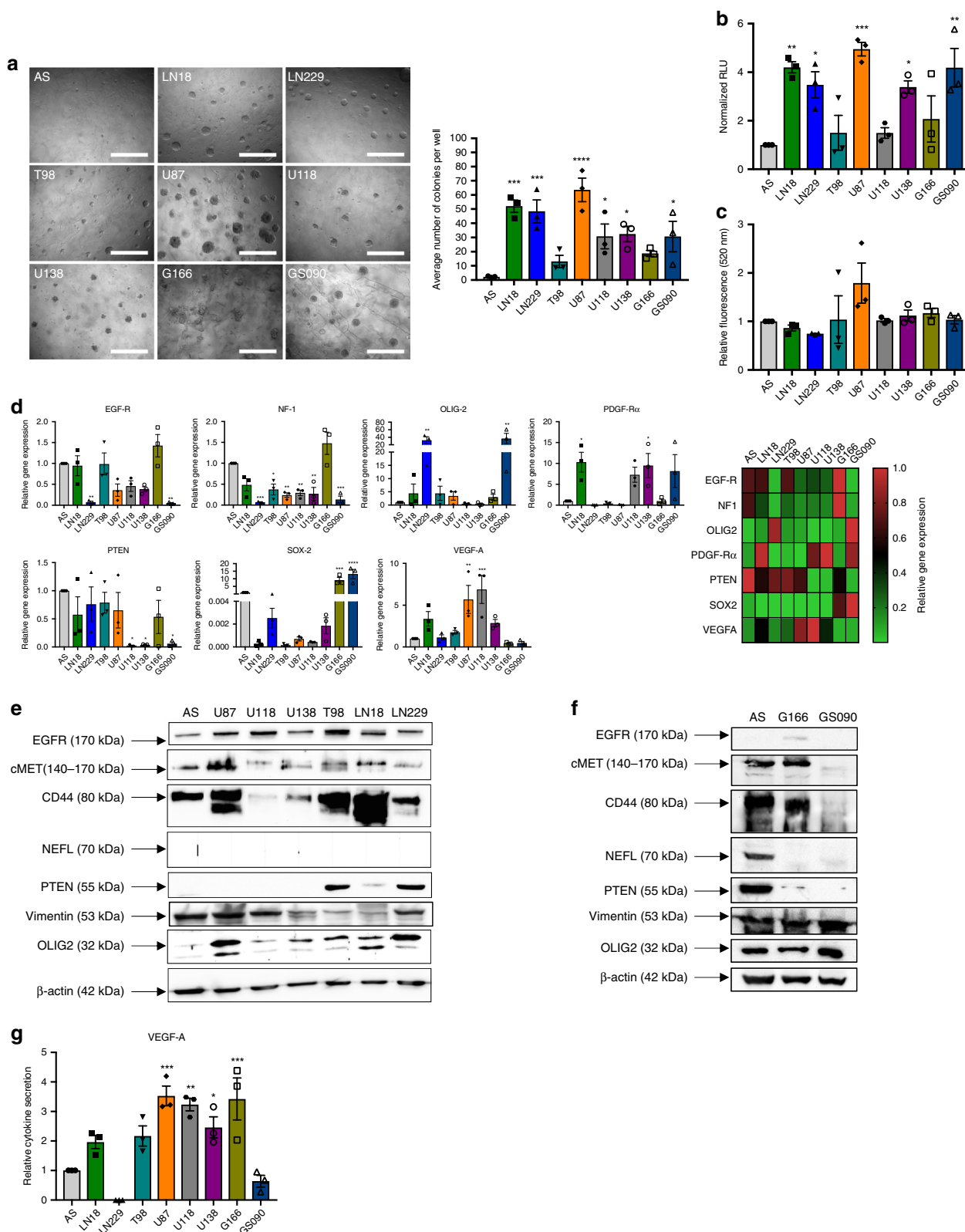
doubling time (25.5 h, $p = 0.0019$ compared to AS), followed by LN229, LN18, and T98 (26.6 h, $p = 0.0023$, 28.2 h, $p = 0.0029$ and 30.1 h, $p = 0.0039$ respectively, $*p < 0.05$, $**p < 0.01$, $***p < 0.001$, $****p < 0.0001$, ordinary one-way ANOVA) (Supplementary Fig. 1B and Supplementary Data 2).

Taken together, our results confirm that AS are quite motile in 2D albeit their low invasiveness potential in 3D. T98 cells had

equally limited migration and invasion capabilities. Despite their restricted in vitro motility, showing both low wound healing and basement membrane invasion, LN18 and LN229 GBM cells were significantly more invasive in HA hydrogels compared to AS (second and third most invasive, respectively) and had short population doubling times. U87, U118, and U138 cells presented higher migration abilities compared to the other GBM cells and

Fig. 1 Astrocytes (AS), GBM cell lines, and GBM patient-derived stem cells present different in vitro invasion capabilities and specific subtype marker expression. **a** AS and GBM cells invasiveness and colony formation abilities using a hyaluronic acid (HA)-based hydrogel assay. Cells were incubated within a HA hydrogel for 7 days. Colony counting was then performed. Scale bar = 400 μm. **b** AS and GBM cell viability in a HA hydrogel-based assay using the CellTiter-Glo® Luminescent Cell Viability Assay. **c** Invasion abilities of AS and GBM cells through an extracellular matrix-coated membrane. Cells were seeded in the top chamber and were allowed to invade the matrix for 24 h in presence or absence of FCS in the bottom chamber. Cells that have passed through the matrix were then detached, lysed, and labeled with CyQuant GR Dye. Fluorescence was then read (480/520 nm filter set). Data obtained in presence of FCS was normalized to data obtained without FCS. Representative images are shown. **d** qRT-PCR analysis of GBM subtype and aggressiveness marker expression in astrocytes, six different GBM cell lines and two different GBM patient-derived stem cells. GAPDH was used as an internal control. Data are shown as normalized to AS data. Heat-map representative of the qRT-PCR data where the data is normalized to the highest level of gene expression. **e** Western blotting analysis of GBM subtype and aggressiveness marker expression in AS and six different GBM cell lines. β-actin was used as an internal control. **f** Western blotting analysis of GBM subtype and aggressiveness marker expression in astrocytes and two different GBM patient-derived stem cells. β-actin was used as an internal control. **g** ELISA analysis of VEGF-A secretion by AS, six different GBM cell lines and two different GBM patient-derived stem cells. Representative images are shown. The mean ± SEM of $n = 3$ independent experiments is shown. *$p < 0.05$, **$p < 0.01$, ***$p < 0.001$, ****$p < 0.0001$ (ordinary one-way ANOVA)

significantly higher invasiveness in HA hydrogels vs. the AS. Among these, only U87 cells displayed the highest basement membrane matrix invasion along with the shortest population doubling time. Amongst the stem cells, only GS090 showed a significantly higher invasive potential, in the HA hydrogels, vs. the AS. Overall, from all the GBM cells that we analyzed, U87 cells had the highest invasion capabilities.

Expression of signature markers in GBM cells and astrocytes. Using the Verhaak et al. classification, we then assessed in our cell line panel the expression of different markers related to the (i) 'classical' (EGF-R), (ii) 'mesenchymal' (Neurofibromatosis type 1 (NF1), CD44), (iii) 'proneural' (PDGF-Rα, Oligodendrocyte transcription factor 2 (OLIG2), SOX2), or (iv) 'neuronal' (NEFL) signatures[2]. In addition, the expression levels of PTEN, vimentin, and vascular endothelial growth factor-a (VEGFA) have been determined with the aim of obtaining further information regarding the tumor cells' aggressiveness.

Gene expression analysis showed significantly lower levels of EGF-R in LN229 and GS090 cells compared to AS (95% lower, $p = 0.005$ and $p = 0.0041$ respectively), while NF1 levels were significantly <50% in all GBM cells when compared to AS, except from G166 cells (+47% compared to AS). OLIG-2 appeared to be expressed ~30× more in LN229 ($p = 0.0072$) and GS090 ($p = 0.0023$) cells than in AS while its levels were low in the other GBM cells. PDGF-Rα expression was observed at its highest in LN18 ($p = 0.0182$) and U138 ($p = 0.0337$) cells (10×-fold and 9×-fold higher compared to AS, respectively). PTEN was present at similar extents in most of the cells, including the AS, except from the U118 ($p = 0.0292$), U138 ($p = 0.0323$), and GS090 ($p = 0.0368$) cells where it was hardly detectable. Finally, regarding VEGF-A, only U87 and U118 cells showed significantly higher levels (>5×-fold higher, $p = 0.0074$ and $p = 0.0009$, respectively) vs. the AS (*$p < 0.05$, **$p < 0.01$, ***$p < 0.001$, ****$p < 0.0001$, ordinary one-way ANOVA) (Fig. 1d and Supplementary Data 3).

Most of these discrepancies were recapitulated by western blotting (Fig. 1e, f, Supplementary Figs. 2 and 3). PTEN was mainly detected in T98 and LN229 cells, while CD44 was highly expressed in LN18, T98, U87, and G166 cells. Similarly, c-Met was over-expressed in U87, T98, LN18, and G166 cells. Regarding NEFL, its expression could only be observed in AS as well as in U118 and U138 cells (Fig. 1e, f, Supplementary Figs. 2 and 3). Finally, ELISA assays demonstrated that VEGF-A cytokine secretion is significantly higher in U87 ($p = 0.0003$), U118 ($p = 0.0011$), U138 ($p = 0.0359$), and G166 ($p = 0.0005$) cells than in AS (*$p < 0.05$, **$p < 0.01$, ***$p < 0.001$, ****$p < 0.0001$, ordinary one-way ANOVA) (Fig. 1g and Supplementary Data 4).

In summary, our genomic/proteomics analyses revealed distinctive expression of GBM subtype markers within the panel of GBM and stem cells that were tested.

Clustering of GBM cells into different signatures. The invasiveness and gene/protein markers' expression data presented in Fig. 1 were put together and compared through clustering analysis resulting in the identification of seven distinctive signatures using non-negative matrix factorization (Fig. 2a and Supplementary Data 5). Then, based on these expression signatures, GBM and stem cells have been compared and clustered together according to their similarities. As shown in Fig. 2b, U118 and U138 were grouped together in a common sub-cluster while U87, T98, G166, GS090, LN229, and LN18 failed to cluster with any other studied GBM cell line (Supplementary Data 5).

Our analysis revealed that LN18, U87, U118, G166, and GS090 GBM cells express distinct parameter/marker signatures, suggesting that they could represent distinct GBM signatures. Hence, a separate four signature clustering of the parameters shown in Fig. 1 has been generated to further describe the LN18, U87, U118, G166, and GS090 cell lines (Fig. 2c and Supplementary Data 5). Signature 1 was mostly characterized by high VEGF expression, high CD44 protein expression, high cMET protein expression, low PTEN protein expression, and high invasiveness potential (high number of 'colonies in HA hydrogels', 'Viability in HA hydrogels' and 'Basement membrane invasion') (Fig. 2c and Supplementary Data 5). Signature 2 was mostly characterized by high PDGF-R, OLIG2, and SOX2 gene expression, as described in GS090 GBM cells (Fig. 2d and Supplementary Data 5). Inversely, signature 3 showed high vimentin protein expression associated with high CD44 protein expression, high NF1 gene expression and high EGF-R gene expression. As seen in Fig. 2d, signature 3 was mainly observed in G166 GBM cells. Signature 4, which was observed in U118 GBM cells, was defined by high VEGF-A gene expression production as well as high vimentin protein expression (Fig. 2d and Supplementary Data 5). Finally, as shown in Fig. 2d, a strong association of signature 1 with LN18 and U87 GBM cells could be observed. In addition, cosine similarity assay confirmed the high similarity between LN18 and U87 (Supplementary Fig. 4 and Supplementary Data 6).

Analysis of GBM cell-derived sEVs size and concentration. Based on our aforementioned clustering results, we decided to focus on these five distinct GBM cells, namely LN18, U87, U118, G166, and GS090. Description of their respective sEV production and proteomic cargo was undertaken in an attempt to identify GBM signature markers in their EVs.
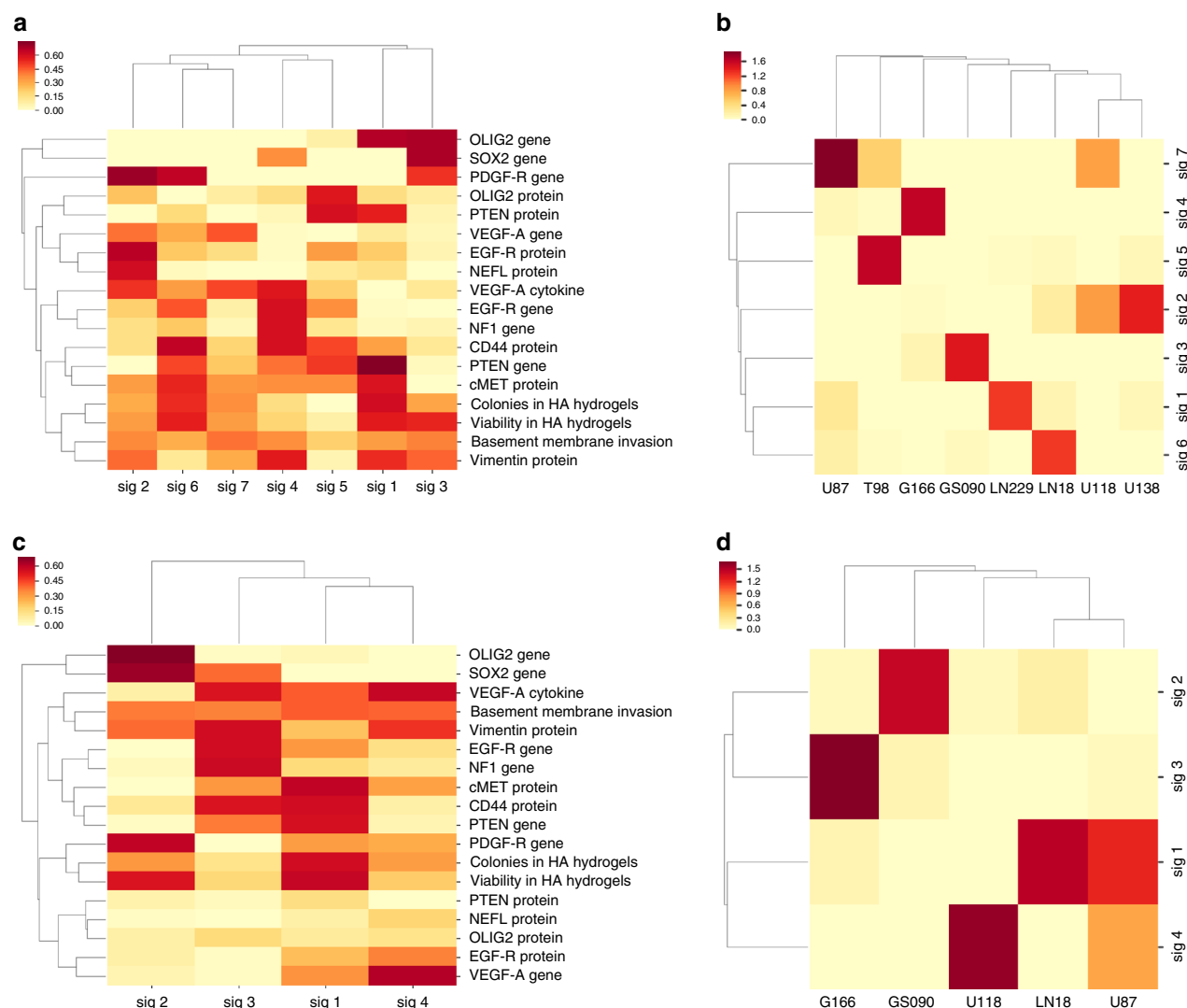
Fig. 2 Different groups of GBM cells can be defined based on invasiveness potential and marker expression data. **a** Clustering heatmap for each parameter shown in Fig. 1, based on the phenotype and marker expression data across all cell lines. Parameters have been clustered in seven different signatures (sig 1–7) in order to reduce the dimensionality of the data. **b** Clustering heatmap for GBM cells based on the signatures defined in **a**. GBM cells have been grouped based on this correlation analysis (U87/T98/G116/GS090/LN229/LN18/U118 & U138). **c** Clustering heatmap for each parameter shown in Fig. 1, based on the phenotype and marker expression data in LN18, U87, U118, G166, and GS090. Parameters have been clustered in four different signatures (sig 1–4) in order to reduce the dimensionality of the data. **d** Clustering heatmap for LN18, U87, U118, G166, and GS090 GBM cells based on the signatures defined in **c**. GBM cells have been grouped based on this correlation analysis (G166/GS090/U118/LN18 & U87)

Size distribution and concentration of sEVs derived from the selected GBM cells were initially determined by NTA. As shown in Fig. 3a, EV concentration (particles /mL/cell) at the size mode was: 60.3 particles/mL/cell for LN18, 59.9 particles /mL/cell for U87, 69 particles /mL/cell for U118, 259.2 particles /mL/cell for G166 and 97.2 particles /mL/cell for GS090. The average EV size modes were: 86.6 nm for LN18, 86.3 nm for U87, 94.6 nm for U118, 80.48 nm for G166 and 81.5 nm for GS090 (Fig. 3b and Supplementary Data 5). Total sEV concentration was 4460 particles /mL/cell for LN18, 3790 particles /mL/cell for U87, 8650 particles /mL/cell for U118, 14,000 particles /mL/cell for G166 and 4520 particles /mL/cell for GS090 GBM cells. As shown in Fig. 3c, concentration of sEVs produced by G166 GBM stem cells was significantly higher than the concentration of sEVs produced by either LN18 ($p = 0.0009$), U87 ($p = 0.0004$) or GS090 ($p = 0.0025$) GBM cells (*$p < 0.05$, **$p < 0.01$, ***$p < 0.001$, ****$p < 0.0001$, ordinary one-way ANOVA) (Fig. 3c and Supplementary Data 7).

Furthermore, coupled to the NTA results, the TEM pictures in Fig. 3d showing vesicles in the well-described size range of 50–150 nm further confirmed the EV isolation from the different GBM cell culture CM[17].

Mass spectrometry (MS) analysis of GBM cell-derived sEVs. Using MS, the proteomic content of the sEVs derived from LN18, U87, U118, G166, and GS090 has been deciphered (Fig. 4 and Supplementary Data 8). Gene enrichment analysis for 'Cellular component' confirmed the 'exosomes' origin of most of the identified proteins (>70% of genes in all GBM cell-derived sEVs) (Fig. 4a). Venn diagrams (Fig. 4b, c) revealed the maximum protein expression overlap between U118 and U87 GBM cell-derived sEV content (46.7%). Proteomic content of sEVs derived from LN18 GBM cells mostly overlapped with the content of U118 (42.2%) and U87 (39.0%) GBM cell-derived sEVs. Proteomic content of sEVs derived from GS090 showed
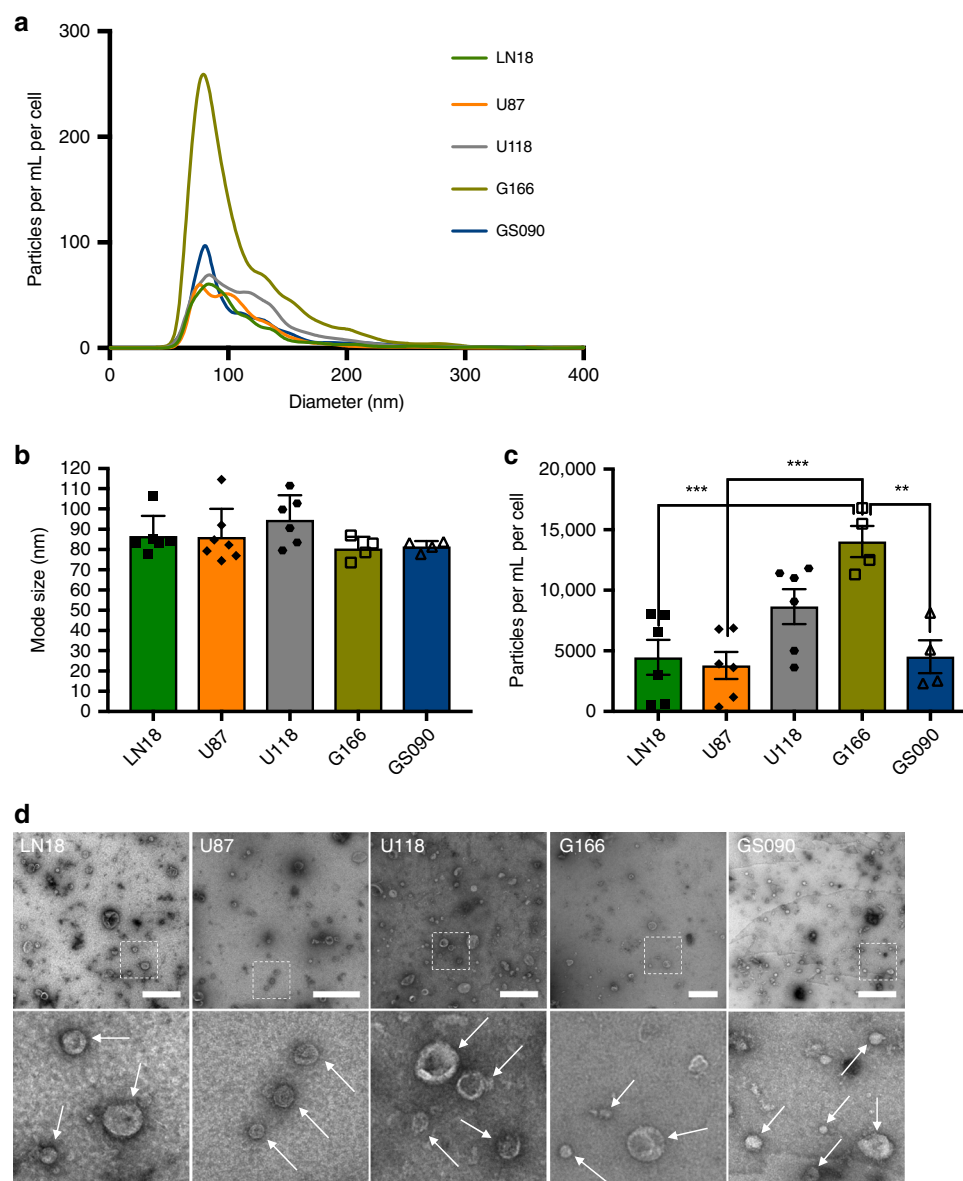
Fig. 3 sEV fractions produced by different GBM cell lines and patient-derived stem cells show variable concentrations and specific patterns of EV markers expression. **a** NTA of GBM cell-derived sEVs. sEV suspension was 1/50 diluted and infused into a Nanosight© NS300 instrument. Five captures of 60 s each were recorded. Particle concentration (particles/mL) and size (nm) were measured. Particles concentration was normalized to the number of cells (particles/mL/cell) at CM harvest. The mean of at least four independent experiments is shown. **b** Mode size (nm) distribution of GBM cell-derived sEVs. sEV mode sizes were determined by NTA. **c** Concentrations (particles/mL/cell) of GBM cell-derived sEVs. sEV concentrations were determined by NTA. **d** TEM detection of GBM cell-derived sEVs (×20k magnification and zoom). White arrows show sEVs. Representative pictures are shown. Scale bar = 500 μm. The mean ± SEM of at least $n = 4$ independent experiments is shown (LN18 $n = 6$, U87 $n = 7$, U118 $n = 6$, G166 $n = 5$, GS090 $n = 4$). *$p < 0.05$, **$p < 0.01$, ***$p < 0.001$, ****$p < 0.0001$ (ordinary one-way ANOVA)

low similarity (<25%) to any other GBM cell-derived sEV proteomic content, with the highest overlap observed with the G166 GBM cell-derived sEV content (23.5%). Altogether, as shown in Fig. 4c, grouping of GBM cell-derived sEV proteomic content distinctly clustered LN18, U87, and U118 together as opposed to G166 and GS090 GBM cells (Fig. 4 and Supplementary Data 8).

Similarly, gene enrichment analysis for 'Biological pathways' and 'Biological processes' showed enrichment of the 'Metabolism' pathway and Metabolism' and 'Energy pathways' processes in the proteomic content of sEVs derived from G166 and GS090 GBM cells, as opposed to the other tumor cell-derived sEVs (Fig. 4d, e). Inversely, our analysis revealed enrichment of pathways such as

'Beta1 integrin cell surface interactions', 'Proteoglycan syndecan-mediated signaling events' or 'VEGF and VEGFR signaling network' in the proteomes of sEVs derived from LN18, U87, and U118 GBM cells. Processes such as 'Signal transduction' and 'Cell communication' were also predominant (>25%) in sEVs derived from those GBM cells (Fig. 4d, e, Supplementary Fig. 5 and Supplementary Data 8).

A further detailed analysis of the proteomes of the studied GBM cell-derived sEVs showed a shared expression of known EV markers or proteins commonly present in EVs, such as Annexin A2 (ANXA2), CD63, fibronectin (FN1), GAPDH, or tubulin (TUBB). Furthermore, other EV markers such as CD82, CD81, CD9, TSG101, or ADAM10 could be detected in sEVs derived
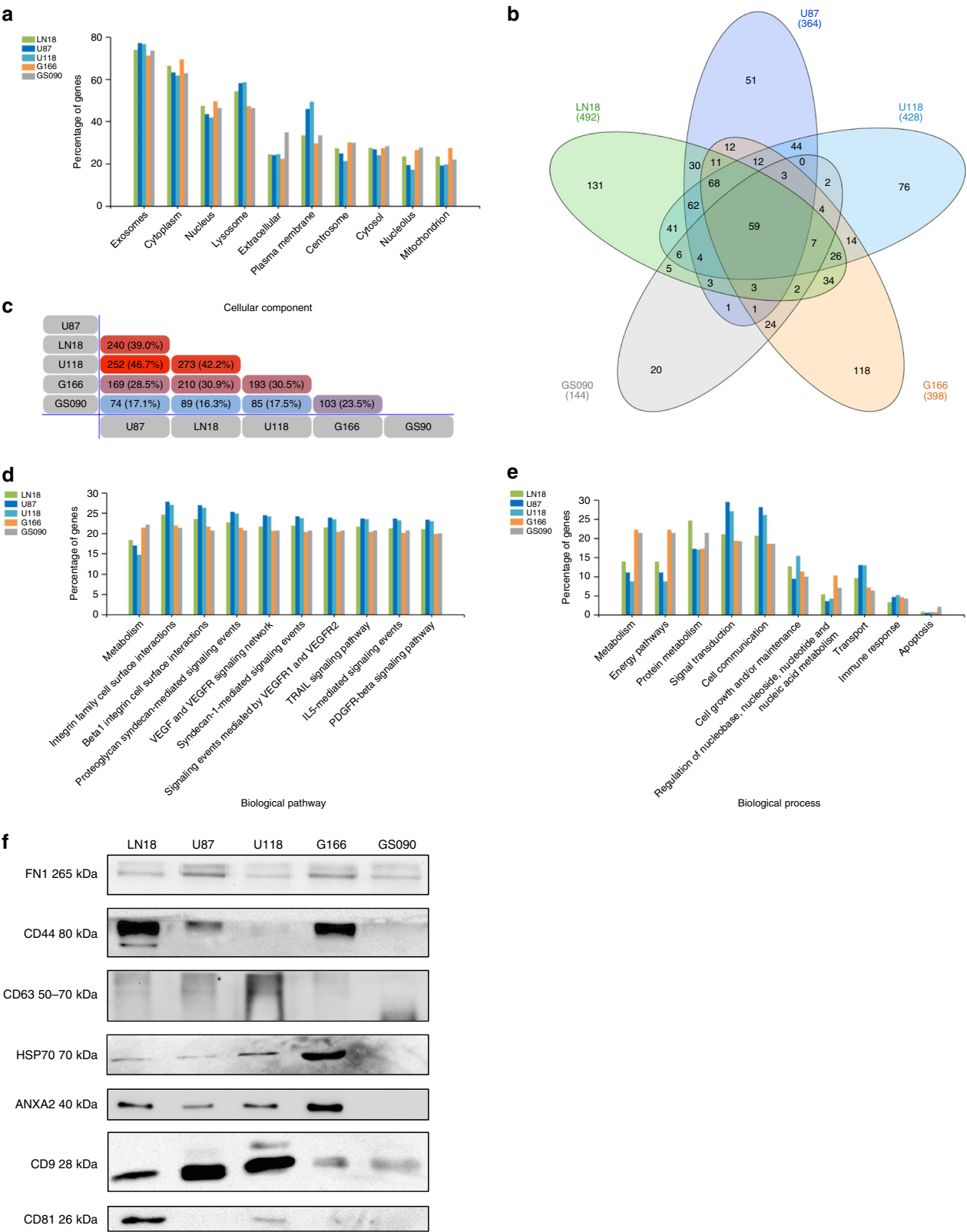
Fig. 4 MS analysis reveals sEV proteomic content that mirrors GBM cell clustering signature and invasiveness in vitro. Protein hits were identified in GBM cell-derived sEVs via MS. Only the protein hits common to at least three biological repeats were considered for each cell line/stem cell (LN18 $n = 3$, U87 $n = 3$, U118 $n = 4$, G166 $n = 5$, GS090 $n = 4$). **a** Gene enrichment analysis for 'Cellular component' was performed based on the MS hits identified from each GBM cell-derived sEVs. **b** Venn diagram based on the identified MS hits. **c** Pairwise comparison diagram showing similarity between the proteome contents of the different GBM cell-derived sEVs. **d** Gene enrichment analysis for 'Biological pathway' was performed based on the MS hits identified from each GBM cell-derived sEVs. **e** Gene enrichment analysis for 'Biological process' was performed based on the MS hits identified from each GBM cell-derived sEVs. **f** Western blotting detection of fibronectin (FBN), CD44, CD63, HSP70, AnnexinA2 (ANXA2), CD9, and CD81 in GBM cell-derived sEVs

from LN18, U87, and U118. CD82 was also observed in G166 GBM cell-derived sEVs (Fig. 4 and Supplementary Data 8). Notably, CD44, a now well-described marker of aggressive mesenchymal GBM, was identified in sEVs derived from LN18, U87, U118, and G166 GBM cells[29] (Supplementary Fig. 6 and Supplementary Data 9).

As we initially grouped LN18 and U87 GBM cells together (signature 1) showing the highest levels of in vitro invasiveness (Fig. 2), we thoroughly looked for potential relevant markers of GBM aggressiveness among the protein hits exclusively present in both sEV fractions derived from these cell lines. By doing so, we identified WNT5a, TGFBI, and SERPINE1, all recently associated with the GBM mesenchymal subtype and tumor invasion[30–32], as well as GDF-15, also known to be linked to GBM progression and poor prognosis[33,34]. TCGA data confirmed the significant association of a high expression of SERPINE1 and TGFBI with mesenchymal subtype in GBM patients (Supplementary Fig. 6 and Supplementary Data 9).

Finally, we further evaluated the distribution of specific markers in sEVs produced by the different GBM cells, including fibronectin, CD63, HSP70, Annexin A2, CD9 CD81, as well as CD44 which has been recently observed at the surface of EVs from different sources, such as ovarian and breast cancer cells but also mesenchymal stem cells, whilst being associated with GBM progression and aggressiveness[23,29,35–37].

Overall, Fig. 4f show that sEVs derived from signature 1-associated LN18 and U87 GBM cells display similar levels of CD63, HSP70, and Annexin A2 while sharing the highest expression of CD63 and CD9 with signature 4 (U118 cells), as compared to sEVs derived from G166 and GS090 stem cells. Both sEV fractions from G166 and GS090 cells had low levels of CD63 and CD9 expression. Highest expression of FBN was observed in U87 and G166 GBM cell-derived sEVs. Furthermore, CD44 was clearly detected only in LN18, U87, and G166 GBM cell-derived sEVs (Fig. 4f and Supplementary Fig. 7).

Discussion

Distinct molecular subtypes have been defined in order to make GBM diagnosis more precise, with direct links to tumor aggressiveness and patients overall survival[2]. Nevertheless, clinical application of such subtyping is still quite limited, due to a lack of reliable and accessible biomarkers. For these reasons, the present study aimed to describe markers for specific GBM signatures in sEVs derived from tumor cells, according to their in vitro invasion potential. We believe that such biomarkers should be detectable in sEVs derived from patients' biofluids (i.e. blood or CSF), thus helping diagnosis and development of future personalized therapies[3].

Indeed, by correlation clustering of our phenotypic and molecular results, we could define distinct signatures to describe the GBM cells that were employed in this study. Interestingly, in accordance with the widely used Verhaak classification and other recent reports, signatures 1 and 2 presented characteristics specifically associated with the mesenchymal and proneural subtype, respectively. Indeed, as often reported for the mesenchymal GBM subtype, signature 1 was mostly characterized by high CD44 and cMET expression, as well as high cell invasiveness. Similarly, proneural markers such as high PDGF-R and OLIG2 expression were the main parameters linked to signature 2. Signature 3 and 4 could not be clearly linked to any of the described GBM subtypes even though signature 3 presented the highest EGF-R gene expression, a marker for the classical GBM subtype.

Interestingly, the cell clustering was mirrored in the proteomic content of sEVs derived from these GBM cells. Indeed, according to our MS data and gene-enrichment analysis, there was a clear separation between LN18, U87, and U118 on one side and G166 and GS090 on the other. Such discrepancy was further supported by the identification of biological pathways and processes in the sEV proteomes. According to our analysis, the content of EVs derived from U87, U118, and LN18 appeared similar while being enriched in signaling pathways, such as 'Integrin family cell surface interaction' or 'VEGF and VEGFR network', known to be directly linked to GBM progression. On the other hand, the EV proteomic signature of G166 and GS090 cells was mostly related to 'normal conditions' machinery/metabolism pathways, e.g. 'Energy pathways' or 'Metabolism'[38,39]. Such discrepancies in the EV cargo between GBM cell lines and GBM stem cells may be due to the remarkable metabolic flexibility of cancer stem cells, as opposed to normal/proliferative cancer cells[40,41], which can have a direct impact on the EV cargo of GBM stem cells[15].

Moreover, differences could also be observed when looking closely at the expression levels of sEV specific markers, such as CD63, HSP70, Annexin A2, and CD9. sEVs derived from LN18, U87, and U118 GBM cells had similar expression patterns when compared to GBM stem cell-derived sEVs. Furthermore, sEVs from signature 2 (GS090 stem cells) only showed clear expression of CD9 and fibronectin, as recently reported in a similar way for 'proneural' GBM cell-derived EVs by Spinelli et al.[23]. In accordance with our present data, authors indeed showed that the GBM stem cell subtype affected EV molecular characteristics as sEVs produced by proneural GBM stem cells had very low levels of CD9, CD63, and CD81 expression compared to sEVs derived from mesenchymal GBM stem cell cultures[23,42]. Finally, the similarities spotted between G166 and LN18 cells (signature 1) and between U118 and U87 cells (signature 4) were partially recapitulated in our proteomic analysis of the EVs-content. Such nuances could be related to the differences in the in vitro migration/invasion capabilities we observed between LN18 and U87 GBM cells. As both cell lines show mesenchymal features (signature 1), we consider LN18 cells to be in an intermediate mesenchymal state, as opposed to the fully invasive mesenchymal U87 cells. Indeed, one could argue that such observation appears similar to a 'go-or-grow' model where LN18 cells would rather 'grow' into a 'tumor friendly' microenvironment characterized by HA abundance than 'go' and migrate through the basement membrane and further invade surrounding tissue layers[43,44].

Taken together, based on the current MS data and specific sEV markers expression, LN18, U87, and U118 appeared to cluster together, as similarly observed in our four-signature clustering that grouped signature 1 (LN18 and U87) along with signature 4 (U118), while our 7-signature clustering also initially grouped LN18 and U118 GBM cells together. Yet, LN18 and U87 on one hand and U118 on the other hand clearly differ in terms of cMET and CD44 expression, as well asin their invasiveness in the HA hydrogels[45]. As a matter of fact, the low expression of CD44 in sEVs derived from U118 GBM cells seems indicative of such difference with LN18 and U87 cells. Our data suggest that sEV-associated CD44 expression could be correlated with GBM cell invasiveness. Yet, as high CD44 has been detected in sEVs derived from low invasive G166 cells, and in accordance with the rest of our results, we thus think that distinct GBM signatures/subtypes might be differently associated with exclusive expression levels of a few selected EV-associated markers. Accordingly, recent reports suggested that profiling the expression of surface EV proteins could provide cancer diagnostic signatures from biofluids[36].

Along with CD44, our results suggest TGFBI and SERPINE1 (PAI-1) as potential sEV-associated biomarkers for the aggressive mesenchymal subtype[31,32]. We especially focused on CD44 as it has often been associated with the mesenchymal phenotype and cell invasion in GBM[29,37,45]. Accordingly, EV-associated CD44 has been linked to tumor progression and resistance to treatment

in breast cancer and myeloma, respectively[37,46,47]. Furthermore, we suggest that such biomarkers could help the follow-up of GBM tumors and the monitoring of recurrence/treatment resistance[24]. In the same way, an increase of the expression of proteins, such as ECM1, CD9, and CD44 has been reported in EVs derived from squamous cell carcinoma cells upon mesenchymal transformation[48,49]. Altogether, both our data and recent publications suggest that changes in the EV-specific marker expression patterns could help identify highly invasive/aggressive tumors.

A few studies have already reported EV-associated markers that could be used for discriminating GBM from normal and stromal CNS cells, such as annexins and integrins[3,42]. Combined with deciphering the expression of specific EV markers and EV-associated GBM subtype markers, such integrated approaches should provide an accurate diagnosis with potential subtype characterization. Nevertheless, both cellular and molecular heterogeneity has been repeatedly reported in GBM tumors[2]. For these reasons, characterizing a GBM tumor subtype based on the respective EV proteomic content appears quite challenging, as markers from various subtypes might be present in patients' samples[5]. Nevertheless, precise quantification of the EV-associated markers should give further information regarding the tumor main molecular signature and, consequently, associated prognosis.

We believe that this study supports the clinical potential of the content of EVs derived from different GBM subtypes[26]. According to our data, EVs may contain reliable protein markers, in particular for the aggressive mesenchymal GBM subtype. Interestingly, although all the different GBM subtypes can be present in the same tumor, it has been suggested that the mesenchymal subtype takes over upon recurrence[50]. Hence, deciphering how specific GBM subtyping influences the EV cargo may help us understand how GBM can progress and recur. In the same way, patient follow-up could also benefit from such work. A limitation of the present study is the use of immortalized tumor cell lines for studying GBM subtypes, despite the concomitant use of two populations of GBM patient-derived stem cells[2]. Nevertheless, we believe that our present report can be of great help for future functional in vitro studies deciphering the role of EVs in GBM[51,52]. Yet, additional work is needed to validate our current conclusions in an in vivo setting, considering the role of the surrounding microenvironment. Furthermore, as presented by Rennert et al. RNA that is detectable in GBM EVs is a rather appealing source of biomarkers as only a small amount of genetic material is needed to perform the analysis of a few key genes. Similarly to the present study, authors suggested that describing EV content expression patterns of the four different GBM subtypes is urgently needed[26]. Also, larger vesicles, such as m/lEVs and oncosomes, might also provide meaningful information for GBM diagnosis and prognosis[21]. Finally, future translational clinical research should be performed in order to assess the application of such observations into a liquid biopsy setup[53].

In summary, our study improves the understanding of the correlation between distinct GBM subtypes and associated potential aggressiveness with respective EV production and content. In addition, our findings suggest the existence of EV-associated biomarker patterns for GBM subtype identification in patients. Consequently, we believe that further clinical work and validation would bring new insight towards the development of more effective therapeutic strategies and personalized treatments.

Methods

Cells and reagents. LN18, LN229, and U118 GBM cells (ATCC) were maintained in Dulbecco's modified Eagle medium (DMEM, Sigma-Aldrich) and T98, U87, and U138 GBM cells (ATCC) were maintained in minimum essential medium (MEM, Sigma-Aldrich). Astrocytes (Human Astrocytes, Sciencell) were maintained in Astrocyte growth medium (ASGM, Cell Applications). Poly-L-lysine (Sigma-Aldrich) at 2 µg cm^{-2} was used to coat every plastic vessel needed for astrocyte culture. Cell line culture medium was supplemented with 100 Units mL^{-1} penicillin, 100 µg mL^{-1} streptomycin, 2 mM L-glutamine (PSG, Sigma-Aldrich) and 10% heat inactivated fetal bovine serum (FBS, First Link).

G166 and GS090 (GBM patient-derived stem cells) were a kind gift from Dr. Angela Bentivegna, University of Milan-Bicocca and Dr. David Nathanson, University of California, Los Angeles, respectively. GBM stem cells were isolated from GBM tumor samples following local Ethical Board approval[54,55]. GBM stem cells were maintained as neurospheres in (DMEM/F-12, Sigma-Aldrich) completed with B-27 without Vitamin A (Life Technologies), Hu EGF (20 µg mL^{-1}), Hu FGF-b (8 µg mL^{-1}), Heparin (2 mg mL^{-1}), 100 Units mL^{-1} penicillin, 100 µg mL^{-1} streptomycin, and Glutamax (Invitrogen). Cells were incubated at 37 °C in a humidified atmosphere at 5% CO$_2$. Medium was changed twice a week. GBM cells (cell lines) and astrocytes were detached at confluence using trypsin/EDTA. GBM stem cells were disassociated using TrypleE Express Enzyme (Gibco) and separated into single cells through a 70 µm cell strainer. The International Cell Line Authentication Committee identifies U118 as a derivative of U138 as they appeared to share a common donor[56,57]. Nevertheless, considering the GBM intra-tumoral heterogeneity, we decided to use both cell lines in the present study to compare them with each other and with the rest of the cells we used[5]. All the cells were tested negative for mycoplasma at the beginning of the study.

Cell invasion assay in HA hydrogels. Cells were incubated with HA hydrogels for 7 days according to the manufacturer's instructions (Biomymesis, Celenys)[58]. 100,000 cells were seeded per well. All the steps conferring properties to HA hydrogels used in cell culture have been described in two Europeans patents: "Improved Crosslinked Hyaluronan Hydrogels for 3D Cell Culture" EP10305666.9, June 22, 2010 and "Method for Harvesting Cells Cultured in 3D Hydrogel Matrices" EP 10305667.7, June 22, 2010. Hyaluronan hydrogels consist of hyaluronan cross-linked with adipic dihydrazide (ADH; Sigma-Aldrich, France) and 1-ethyl-3 [3-(dimethylamino)-propyl] carbodiimide (EDCI; Sigma-Aldrich). High molecular weight hyaluronan (>106 Da; Sigma-Aldrich) is used to prepare the hydrogel plates, as originally described by Prestwich et al.[59]. Briefly, the ratios ADH:hyaluronan (10:1) and hyaluronan:EDCI (1:1) have been optimized for cell adhesion and culture. Hyaluronan and ADH are dissolved in milliQ-water. 0.1 N HCl is used to adjust the pH to 4.6. The reaction mixture is then completed with carbodiimide reagent (EDCI) and allowed to set for 2 h, with gentle agitation. Hyaluronan hydrogels are then dialyzed against 0.1 N NaCl for 2 days, then in a water:ethanol mixture (3:1 v/v) for other 2 days, and in milliQwater for 2 days in order to remove excess of ADH and EDCI. In the next step, the dialyzed hydrogel is placed in a plastic container and frozen. Following freezing, the hydrogels are placed in a lyophilizer (Alpha 1–2, Christ, Germany; performances, 2 kg ice per 24 h, $T = -55$ °C) for 4–5 days. The lyophilized hydrogels are then stored at −20 °C. Hydrogels are sterilized at 100 °C. The gel pH post-rehydration has been shown to be ~8.4. The swelling ratio of hyaluronan hydrogels at room temperature in culture medium should be 37 g g^{-1} [60]. Colony counting was performed on six pictures randomly taken from each gel using an EVOS FLC imaging system (Life Technologies) at ×10 magnification. Cell viability was assessed using the CellTiter-Glo® Luminescent Cell Viability Assay. To do so, 100 µL of Cell-Titer-Glo® Reagent (CellTiter-Glo® Luminescent Cell Viability Assay, Promega) was added to each well. Plate was agitated on a plate mixer for 2 min and left for 10 min at room temperature before luminescence was recorded using a GloMax Explorer plate reader (Promega). Graphs show an average of three experiments.

Cell invasion assay through a basement membrane matrix. The QCM™ 96-well plate (Merck) was used to perform the cell invasion assay. The assay allows for measurement of cell invasion through a reconstituted basement membrane matrix. Cells were starved in serum-free medium for 24 h before the assay, according to the manufacturer's instruction. The basement membrane matrix was rehydrated with warm cell culture medium for 2 h. Medium was discarded from the inserts and either serum-free medium (control) or 10% FCS medium was added to the feeder tray (lower chamber). 100,000 cells per well were then seeded and allowed to invade the matrix for 24 h. Following incubation, the cell suspension was carefully removed from the top chamber and inserts were rinsed in sterile PBS for 1 min. Cell detachment solution was then added to a new feeder tray and the plate was incubated for 30 min so invading cells are dissociated from underside. In order to label the cells, CyQuant GR Dye/4x Lysis Buffer solution was then added to the wells. The plate was incubated for an additional 15 min at room temperature. Finally, fluorescence was read using a GloMax Explorer plate reader (480/520 nm filter set, Promega). Data obtained in presence of FCS was normalized to data obtained without FCS. Graph shows an average of three experiments.

Cell proliferation assay. Cells were plated in a 96-well plate (5000 cells per well) in 10% FCS medium. Cells were incubated for 24 and 96 h, washed once with sterile PBS and then fixed using 4% paraformaldehyde for 20 min. Following, cells were washed with PBS again and stained using a 0.1% crystal violet solution for 30 min. Crystal violet dye was then extracted from the cells using 10% acetic acid.

Plates were placed on a plate shaker for 30 min. Absorbance was then read at 590 nm for both t24 and t96 time points using a GloMax Explorer plate reader (Promega). Doubling time (h) was calculated using this formula: doubling time = $72/(\log(\text{absorbance}_{590nm} \text{ at t96}) - \log(\text{absorbance}_{590nm} \text{ at t24}))/\log 2)$. Graph shows an average of three experiments.

Wound healing assay. Cells were plated at 100,000 cells per well in a 24-well plate in 10% FCS medium until they reach 80% of confluence. Then, cells were washed once with sterile PBS and medium was changed for 0% FCS medium before a scratch was performed in the cell layer using a 200 µL tip. Cells were incubated for 48 h. A total of three pictures per wound were taken using an EVOS FLC imaging system (Life Technologies) at ×10 magnification. The size of the wound was then measured on each picture. Graphs show an average of three experiments. The wound healing assay could not be performed using G166 or GS090, as previously reported[61].

Western blotting. Cell protein lysates were extracted using RIPA buffer (Sigma) including fresh protease and phosphatase inhibitors and standard western blotting protocol was performed as described before[62]. For the EV marker analysis, 1×10^{11} sEVs mL^{-1} was loaded on the SDS gel. Primary antibodies: Anti-AnnexinA2 (Genscript A01471, 1/1000 dilution), anti-β-Actin (Abcam ab6276, 1/5000 dilution), anti-CD-9 (System Biosciences EXOAB-CD9A-1, 1/10000 dilution), anti-CD44 (Cell Signaling #3570, 1/1000 dilution), anti-CD63 (System Biosciences EXOAB-CD63A-1, 1/10,000 dilution), anti-CD81 (System Biosciences EXOAB-CD81A-1, 1/10,000 dilution), anti-Fibronectin (Abcam ab2413, 1/1000 dilution), anti-HSP-70 (System Biosciences EXOAB-HSP70A-1,1/10,000 dilution), anti-NEFL (Cell Signaling #2837, 1/1000 dilution), anti-OLIG2 (Genscript A01474, 1/1000 dilution), and anti-PTEN (Cell Signaling #9188, 1/1000 dilution). Secondary antibodies used: Polyclonal Goat Anti-Rabbit/Mouse Immunoglobulins/HRP (Dako P0447/8, 1/3000 dilution) antibodies and Anti-Rabbit Immunoglobulins/HRP (ExoAb antibody Kit, System Biosciences EXO-AB-HRP, 1/3000 dilution). Chemiluminescence was observed using a UVP Chemstudio instrument (Analytik Jena) and the Vision Works software. All experiments have been repeated at least three times.

Real-time polymerase chain reaction. RNA was purified from cell pellets using the RNeasy® mini kit (Qiagen) quick start protocol. Reverse transcription was carried out using a cDNA synthesis kit (Applied Biosystems). Taqman (Applied Biosystems) and cDNA were mixed with primers (Applied Biosystems) specific for the markers of interest and run on a One-Step® Plus machine (Applied Biosystems). Data was evaluated using One-Step® Plus software (Applied Biosystems). Each result has been normalized to GAPDH values. Graphs show an average of at least three experiments. All the primers (Table 1) were obtained from Applied Biosystems (Thermofisher), except primers for PDGF-Rα and GAPDH (Qiagen).

VEGF-A ELISA. Human VEGF DUOSET ELISA (R&D System) was used to measure VEGF-A levels in culture medium according to the manufacturer's instructions. Absorbance was measured at 450 nm using a GloMax Explorer plate reader (Promega). Graphs show an average of three experiments.

Extracellular vesicle concentration. In order to collect sEVs derived from GBM cell lines (LN18, U87, and U118), cells were seeded in $4–5 × 175$ cm^2 flasks and grown in 10% FCS medium until they reach confluence. Then, cells were washed with sterile PBS and 15 mL of corresponding serum-free medium was added to each flask for 24 h. Following this incubation, conditioned medium (CM) was collected and kept at either 4 °C for a very short time (up to 24 h) or at −20 °C for longer periods (up to 6 months) before sEV concentration.

To collect sEVs from GBM stem cells (G166 and GS090) in suspension cell culture (neurospheres), medium was changed at confluence (neurospheres of 150–200 µm diameter) and incubated for 24 h before CM collection. To do so, culture supernatant and neurospheres were centrifuged at $400 × g$ for 4 min and CM was collected (35 mL). CM from GBM stem cell cultures was then kept at

either 4 °C for a very short time (up to 24 h) or at −20 °C for longer periods (up to 6 months) before sEV concentration. In accordance with the latest minimal information for studies of EVs, cell count at time of collection was recorded and used to normalize the final sEV concentration (particles/mL/cell)[21].

Concentration of sEVs was performed using an ultracentrifugation-based protocol[63]. Every step of the concentration protocol was performed at 4 °C. An initial $300 × g$ centrifugation was performed for 10 min to discard any floating cells from the CM, followed by a 10 min centrifugation step at $2000 × g$ to remove any floating cell debris and dead cells (Hettich Universal 320R centrifuge). A $10,000 × g$ ultracentrifugation step (Beckman optima LE 80-k ultracentrifuge, Beckman Type 70 Ti rotor, Beckman polypropylene centrifuge $14 × 89$ mm tubes, full dynamic braking, $k_{adj} = 15,638$) was performed for 30 min to remove any further cell debris and large vesicles (m/lEVs) from the CM. Finally, a first $100,000 × g$ ultracentrifugation run was performed for 1 h30 min to pellet the sEVs ('exosomes') from the CM (Beckman optima LE 80-k ultracentrifuge, Beckman Type 70 Ti rotor, Beckman polypropylene centrifuge $14 × 89$ mm tubes, full dynamic braking, $k_{adj} = 494$). Supernatant was stored at −20 °C. The sEV pellet was then washed in filtered sterile PBS and centrifuged again for 1 h30 min at $100,000 × g$ in order to discard contaminants. The final sEV pellet was re-suspended in 100 µL filtered sterile PBS and immediately characterized through nanoparticle tracking analysis (NTA).

Further characterization of the sEVs was performed through western blotting (see subsection 'Western blotting' in "Methods" section) by measuring the expression of EV membrane associated markers, such as CD63, CD9, CD81 (mainly associated with light sEVs) and fibronectin (mainly associated with dense sEVs), and EV cytosolic markers such as HSP70 and Annexin A2[17,21].

Nanoparticles tracking analysis (NTA). Vesicle concentration and size were determined using a Nanosight© NS300 and the Nanosight© NTA 3.2 software (Malvern Instruments). The following conditions were applied for the NTA analysis at the Nanosight instrument: temperature was 20–25 °C; viscosity was ~0.98 cP; camera type was sCMOS; laser type was Blue488; camera levels were either 14 or 15; syringe Pump Speed was set to 70 AU; five measurements of 60 s each were recorded. Graphs show an average of at least four experiments.

Transmission electron microscopy. Transmission electron microscopy (TEM) has been performed on sEV preparations in order to visualize and assess/confirm the size range of the vesicles, as described before[63]. Samples were visualized using a JEOL JEM1400-Plus (120 kV, LaB6) microscope equipped with a Gatan OneView 4K camera at ×20k magnification. 10–15 pictures per grid were taken.

Mass spectrometry. In order to elucidate the protein content of the GBM cell-derived sEVs, MS analysis was performed. To do so, a Bradford assay was performed to determine the protein concentration of each sEV sample and 100 ng was then loaded on a SDS–PAGE gel for protein separation. Following Coomassie blue staining, 5 slices/lane were then cut out of the gel and further processed for in-gel trypsin digestion and MS run. De-staining was performed through 3 changes/washes with 50% acetonitrile (MeCN), 25 mM NH$_4$HCO$_3$, with 5 min shaking between each change. Reduction and alkylation were performed, respectively, with 10 mM dithiothreitol (DTT), in 25 mM NH$_4$HCO$_3$ (45 min at 50 °C) and 50 mM chloracetamide, 25 mM NH$_4$HCO$_3$ (45 min in the dark at room temperature). Subsequently, 12.5 ng µL^{-1} trypsin (in 25 mM NH$_4$HCO$_3$) was added to the samples, followed by an overnight incubation at 37 °C. The digest solution was then transferred to clean tubes. Next, 70% acetonitrile/5% trifluoroacetic acid was added to the gel pieces. Following 5 min shaking, the supernatant was transferred to the corresponding clean tubes. A similar further extraction was repeated another two times in order to completely dehydrate the gel pieces and consequently recover the rest of the peptides. Sample volume was reduced to 20 µL using a vacuum concentrator. Samples were then processed through a LTQ-Orbitrap mass spectrometer coupled to a Dionex NCP-3200 nanoLC system. The raw data was searched using Maxquant (Max Planck Institute of Biochemistry) against a SwissProt database (Proteome ID: UP000005640, Taxonomy: 9606—Homo sapiens). The following settings were used: trypsin was the enzyme with up to two missed cleavages, oxidation (M) and acetyl (Protein N-term) were set as variable modifications, Carbamidomethyl (C) was set as fixed modification, minimum peptide length was seven amino acids, maximum peptide mass was 4600 Da, minimum and maximum peptide length for unspecific search was 8 and 25 amino acids, respectively, peptides and protein false discovery rates (FDR) were both 0.01 and minimum razor + unique peptides was set to 1 (minimum of 1 peptide for protein identification). Finally, results ('protein groups') were exported to Microsoft Office Excel and further processed. The MS analysis was repeated at least three times for each GBM cell lines/stem lines, using independent samples. Through comparison of independent experiments for each cell line/stem cell, we described as 'hits' the identified proteins that appeared in at least two independent identifications. Obvious contaminants (keratins) were removed from the protein group lists. In addition, proteomic data were further deciphered by loading the gene symbols identified from the MS data in Functional Enrichment Analysis Tool (FunRich) for gene-enrichment analysis of 'Biological pathways', 'Biological process', 'Cellular

Table 1 Primers used for RT-PCR assays

Gene	Primer	Source
EGF-R	Hs01076090_m1	Applied Biosystems (Thermofisher)
PTEN	Hs02621230_s1	Applied Biosystems (Thermofisher)
NF1	Hs01035108_m1	Applied Biosystems (Thermofisher)
VEGF-A	Hs00900055_m1	Applied Biosystems (Thermofisher)
OLIG2	Hs00300164_s1	Applied Biosystems (Thermofisher)
SOX2	Hs00415716	Applied Biosystems (Thermofisher)
GAPDH	Hs99999905_m1	Applied Biosystems (Thermofisher)
PDGF-Rα	Hs_PDGFRA_1_SG	Qiagen
GAPDH	Hs_GAPDH_2_SG	Qiagen

component' and 'Pairwise comparison diagram'. The InteractiVenn (www.interactivenn.net) online software was used to make Venn diagrams[64].

TCGA data. Information about the distribution of specific gene hits among the different GBM subtypes has been obtained from The Cancer Genome Atlas (TCGA) through the 'Expression box plot (Affymetrix HT HG U133A)' and 'Expression box plot (Affymetrix Human Exon 1.0 ST)' graphs on the Betastasis website (www.betastasis.com) that organize patients' samples according to their GBM subtypes.

Experimental design and statistics. Sample size was set to a minimum of three independent experiments (biological repeats) based on the magnitude and consistency of differences between cells/conditions. Experimental findings were reliably reproduced. All the results were normalized to control and reported as mean ± standard error of the mean (SEM). Ordinary one-way ANOVA tests were employed to determine the significance of the observed differences. Tukey's test was used for multiple comparison. Differences were considered statistically significant at $p < 0.05$ (95% confidence interval, $*p < 0.05$; $**p < 0.01$; $***p < 0.001$). Pearson correlation coefficient was used to measure the relationship between the considered parameters shown in Fig. 1. Mean phenotype parameter measurement across all available cell lines was decomposed into seven different signatures (sig 1–7, Fig. 2a) to reduce the dimensionality of the data and provide a method of clustering the cell lines by phenotype similarity. Additionally the LN18, U87, U118, G166, and GS090 cell lines alone were decomposed into four signatures (sig 1–4, Fig. 2c). This decomposition was achieved using non-negative matrix factorization (NMF). Each cell-line's mean parameter measurement was used to build a feature matrix. NMF was used to decompose these features into two separate matrices, the basis, which describes the composition of each signature and the coefficient, which reports how prominent each signature is in each cell line and stem cell. The number of components parameter used for each decomposition was decided by running many NMF decompositions with increasing parameters, and choosing the number of components where the reconstruction error plateaued. Finally, we used hierarchical clustering on the coefficient matrices in order to cluster GBM cell lines and stem cells based on signature composition similarity (Fig. 2b, d, respectively).

Reporting summary. Further information on research design is available in the Nature Research Reporting Summary linked to this article.

Data availability

All relevant data are available from the authors upon request. The mass spectrometry proteomics data have been deposited to the ProteomeXchange Consortium via the PRIDE partner repository with the dataset identifier PXD014579[65].

References

1. Louis, D. N. et al. The 2016 World Health Organization Classification of Tumors of the Central Nervous System: a summary. *Acta Neuropathol.* **131**, 803–820 (2016).
2. Verhaak, R. G. et al. Integrated genomic analysis identifies clinically relevant subtypes of glioblastoma characterized by abnormalities in PDGFRA, IDH1, EGFR, and NF1. *Cancer Cell* **17**, 98–110 (2010).
3. Mallawaaratchy, D. M. et al. Comprehensive proteome profiling of glioblastoma-derived extracellular vesicles identifies markers for more aggressive disease. *J. Neuro-Oncol.* **131**, 233–244 (2017).
4. Phillips, H. S. et al. Molecular subclasses of high-grade glioma predict prognosis, delineate a pattern of disease progression, and resemble stages in neurogenesis. *Cancer Cell* **9**, 157–173 (2006).
5. Patel, A. P. et al. Single-cell RNA-seq highlights intratumoral heterogeneity in primary glioblastoma. *Science* **344**, 1396–1401 (2014).
6. Cruickshanks, N. et al. Role and therapeutic targeting of the HGF/MET pathway in glioblastoma. *Cancers* **9**, https://doi.org/10.3390/cancers9070087 (2017).
7. Quail, D. F. & Joyce, J. A. The microenvironmental landscape of brain tumors. *Cancer cell* **31**, 326–341 (2017).
8. Liebelt, B. D. et al. Glioma stem cells: signaling, microenvironment, and therapy. *Stem Cells Int.* **2016**, 7849890 (2016).
9. Bao, S. et al. Glioma stem cells promote radioresistance by preferential activation of the DNA damage response. *Nature* **444**, 756–760 (2006).
10. Okawa, S. et al. Proteome and secretome characterization of glioblastoma-derived neural stem cells. *Stem Cells* **35**, 967–980 (2017).
11. Orzan, F. et al. Genetic evolution of glioblastoma stem-like cells from primary to recurrent tumor. *Stem Cells* **35**, 2218–2228 (2017).
12. Reinartz, R. et al. Functional subclone profiling for prediction of treatment-induced intratumor population shifts and discovery of rational drug combinations in human glioblastoma. *Clin. Cancer Res.* **23**, 562–574 (2017).
13. Abou-Antoun, T. J., Hale, J. S., Lathia, J. D. & Dombrowski, S. M. Brain cancer stem cells in adults and children: cell biology and therapeutic implications. *Neurotherapeutics* **14**, 372–384 (2017).
14. Kawamura, Y., Takouda, J., Yoshimoto, K. & Nakashima, K. New aspects of glioblastoma multiforme revealed by similarities between neural and glioblastoma stem cells. LID-https://doi.org/10.1007/s10565-017-9420-y.
15. Wendler, F. et al. Extracellular vesicles swarm the cancer microenvironment: from tumor–stroma communication to drug intervention. *Oncogene*. LID-https://doi.org/10.1038/onc.2016.253 (2016).
16. Haraszti, R. A. et al. High-resolution proteomic and lipidomic analysis of exosomes and microvesicles from different cell sources. *J. Extracell. Vesicles* **5**, 32570 (2016).
17. Kowal, J. et al. Proteomic comparison defines novel markers to characterize heterogeneous populations of extracellular vesicle subtypes. *Proc. Natl Acad. Sci. USA* **113**, E968–E977 (2016).
18. Gourlay, J. et al. The emergent role of exosomes in glioma. *J. Clin. Neurosci.* **35**, 13–23 (2017).
19. Treps, L., Perret, R., Edmond, S., Ricard, D. & Gavard, J. Glioblastoma stem-like cells secrete the pro-angiogenic VEGF-A factor in extracellular vesicles. *J. Extracell. Vesicles* **6**, 1359479 (2017).
20. Yang, J. K. et al. Exosomal miR-221 targets DNM3 to induce tumor progression and temozolomide resistance in glioma. *J. Neuro-Oncol.* **131**, 255–265 (2017).
21. Thery, C. et al. Minimal information for studies of extracellular vesicles 2018 (MISEV2018): a position statement of the International Society for Extracellular Vesicles and update of the MISEV2014 guidelines. *J. Extracell. Vesicles* **7**, 1535750 (2018).
22. Simon, T. et al. Shedding of bevacizumab in tumour cells-derived extracellular vesicles as a new therapeutic escape mechanism in glioblastoma. *Mol. Cancer* **17**, 132 (2018).
23. Spinelli, C. et al. Molecular subtypes and differentiation programmes of glioma stem cells as determinants of extracellular vesicle profiles and endothelial cell-stimulating activities. *J. Extracell. Vesicles* **7**, 1490144 (2018).
24. Osti, D. et al. Clinical significance of extracellular vesicles in plasma from glioblastoma patients. *Clin. Cancer Res.* **25**, 266–276 (2019).
25. Rooj, A. K., Mineo, M. & Godlewski, J. MicroRNA and extracellular vesicles in glioblastoma: small but powerful. *Brain Tumor Pathol.* **33**, 77–88 (2016).
26. Rennert, R. C., Hochberg, F. H. & Carter, B. S. ExRNA in biofluids as biomarkers for brain tumors. *Cell. Mol. Neurobiol.* **36**, 353–360 (2016).
27. Al-Nedawi, K., Meehan, B., Kerbel, R. S., Allison, A. C. & Rak, J. Endothelial expression of autocrine VEGF upon the uptake of tumor-derived microvesicles containing oncogenic EGFR. *Proc. Natl Acad. Sci. USA* **106**, 3794–3799 (2009).
28. Chen, W. W. et al. BEAMing and droplet digital PCR analysis of mutant IDH1 mRNA in glioma patient serum and cerebrospinal fluid extracellular vesicles. *Mol. Ther. Nucleic Acids* **2**, e109 (2013).
29. Guo, J. Y. et al. Serglycin in tumor microenvironment promotes non-small cell lung cancer aggressiveness in a CD44-dependent manner. *Oncogene* **36**, 2457–2471 (2017).
30. Binda, E. et al. Wnt5a drives an invasive phenotype in human glioblastoma stem-like cells. *Cancer Res.* **77**, 996–1007 (2017).
31. Pan, Y. B. et al. Transforming growth factor beta induced (TGFBI) is a potential signature gene for mesenchymal subtype high-grade glioma. *J. Neuro-Oncol.* **137**, 395–407 (2018).
32. Patil, V. & Mahalingam, K. Comprehensive analysis of Reverse Phase Protein Array data reveals characteristic unique proteomic signatures for glioblastoma subtypes. *Gene* **685**, 85–95 (2019).
33. Codo, P. et al. Control of glioma cell migration and invasiveness by GDF-15. *Oncotarget* **7**, 7732–7746 (2016).
34. Brandao, M., Simon, T., Critchley, G. & Giamas, G. Astrocytes, the rising stars of the glioblastoma microenvironment. *Glia* **67**, 779–790 (2019).
35. Buzás, E. I., Tóth, E. Á., Sódar, B. W. & Szabó-Taylor, K. É. Molecular interactions at the surface of extracellular vesicles. *Semin. Immunopathol.* **40**, 453–464 (2018).
36. Belov, L. et al. Extensive surface protein profiles of extracellular vesicles from cancer cells may provide diagnostic signatures from blood samples. *J. Extracell. Vesicles* **5**, 25355–25355 (2016).
37. Nakamura, K. et al. Exosomes promote ovarian cancer cell invasion through transfer of CD44 to peritoneal mesothelial cells. *Mol. Cancer Res.* **15**, 78–92 (2017).
38. Simon, T., Gagliano, T. & Giamas, G. Direct effects of anti-angiogenic therapies on tumor cells: VEGF signaling. *Trends Mol. Med.* **23**, 282–292 (2017).
39. Wang, R. & Dashwood, R. H. Endothelins and their receptors in cancer: identification of therapeutic targets. *Pharmacol. Res.* **63**, 519–524 (2011).

40. Snyder, V., Reed-Newman, T. C., Arnold, L., Thomas, S. M. & Anant, S. Cancer stem cell metabolism and potential therapeutic targets. *Front. Oncol.* **8**, 203–203 (2018).

41. Sancho, P. et al. MYC/PGC-1alpha balance determines the metabolic phenotype and plasticity of pancreatic cancer stem cells. *Cell Metab.* **22**, 590–605 (2015).

42. Ricklefs, F. et al. Extracellular vesicles from high-grade glioma exchange diverse pro-oncogenic signals that maintain intratumoral heterogeneity. *Cancer Res.* **76**, 2876–2881 (2016).

43. Oliveira, A. I. et al. Crosstalk between glial and glioblastoma cells triggers the "go-or-grow" phenotype of tumor cells. *Cell Commun. Signal.* **15**, 37 (2017).

44. Xie, Q., Mittal, S. & Berens, M. E. Targeting adaptive glioblastoma: an overview of proliferation and invasion. *Neuro-Oncol.* **16**, 1575–1584 (2014).

45. Simon, T. et al. Direct effect of bevacizumab on glioblastoma cell lines in vitro. *Neuromol. Med.* **16**, 752–771 (2014).

46. Harshman, S. W. et al. Proteomic characterization of circulating extracellular vesicles identifies novel serum myeloma associated markers. *J. Proteom.* **136**, 89–98 (2016).

47. Wang, M. et al. Effect of exosome biomarkers for diagnosis and prognosis of breast cancer patients. *Clin. Transl. Oncol.* **20**, 906–911 (2018).

48. Garnier, D., Magnus, N., Meehan, B., Kislinger, T. & Rak, J. Qualitative changes in the proteome of extracellular vesicles accompanying cancer cell transition to mesenchymal state. *Exp. Cell Res.* **319**, 2747–2757 (2013).

49. Choi, D. et al. The impact of oncogenic EGFRvIII on the proteome of extracellular vesicles released from glioblastoma cells. *Mol. Cell. Proteom.* **17**, 1948–1964 (2018).

50. Behnan, J., Finocchiaro, G. & Hanna, G. The landscape of the mesenchymal signature in brain tumours. *Brain* **142**, 847–866 (2019).

51. Umakoshi, M. et al. Macrophage-mediated transfer of cancer-derived components to stromal cells contributes to establishment of a pro-tumor microenvironment. *Oncogene* https://doi.org/10.1038/s41388-018-0564-x (2018).

52. Wang, Q. et al. Tumor evolution of glioma-intrinsic gene expression subtypes associates with immunological changes in the microenvironment. *Cancer Cell* **32**, 42–56.e46 (2017).

53. Hallal, S. et al. The emerging clinical potential of circulating extracellular vesicles for non-invasive glioma diagnosis and disease monitoring. *Brain Tumor Pathol.* **36**, 29–39 (2019).

54. Pollard, S. M. et al. Glioma stem cell lines expanded in adherent culture have tumor-specific phenotypes and are suitable for chemical and genetic screens. *Cell Stem Cell* **4**, 568–580 (2009).

55. Baronchelli, S. et al. Delineating the cytogenomic and epigenomic landscapes of glioma stem cell lines. *PLoS ONE* **8**, e57462–e57462 (2013).

56. Bady, P. et al. DNA fingerprinting of glioma cell lines and considerations on similarity measurements. *Neuro-Oncology* **14**, 701–711 (2012).

57. Allen, M., Bjerke, M., Edlund, H., Nelander, S. & Westermark, B. Origin of the U87MG glioma cell line: Good news and bad news. *Sci. Transl. Med.* **8**, 354re353 (2016).

58. David, L. et al. Hyaluronan hydrogel: an appropriate three-dimensional model for evaluation of anticancer drug sensitivity. *Acta Biomater.* **4**, 256–263 (2008).

59. Prestwich, G. D., Marecak, D. M., Marecek, J. F., Vercruysse, K. P. & Ziebell, M. R. Controlled chemical modification of hyaluronic acid: synthesis, applications, and biodegradation of hydrazide derivatives. *J. Control. Release.* **53**, 93–103 (1998).

60. Kassim, Y. L. T. et al. Dimensional cell culturing: colorectal cancer micro-tissue engineering. *J. Clin. Exp. Oncol.* **3**, https://doi.org/10.4172/2324-9110.1000123 (2014).

61. Cilibrasi, C. et al. Resveratrol impairs glioma stem cells proliferation and motility by modulating the wnt signaling pathway. *PLoS ONE* **12**, e0169854 (2017).

62. Giamas, G. et al. Phosphorylation of CK1delta: identification of Ser370 as the major phosphorylation site targeted by PKA in vitro and in vivo. *Biochem. J.* **406**, 389–398 (2007).

63. Thery, C., Amigorena, S., Raposo, G. & Clayton, A. Isolation and characterization of exosomes from cell culture supernatants and biological fluids. *Curr. Protoc. Cell Biol.* **Chapter 3**, Unit 3.22 (2006).

64. Heberle, H., Meirelles, G. V., da Silva, F. R., Telles, G. P. & Minghim, R. InteractiVenn: a web-based tool for the analysis of sets through Venn diagrams. *BMC Bioinforma.* **16**, 169 (2015).

65. Perez-Riverol, Y. et al. The PRIDE database and related tools and resources in 2019: improving support for quantification data. *Nucleic Acids Res.* **47**, D442–d450 (2019).

Acknowledgements

Author contributions

T.S. and G.G. conceived the idea. R.L., T.S., M.V., B.S., B.K. and N.S. performed the experiments. G.C., G.B.-H., F.P., T.S. and G.G. helped with the analysis of the data. G.G., T.S., R.L. and J.S. wrote the manuscript.

Additional information

Supplementary information accompanies this paper at https://doi.org/10.1038/s42003-019-0560-x.

ARTICLE

Distinct co-acquired alterations and genomic evolution during TKI treatment in non-small-cell lung cancer patients with or without acquired T790M mutation

This article has been corrected since Advance Online Publication and a correction is also printed in this issue

Ying Jin[1,2,3] · Hua Bao[4] · Xiuning Le[5] · Xiaojun Fan[4] · Ming Tang[5] · Xun Shi[1,2] · Jun Zhao[1,2] · Junrong Yan[6] · Yang Xu[4] ·
Kelly Quek[5] · Yasir Y. Elamin[5] · Jianhua Zhang[7] · P. Andrew Futreal[7] · Ignacio I. Wistuba[8] · John V. Heymach[5] ·
Guangyuan Lou[1,2] · Lan Shao[1,2] · Qiong He[1,2] · Chen Lin[1,2] · Xue Wu[4] · Yang W. Shao[6] · Xiaonan Wang[6] ·
Jiachen He[6] · Yamei Chen[1,3] · Justin Stebbing[9] · Ming Chen[1,3] · Jianjun Zhang[5,7] · Xinmin Yu[1,2]

Abstract

EGFR-mutant non-small-cell lung cancer (NSCLC) patients inevitably develop drug resistance when treated with EGFR tyrosine kinase inhibitors (TKIs). Systematic genetic analysis is important to understand drug-resistant mechanisms; however, the clinical significance of co-occurring genetic alterations at baseline, co-acquired mutations at progressive disease (PD), and the clonal evolution remain underinvestigated. We performed targeted sequencing of pre-treatment and PD tumor samples from 54 *EGFR*-mutant NSCLC patients. Ten additional patients were sequenced using whole-exome sequencing to infer the clonal evolution patterns. We observed a domain-dependent effect of PIK3CA mutation at baseline on patient progression-free survival (PFS). In addition, at baseline, 9q34.3/19p13.3 (*NOTCH1/STK11/GNA11*) showed a co-deletion pattern, which was associated with a significantly worse PFS ($p = 0.00079$). T790M-postive patients with other concurrent acquired oncogenic mutations had a significantly shorter PFS ($p = 0.005$). Besides acquired T790M mutation, chromosomal instability (CIN) related genes, including *AURKA* and *TP53* alterations, were the most frequently acquired events. CIN significantly increased during TKI treatment in T790M-negative patients and is a candidate resistance mechanism to the first-generation TKIs. Clonal evolution analyses suggest that the composition and relationship among resistant subclones, particularly relationship with T790M subclone, affect patients' outcomes. Overall, our findings of novel co-occurring alterations and clonal evolution patterns can be served as predictive biomarkers to stratify patients and help to better understand the drug-resistant mechanism to TKIs.

These authors contributed equally: Ying Jin, Hua Bao, Xiuning Le

Supplementary information The online version of this article (https://doi.org/10.1038/s41388-019-1104-z) contains supplementary material, which is available to authorized users.

✉ Ming Chen
chenming@zjcc.org.cn

✉ Jianjun Zhang
jzhang20@mdanderson.org

✉ Xinmin Yu
yuxm@zjcc.org.cn

1 Institute of Cancer and Basic Medicine, Chinese Academy of Sciences, Hangzhou, Zhejiang, China

2 Department of Medical Oncology, Cancer Hospital of the University of Chinese Academy of Sciences & Zhejiang Cancer Hospital, Hangzhou, Zhejiang, China

3 Zhejiang Key Laboratory of Radiation Oncology, Hangzhou, Zhejiang, China

Introduction

The current paradigm in cancer therapy is to treat oncogene-positive disease primarily through targeting a single

4 Translational Medicine Research Centre, Geneseeq Technology Inc., Toronto, ON, Canada

5 Department of Thoracic/Head and Neck Medical Oncology, University of Texas MD Anderson Cancer Center, Houston, TX 77030, USA

6 Nanjing Geneseeq Technology Inc., Nanjing, Jiangsu, China

7 Department of Genomic Medicine, University of Texas MD Anderson Cancer Center, Houston, TX 77030, USA

8 Department of Translational Molecular Pathology, University of Texas MD Anderson Cancer Center, Houston, TX 77030, USA

9 Department of Surgery and Cancer, Division of Cancer, Imperial College London, Imperial Centre for Translational and Experimental Medicine (ICTEM), London, W12 0NN, UK

oncogenic alteration, such as treating *EGFR*-mutant non-small-cell lung cancer (NSCLC) patients with EGFR tyrosine kinase inhibitors (TKIs) [1–4]. Targeted therapy typically induces an incomplete tumor response due to the intratumor heterogeneity, and some residual tumor clones within therapy-sensitive tumors can survive the initial treatment, resulting in the accumulation of a drug-resistant population that eventually leads to therapy failure [5]. Despite the high response rate to EGFR TKIs (>70%), almost all patients with *EGFR*-mutant NSCLC inevitably acquire drug resistance [6–9]. *EGFR*-T790M is a well-known acquired resistant mutation to the first-generation EGFR TKIs (e.g., gefitinib, erlotinib, and icotinib) and is rarely detected at baseline. Besides T790M, resistant genetic alterations from multiple other genes/pathways have been reported, including *PIK3CA*, *KRAS*, *BRAF*, *PTEN*, as well as somatic copy number alterations (SCNAs) of different receptor tyrosine kinases (RTKs) [10–13].

Although molecular mechanisms of acquired resistance to the first-generation EGFR inhibitors have been identified extensively, co-occurring somatic alterations and pathways associated with the innate resistance are largely unknown [14–16]. In addition, little is known about how these multiple co-occurring genetic clones evolve during the EGFR TKI therapy [17]. An open question in the field is to what extent multiple co-occurring genetic events cooperate with a primary *EGFR*-mutant to promote tumor progression and therapy resistance in both the targeted-therapy-naïve and acquired-resistance settings. Understanding the biological links between subclones and co-occurring genetic mutations, elucidating the therapy-resistant tumor progression, as well as identifying and targeting subclonal tumor cells, are essential in enhancing therapeutic responses.

Although T790M mutation is a major TKI resistance mechanism, one unexplored question is whether any co-acquired alterations are cooperating with T790M. It is known that T790M-positive patients have better PFS compared with T790M-negative patients [18]; however, whether any subgroups within T790M-positive or T790M-negative patients would show distinct clinical outcomes has not been systematically investigated. Despite extensive studies on EGFR TKIs, there are still 10–30% cases whose resistance mechanisms are unknown [19–21]. Furthermore, although T790M is generally considered as a subclone, its competition with other resistant subclones and the resulting patients' outcomes is not well studied. Indeed, understanding of clonal evolution during pre- and post-TKI treatment is still lacking as previous studies mainly sequenced and analyzed small panels of genes.

The introduction of next-generation sequencing (NGS) into cancer genetic interrogation achieved tremendous success in acquiring cancer genomic information comprehensively and efficiently [22]. In this study, we performed targeted NGS for patients with *EGFR*-mutant NSCLC at both baseline and progressive disease (PD) during EGFR TKI treatment. We then investigated the co-occurring intrinsic resistant genetic alterations and analyzed the difference in co-acquired landscape between T790M-positive and T790M-negative patients. Lastly, we performed whole-exome sequencing (WES) to depict the subclonal architecture and clonal evolution patterns during TKI treatment and correlated them with patients' clinical results.

Materials and methods

Patient enrollment and sample preparation

Pretreatment and paired PD tumor samples from 64 patients (Table S1) with *EGFR*-mutant NSCLC, who were treated with first-generation EGFR TKIs, underwent WES ($n = 10$) or targeted sequencing of 416 cancer genes ($n = 54$). Circulating cell-free DNA (cfDNA) was collected at the time of acquired resistance and was also subject to targeted sequencing of 416 cancer genes. Acquired resistance to EGFR TKIs was evaluated by "Jackman criteria" [23].

All patients were informed of sample collection and intended research usage. Written consent was collected according to the ethical regulations of the Zhejiang Cancer Hospital. The tests were performed in a centralized clinical testing center (Nanjing Geneseeq Technology Inc., China) according to protocols reviewed and approved by the ethical committee of the Zhejiang Cancer Hospital. All methods were performed in accordance with the relevant guidelines and regulations.

Overall, 5 mL of peripheral blood was collected from each patient and placed into EDTA-coated tubes (BD Biosciences). Formalin-fixed paraffin-embedded (FFPE) blocks/sections were obtained from the hospitals and shipped to the central testing laboratory by required conditions. Diagnosis and tumor purity of the samples were confirmed by pathologists from the Zhejiang Cancer Hospital. Samples with tumor cell content above 20% were considered qualified.

DNA extraction and quantification

Genomic DNA from white blood cells was extracted using DNeasy Blood & Tissue kit (Qiagen). FFPE samples were de-paraffinized with xylene, and genomic DNA was extracted using QIAamp DNA FFPE Tissue Kit (Qiagen). Purified genomic DNA was qualified by Nanodrop2000 for A260/280 and A260/A230 ratios (Thermo Fisher Scientific). All DNA samples were quantified by Qubit 3.0 using

the dsDNA HS Assay Kit (Life Technologies) according to the manufacturer's recommendations.

Library preparation, targeted and exome NGS

Sequencing libraries were prepared using KAPA Hyper Prep kit (KAPA Biosystems) with an optimized manufacturer's protocol. In brief, 1–2 μg of genomic DNA, which was sheared into 350 bp fragments using Covaris M220 instrument (Covaris), underwent end-repairing, A-tailing and ligation with indexed sequencing adapters sequentially, followed by size selection for genomic DNA libraries using Agencourt AMPure XP beads (Beckman Coulter). Finally, libraries were amplified by PCR and purified using Agencourt AMPure XP beads.

Customized xGen lockdown probes panel (Integrated DNA Technologies) were used to selectively enrich for 416 predefined genes. The enriched libraries were sequenced on Hiseq 4000 NGS platforms (Illumina) to coverage depths of at least 100×, 300×, and 3000× after removing PCR duplicates for blood, FFPE, and ctDNA, respectively. Exome capture was performed using the IDT xGen Exome Research Panel V1.0 (Integrated DNA Technologies) and sequenced using the Illumina HiSeq 4000 platform to reach the mean coverage depth of ~60× for the normal control (white blood cells samples) and ~150× (~3000×) for the tumor tissue (plasma) samples.

Bioinformatics analyses

Paired-end sequencing data were aligned to the reference human genome (build hg19) with the Burrows–Wheeler Aligner (bwa-mem) [24] and further processed using the Picard suite (http://picard.sourceforge.net/) and the Genome Analysis Toolkit (GATK). MuTect [25] was applied to paired normal and tumor BAM files for the identification of somatic single nucleotide variants (SNVs). Small insertions and deletions (indels) were detected using SCALPEL (http://scalpel.sourceforge.net). Tumor purity was estimated by ABSOLUTE [26]. Purity-adjusted gene-level and segment-level copy number were calculated by CNVKit [27]. Chromosome instability score (CIS) was defined as the proportion of the genome with aberrant (purity-adjusted segment-level copy number ≥3 or ≤1) segmented copy number. Intratumor heterogeneity score (ITH) was defined by mutant-allele tumor heterogeneity [28]. Tumor mutation burden (TMB) was defined as the number of nonsilent mutations per sample. For subclonal evolution analysis, PyClone [29] was used for cancer cell fraction estimation and phylogenetic tree was built using the SCHISM package [30]. Detailed information including criteria for SNV and SCNA calling were shown in Supplementary method note.

Results

## Patient cohort and clinical characteristics

For panel sequencing, after excluding samples from two patients with deamination damaging or contamination (assessed by GATK), samples from 52 patients met the quality requirement. Among the 52 patients who had baseline (pre-treatment) tissue samples, 42 had both paired PD tissue and plasma samples, 8 patients only had PD plasma samples and 2 patients' PD samples were excluded due to oxidative damaging (Fig. S1). For the acquired mutation analysis, 50 patients were included. Due to general low tumor content for plasma samples and difficulty to detect SCNAs, the acquired SCNA analysis was performed on 42 patients with paired baseline and PD tissue samples. Paired pretreatment and PD tissue samples from 10 additional patients were sequenced by WES.

Of the 62 patients, the number of male and female patients was similar (48% vs. 52.0%) and more than half of them had no smoking history (62.9%). The median age of all patients was 60.5 years old (range from 32 to 82 years old) and most of them were diagnosed as adenocarcinoma. Twenty-eight patients (45.2%) harbored *EGFR* Exon 19 deletion, 32 patients (51.6%) harbored *EGFR* L858R mutation, and 2 patients (3.2%) had *EGFR* L861Q mutation. For the first-line treatment, 40 patients (64.5%) received icotinib, 19 patients (30.6%) received gefitinib, and 3 patients (4.9%) received erlotinib. The objective response rate was 75.8% (1 patient had complete response, CR; 46 patients had partial response, PR; 15 patients had stable response, SD). The median progression-free survival (PFS) was 11.95 months (range: 2.2–38.3 months). We observed no significant ($p > 0.1$) difference in PFS among three TKIs in both panel sequencing cohort ($n = 52$) and panel plus WES cohort ($n = 62$) (Fig. S2). In addition, there were no significant differences in the distribution of clinical features such as gender, age, smoking history, mutational, or copy number alteration spectrum among patients treated with various TKIs. Detailed information, as well as summarized data of the included patients, was shown in Table S1.

Domain-specific *PIK3CA* alterations and co-deletion of *NOTCH1/STK11/GNA11* (9q34.3/19p13.3) at baseline were associated with primary resistance to EGFR TKI treatment

In order to elucidate the effects of baseline genetic features on the clinical response to EGFR TKIs, somatic mutations and SCNAs were identified and linked to PFS. As shown in Fig. 1, widespread baseline genetic alterations were co-occurring with *EGFR* mutations, with *TP53* (62%) and

Fig. 1 Comutation plot of genomic alterations at baseline. Baseline mutations and SCNAs of the most frequently changed genes were detected by next-generation sequencing of 52 patients with *EGFR*-mutant NSCLC prior to EGFR TKI treatment. Patients were divided into two groups with the median PFS as the cutoff value. Two patients had no qualified tissue and plasma samples at PD, so their T790M status were unknown (not available)

Genomic alterations at baseline (n=52)
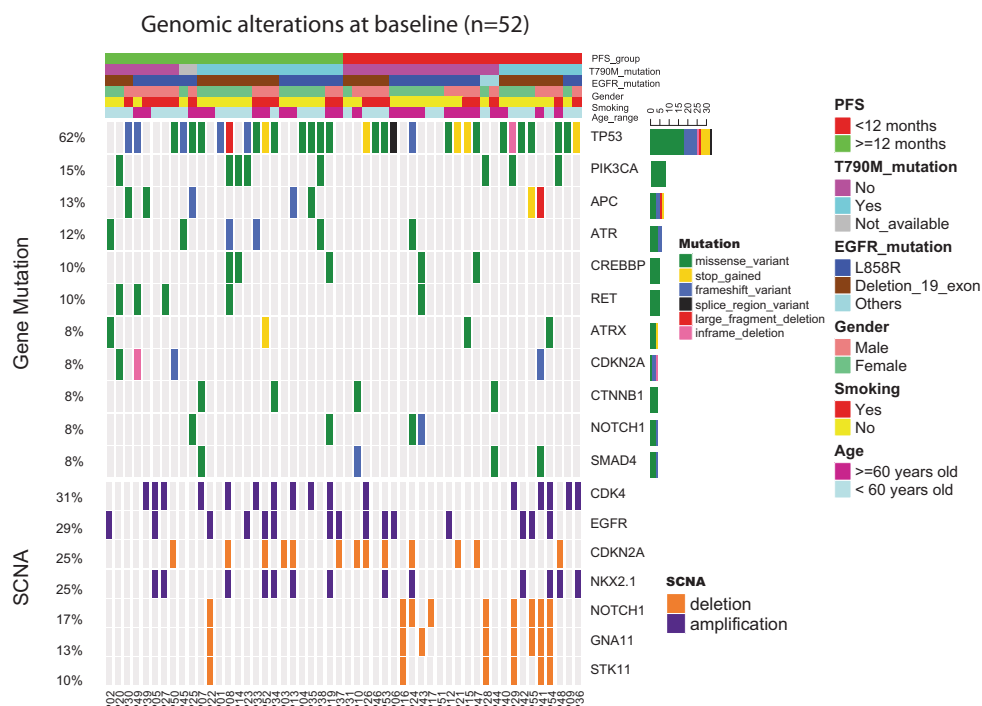
PIK3CA (15%) being the top two most frequently comutated genes. Several genes that have been reported in NSCLC [31–33] were found to be comutated with *EGFR*, including *APC* (13%), *ATR* (12%), *CREBBP* (10%), *RET* (10%), *CDKN2A* (8%), *CTNNB1* (8%), and *SMAD4* (8%). 31% of patients had *CDK4* amplification, which is the most frequent SCNA in our cohort, followed by *EGFR* amplification (29%) and *NKX2-1* amplification (25%). On the pathway level [34], alterations in RTK-RAS (other than EGFR), PI3K, NOTCH, cell cycle, and TGF-beta pathways frequently co-occurred with *EGFR* mutations in baseline samples (Table S2).

We then correlated these somatic mutations with patients' clinical outcomes. Among mutated genes occurring in four or more patients, only *PIK3CA* mutation status was found significantly associated with PFS ($p < 0.05$). Patients with baseline *PIK3CA* mutation had a longer PFS compared with patients without *PIK3CA* mutation ($p = 0.04$, Fig. 2a). *PIK3CA* mutations showed a domain-dependent effect on PFS. Mutations in kinase domain (Y1021H and H1047R, KD), helical domain (E542K, HD), and C2 domain (N345K) were associated with a worse PFS whereas mutations in p85 binding domain (R88Q, R108H, and K111E) were associated with an improved PFS (Fig. 2b). At baseline, there were two patients with *PIK3CA* amplification and four patients with *PIK3R2* (p85-β subunit) amplification. Based on the affected domains, the patients were classified into three groups: (1) p85-related group included three patients with *PIK3CA* p85 binding domain mutation and four patients with *PIK3R2* amplification; (2)

kinase-related group included four patients with KD/HD/C2 mutation and two patients with *PIK3CA* amplification; (3) all other patients without the above alterations. Consistent with the results in Fig. 2b, kinase-related group had a significantly worse PFS than p85-related group ($p = 0.0006$, Fig. S3), suggesting a domain-specific effect of *PIK3CA* alterations on TKI treatment.

In addition to mutations, several gene deletions such as *NOTCH1*, *STK11*, *GNA11*, and *SMAD4* were associated with a worse PFS. Interestingly, *NOTCH1* (9q34.3), *STK11* and *GNA11* (19p13.3) showed a significant co-deletion pattern (*NOTCH1* and *GNA11*, $p = 2.727e{-}05$; *NOTCH1* and *STK11*, $p = 4.848e{-}05$; *GNA11* and *STK11*, $p = 8.08e{-}06$; Fisher's exact test, two-sided) in 10 patients (Fig. 1). Two co-deletion cases were shown in Fig. 2c. Five patients had co-deletion of the above three genes using our default cutoffs and we further confirmed another four patients (Fig. S4c) harbored co-deletion of the three genes by manually inspecting the scatter plot of log2 depth ratio and the raw data. Both *GNA11* and *STK11* are located on chromosome 19p13.3 and co-deletion of the two genes has been previously reported [35]. We also observed the co-deletion of *NOTCH1* and *STK11* ($p < 0.001$, Fisher's exact test, two-sided) in a TCGA lung adenocarcinoma cohort. The co-deletion of *NOTCH1*, *GNA11*, and *STK11* (9q34.3/19p13.3) ($n = 9$) at baseline imposed a negative impact on PFS ($p = 0.00079$) (Fig. 2d). Deletion of TGF-beta pathway including *SMAD2*, *SMAD3*, *SMAD4*, and *TGFBR2* was also associated with a shorter PFS than patients without SCNAs in this pathway ($p = 0.011$) (Fig. 2e).
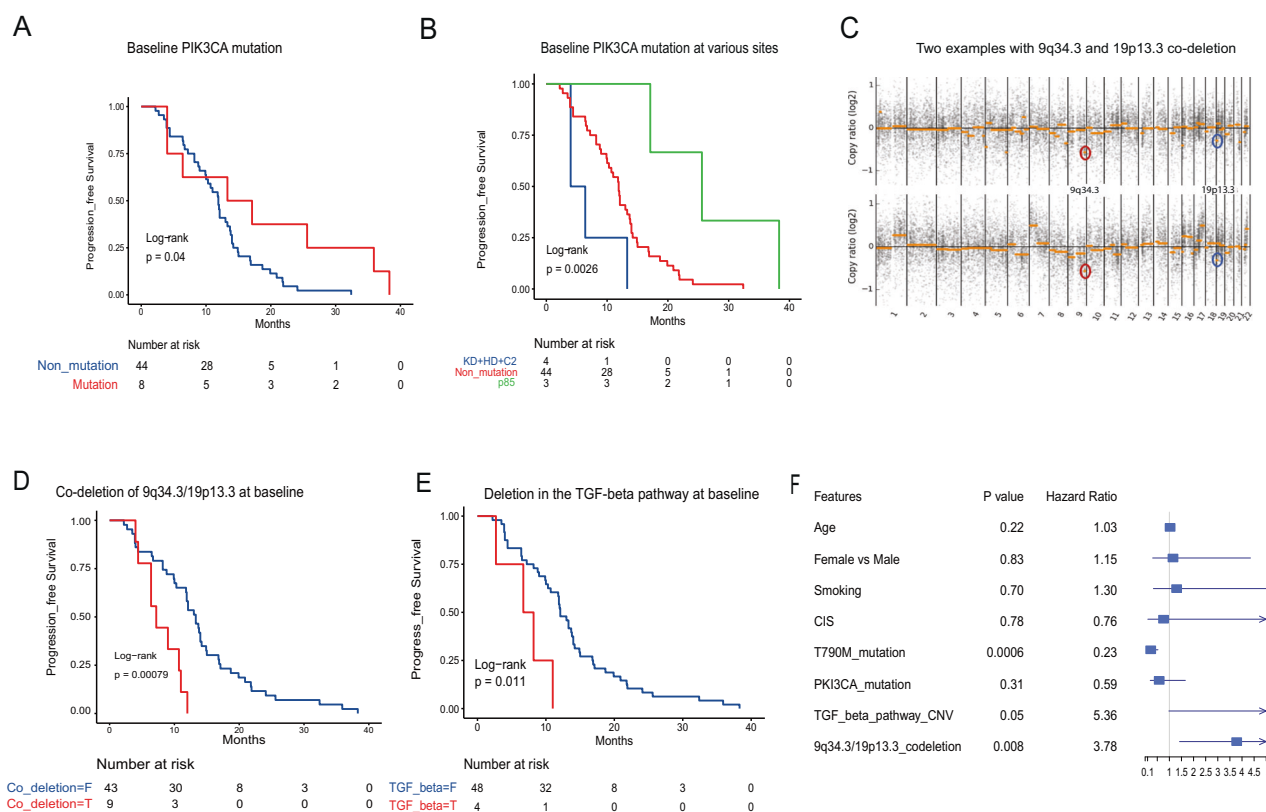
Fig. 2 Baseline genetic features affected the clinical response to EGFR TKI treatment. Kaplan–Meier curves showing different effects of baseline genetic features on patients' PFS: **a** The overall effect of baseline *PIK3CA* mutation. **b** Baseline *PIK3CA* mutations in individual domains (one mutation was not a hotspot mutation and thus not included in the analysis). **c** Co-deletion of *NOTCH1* (9q34.3) and *GNA11/STK11* (19p13.3) in two cases. **d** Baseline co-deletion of 9q34.3/19p13.3was associated with patient PFS. **e** Baseline deletion of TGF-beta pathway. **f** Forest plot of hazard ratio (HR) and *p* value for multivariate Cox regression analysis. Bars represent the 95% CI of HR of included variables, including age, gender (female vs. male), smoking history (smoker vs. nonsmoker), baseline CIS, acquired *EGFR*-T790M mutation, baseline *PIK3CA* mutation, baseline deletion of TGF-β pathway and baseline co-deletion of 9q34.3/19p13.3

We then conducted a multivariate regression analysis including significant variables in univariate analysis as well as important clinical and molecular features such as age, gender, smoking, and CIS (Fig. 2f). Besides the above baseline features, we included acquired T790M mutation in the model since previous studies have shown T790M mutation is a favorable factor for PFS [18]. The 9q34.3/19p13.3 co-deletion still maintained its significant negative effects on PFS [HR = 3.78 (95% CI: 1.42–10.07), *p* = 0.008] in the multivariate analysis. Kaplan–Meier results also showed the effect of the co-deletion on PFS was T790M-independent (Fig. S4b). We next combined the two important baseline features, 9q34.3/19p13.3 co-deletion and *PIK3CA* alterations, to investigate their effect on patients' outcomes. The three patients with both co-deletion and *PIK3CA* kinase mutations had the worst PFS (median PFS: 6.40 months) among all patients, although the result is not statistically significant due to the small sample size. Patients with the co-deletion or *PIK3CA* kinase domain alterations alone did not show significant difference in PFS. In addition, all of the patients with *PIK3CA* p85 binding domain

alterations had no 9q34.3/19p13.3 co-deletion and they had the best PFS among all patients (Fig. S4c).

Increased CIN and acquired alterations of CIN-related genes from baseline to progressive disease

After assessing the baseline mutations/SCNAs, we further identified acquired alterations, defined as genetic changes that were absent at baseline but detected at PD. On average, we observed four acquired mutations per patient. The number of shared, pre-treatment specific and PD sample-specific mutations were shown in Fig. S5. Fifty patients had paired baseline and PD samples, and 25 of them (50%) had acquired T790M at PD, which was similar to the TKI-induced T790M frequency in other studies [36]. Moreover, patients carrying exon 19 deletion at baseline were prone to develop T790M mutation compared with those carrying L858R mutation (*P* = 0.04, Fisher exact test, two-sided), which was consistent with previous studies [37]. Besides T790M mutation, acquired mutations frequently happened at other loci of *EGFR* (8/50, 16%), such as G796D, L861M,
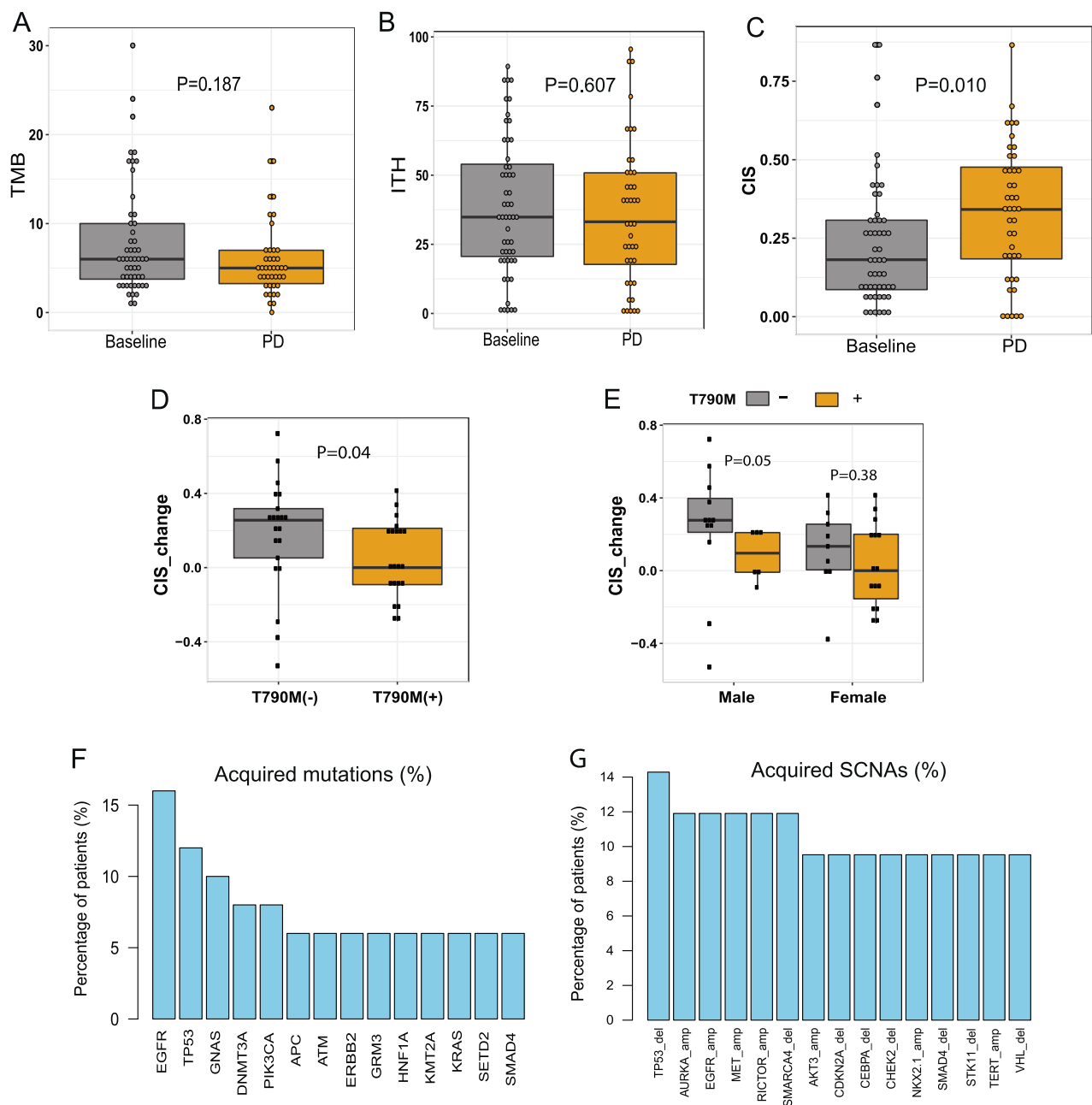
Fig. 3 Acquired somatic alterations from baseline to progressive disease. Box plot comparing baseline and PD genomic features of TMB (**a**), ITH (**b**), CIS (**c**), CIS change (CIS_at_PD - CIS_at_baseline) in T790M-positive and -negative group (**d**), and CIS change of male and female patients in T790M-positive and -negative group (**e**). Bar graphs showing the top acquired gene mutations (**f**) and acquired SCNAs (**g**) at PD. Wilcoxon's rank–sum test was used for inter-group comparison and *p* value calculation (two-sided)

A289V, and exon 20 insertion (Fig. S6b). Other known resistant alterations against the first-generation TKIs, including mutation of *TP53* (6/50, 12%), *PIK3CA* (4/50, 8%), *KRAS* (3/50, 6%), *ERBB2* (3/50, 6%) and deletion of *TP53* (6/42, 14%), amplification of *EGFR* (5/42, 12%) and *MET* (5/42, 12%), were also detected in our cohort (Fig. 3f, g, Fig. S6). These acquired alterations involved multiple pathways, particularly RTK-RAS and PI3K pathway (Fig. 3f, g, Fig. S6, Table S2). For cell cycle pathway, acquired

alterations were mainly SCNAs rather than gene mutations (Fig. S6, Table S2). We further analyzed changes of mutation clonality and observed most (~90%) of acquired mutations were subclones in PD samples. Three *EGFR* T790M, two *RET*, and two *SMAD4* mutations became clonal at PD (Table S3). One patient (P30, male, 46 years old, smoker, exon 19 deletion) was pathologically confirmed to be transformation from adenocarcinoma to small cell lung cancer at PD, with acquired *RB1* deletion.

By analyzing changes at the genome-wide level, we found that TMB ($p = 0.187$) or ITH ($p = 0.607$) was not significantly different when comparing baseline and PD (Fig. 3a, b). In contrast, there was a significant increase in CIS ($p = 0.01$) at PD (Fig. 3c). The increase of CIS was more significant ($p = 0.04$) in T790M-negative patients (Fig. 3d) and the trend was more evident in male patients (Fig. 3e). These results suggest increased CIN may be one of the acquired resistant mechanisms in T790M-negative patients, particularly in male patients. Interestingly, acquired deletion of *TP53* and amplification of *AURKA* gene, the two genes that are closely associated with chromosome instability, were among the top acquired events (Fig. 3g). Patients with acquired SCNAs of *TP53* and *AURKA* had a more significant increase of CIS from baseline to PD than those without these alterations (Fig. S7). For example, CIS of patient P20 with *AURKA* amplification changed from 0.21 at baseline to 0.78 at PD. Although acquired SCNAs of *TP53* and *AURKA* were found in both T790M-positive and T790M-negative patients, their effects on the increase of CIS seemed more obvious in T790M-negative patients for either *TP53* or *AURKA* or both (Fig. S7).

Distinct co-acquired alterations in T790M-positive and T790M-negative patients

We were particularly interested in two questions: first, are there any profound differences in acquired resistant mechanisms in T790M-positive and T790M-negative patients other than T790M "gatekeeper" mutation? Second, will these differences influence treatment decisions and patients' outcomes? To answer these questions, we firstly identified alterations that were enriched in T790M-positive and -negative patients, respectively (Fig. 4a, b). Unfortunately, due to limited cases with each acquired genetic alteration, we could not statistically assert their enrichment in a certain group, particularly for gene mutations. Nevertheless, we observed some trends within the PD samples: *NKX2-1* amplification and *VHL* deletion were only seen in T790M-positive group, and *CDKN2A* deletion was only in T790M-negative group (Fig. 4b); *IDH1* and *IDH2* mutations, which are rare in NSCLC (1.1%) [38], were acquired in 2 T790M-negative patients (*IDH1*:R132S in patient 39; *IDH2*: F126L and R140Q in patient 39 and patient 17).

Acquired events also affect patient response to the first-generation TKIs and response duration. In order to explore the clinical significance of these acquired events, we filtered potential oncogenic and actionable alterations from T790M-negative and -positive group separately based on the OncoKB database (https://oncokb.org/) (Fig. S8a, b). T790M was accompanied by other acquired oncogenic alterations, especially gene mutations. Some known resistant alterations like *KRAS* and *ERBB2* activating mutations could be co-acquired with T790M. Among 25 T790M-positive patients, 6 patients (24%) with other oncogenic mutations had a worse PFS ($p = 0.005$, Fig. 4c). Six T790M-negative patients had acquired oncogenic mutations; however, their PFS was not negatively affected ($p = 0.34$, Fig. 4d). In addition, oncogenic SCNAs did not significantly affect patients' PFS in both T790M-negative and T790M-positive patients (Fig. S8c, d).

Other acquired genetic events also affected patients' PFS. It has been reported that T790M-positive patients generally have a longer PFS than T790M-negative patients under TKI treatments. Our study confirmed that T790M mutation is a favorable factor in lung cancer patients undergoing first-generation TKI treatment ($p = 0.00068$, Fig. S9a). SCNAs of specific genes may affect patients' outcomes, for example, *PTEN* deletion in T790M-negative patients seemed to further worsen the PFS of these patients ($p = 0.06$, Fig. S9b). Furthermore, alterations in certain pathways may be associated with patient outcomes. We found acquired mutations in the RTK-RAS pathway occurred in both T790M-positive and T790M-negative patients; however, the negative effect on PFS was only observed in T790M-positive patients ($p = 0.03$, Fig. 4e, f). Considering a proportion of mutations in the pathway belong to oncogenic mutation, the result was consistent with the former result that co-commitment of T790M with other oncogenic mutations was associated with a worse PFS.

CIN is a candidate resistance mechanism against TKIs in T790M-negative patients without acquired oncogenic alterations

Intriguingly, we found ~50% of T790M-negative patients had neither oncogenic mutations nor oncogenic SCNAs, suggesting some unidentified resistant mechanisms in these patients. Because increased CIN is a major hallmark event in T790M-negative patients, we further analyzed the relationship among CIN, oncogenic alterations, and PFS. We divided the patients into four groups according to their T790M status and whether having acquired oncogenic mutations and examined the CIS changes (Fig. 5a). Interestingly, for T790M-negative patients, there was a more profound increase of CIS in patients without acquired oncogenic mutations compared with those having acquired oncogenic mutations ($p = 0.05$); among those T790M-negative patients with acquired oncogenic mutations, the increase of CIS was similar to that in T790M-positive patients ($p = 0.70$). In contrast, for T790M-positive patients, the change of CIS was found to be independent of the oncogenic mutation status ($p = 0.73$). Moreover, T790M-negative patients also had more
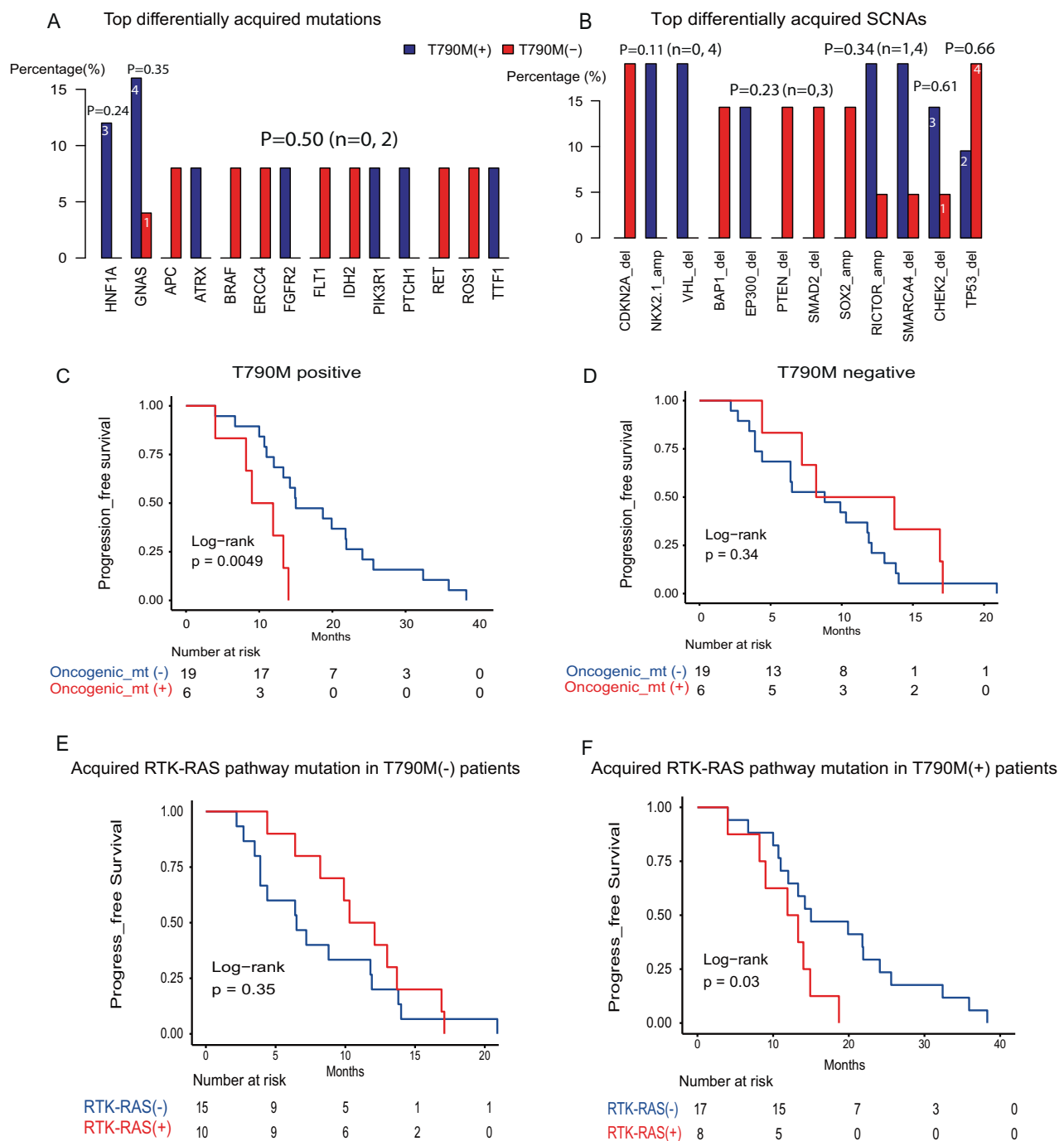
Fig. 4 Distinct landscape of acquired alterations between T790M-positive and T790M-negative patients. Bar graphs showing the top differentially acquired gene mutations (**a**) and acquired SCNAs (**b**) between T790M-positive and -negative group at PD. *n, m* represents the altered genes occurred in *n* patients in one group and *m* in another group. Fisher exact test was used for inter-group comparison and *p* value calculation (two-sided). *P* values were not adjusted. Effect of concurrent acquired oncogenic mutations on patient PFS in T790M-positive group (**c**) and T790M-negative group (**d**). Effect of acquired mutations in the RTK-RAS pathway inT790M-negative patients (**e**) and T790M-positive patients (**f**)

specific oncogenic SCNAs than T790M-positive patients (Fig. S8b). In T790M-negative patients, CIS change showed a nonlinear correlation with patients' PFS. Patients in the third quartile of CIS increase had the worst PFS followed by patients with minimum CIS increase who

generally harbored oncogenic mutations, while patients whose CIS increased most drastically had a better PFS (Fig. 5b), which severe CIN may be detrimental to tumor cells instead. We did not observe such a pattern in T790M-positive patients (Fig. 5c). These results suggest CIN may
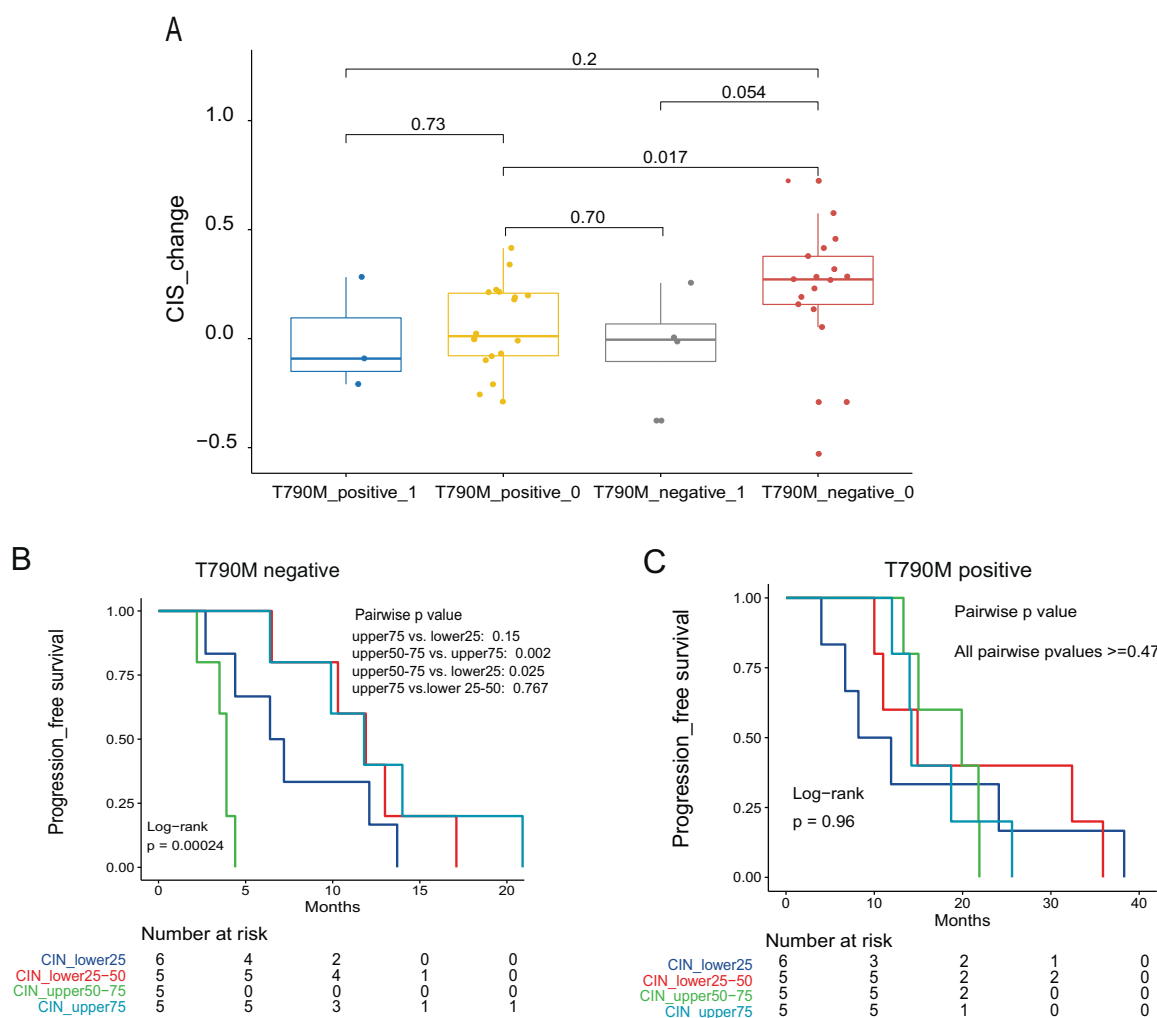
Fig. 5 CIN is a candidate T790M-independent resistance mechanism. **a** CIS change in the four groups classified based on patient's T790M status and oncogenic mutation status. "T790M_positive_1" represents T790M positive and at the same time, having one or more oncogenic mutations, and so on (that is, 1 represents having oncogenic mutations and 0 represents having no oncogenic mutations). Wilcoxon's

rank–sum test was used for inter-group comparison and *p* value calculation (two-sided). Effect of CIS change on patient PFS in T790M-negative group (**b**) and T790M-positive group (**c**). Patients were divided into four groups according to their CIS change ordered from small to big. "CIN_low25" represents the 25th percentile, and so on

be a candidate resistant mechanism and has impacts on PFS of T790M-negative patients.

Depicting genomic evolution of *EGFR*-mutant NSCLC under EGFR TKI therapy

In order to investigate the subclonal architecture and clonal evolution during the acquisition of drug resistance in *EGFR*-mutant tumors, we performed WES in 10 patients at both baseline and PD and inferred clonal evolution. We observed a low proportion of shared mutations between baseline and PD samples, suggesting a highly dynamic elimination-and-emergence process during TKI treatment and progression (Fig. S5). The proportion of clonal mutations increased at PD in 7 (70%) patients (Fig. S10, Table S4).

Among 10 patients, 4 of them developed T790M subclone, from which we identified two subtypes. The first subtype was a parallel evolution of T790M with other drug-resistant subclones (Fig. 6a, b). In this situation, the competitive advantage of T790M subclone relative to other resistant subclones was associated with PFS. In P56 case (Fig. 6a), two subclones, including T790M, developed during TKI therapy; the existence of the co-expending "purple" subclone seemed to restrict the growth of T790M subclone, and this patient had the shortest PFS (7.2 months) among the 4 T790M-positive patients. Patient P58 (Fig. 6b) showed another possibility; in this case, although there was another coexistent subclone which was probably a primary drug-resistant subclone, the T790M subclone was expanded gradually; the PFS of the patient was relatively longer (16.2 months). The second subtype was T790M-dominant
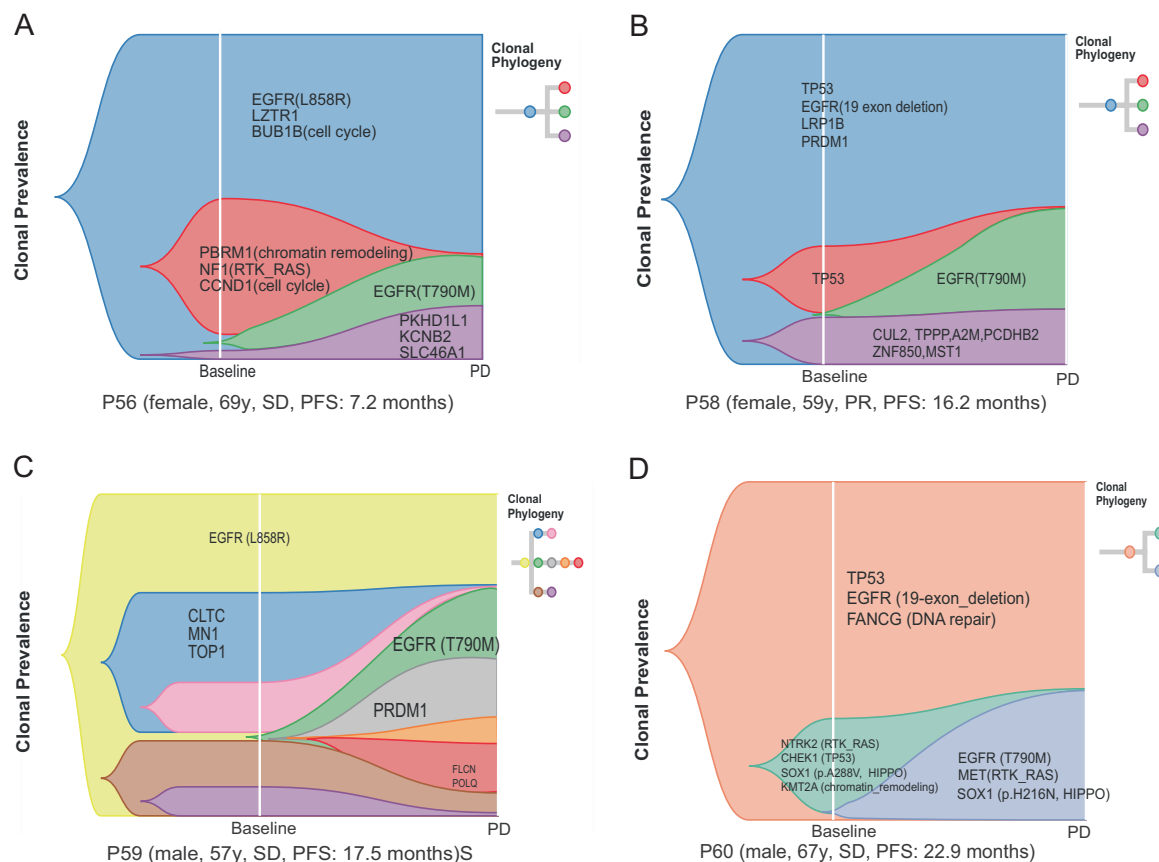
Fig. 6 Clonal evolution from baseline to progressive disease during TKI treatment. Fish plots showing progression of patients with acquired T790M mutation (including four T790M-positive patients)

evolution without parallel subclones. Patient P59 has a dominant T790M subclone and several other subclones within the T790M. This patient had a longer PFS (17.5 months) (Fig. 6c). The fourth patient (P60) with a PFS of 22.9 months had a dominant T790M subclone without any other acquired subclones (Fig. 6d). Both subtypes indicate that higher competitive advantage of T790M was associated with improved PFS. Interestingly, we observed a similar pattern of association between PFS and subclone competition in six T790M-negative patients (Figs. S11 and S12). In three patients with relatively long PFS, all patients had dominant acquired subclones. In contrast, we observed parallel acquired subclones in two out of three patients with short PFS (Figs. S11 and S12). The effect of subclone competition on PFS was probably T790M-independent since the three T790M-negative patients with dominant acquired subclones had relatively long PFS (21.8, 17.3, and 10.3 months), even longer than that T790M-positive patient with multiple competitive subclones (7.2 months). Limited by few samples, the finding requires more cases to validate. Taken together, these results indicate that the rapid progression group is correlated with the coexistence of parallel acquired subclones. In contrast, the evolution of the

attenuated progression group is associated with acquired mono-clone, particularly *EGFR* T790M clone.

Discussion

Recent studies have found co-occurring genomic alterations were common in *EGFR*-mutated lung cancers, especially in advanced-stage cancers [17]; however, the biological significance of these co-occurring events and their correlation with clinical features were largely unknown. In the present study, we found there were extensive accompanying genomic alterations, including various SNVs and SCNAs that co-occurred with canonical *EGFR* driver mutations in NSCLC; for example, 60% patients had mutations in two or more cancer signaling pathways, such as P53, cell cycle, NOTCH, RTK_RAS, WNT and so on. These accompanying events may change the patient's sensitivity to EGFR-TKI therapy; thereby, may serve as predictive biomarkers to stratify patients and improve the efficacy of targeted therapy.

We observed a domain-dependent effect of baseline *PIK3CA* mutation on PFS. So far, the predictive/prognostic

value of *PIK3CA* mutation for lung cancer patients receiving TKI treatment is inconclusive. Although PIK3CA mutations including p85 binding domain mutations are confirmed to be gain-of-function in vitro [39–41], many studies showed *PIK3CA* mutations would not affect the response to TKI treatment or PFS [14, 42, 43]. Due to the low frequency of p85 binding domain mutation, data regarding the domain-specific effect of *PIK3CA* mutation are absent. However, a study showed that p85 binding domain mutation did increase the sensitivity to radiation compared with mutations in other domains [44]. Also, in glioblastoma, unlike mutations in HD and KD, mutations in p85 binding domain did not increase PI3K activity, migration, or colony formation of immortalized human astrocytes [45]. The domain-specific effect was also reflected in SCNA level in our study. Amplification of *PIK3R2* was associated with a better PFS and amplification of *PIK3CA* was the opposite. Despite the fact that these results still need to be validated in larger cohorts, our study highlights the necessity of treating *PIK3CA* mutation differentially.

Another baseline genetic feature associated with a worse PFS was co-deletion of 9q34.3/19p13.3. The co-deletion pattern of 9q34.3/19p13.3 was observed in both our cohort and the TCGA cohort, and the high frequency of 19p loss in NSCLC was also identified in other studies [46]. The representative cancer-related gene in 9q34.3 is *NOTCH1*, which possesses both oncogenic and tumor suppressor roles depending on specific tissue and cancer types [47]. Influence of *NOTCH1* on NSCLC prognosis is unclear and controversial in various studies [48, 49]. *STK11*, located in 19p13.3, is a tumor suppressor gene that is frequently mutated/deleted in lung adenocarcinoma [50]. Deficiency of *STK11* has been linked to primary resistance to EGFR TKI [51]. Moreover, mutation of *STK11* was found to be a primary resistant factor for anti-PD-1 immunotherapy [52]. A bunch of STK11-targeted therapies have been investigated [53]. Given that patients carrying inactivated *STK11* is insensitive to TKIs or immunotherapy, the new STK11-targeted drugs alone or combining with current standard TKI therapy may improve the prognosis of this subgroup of patients.

We did not observe baseline *TP53* mutations were associated with patients' PFS no matter including all *TP53* mutations, or functional mutations (truncation, frame-shift and splicing), or mutations in specific exons (for example, exon 8), which seems to be inconsistent with previous study [54]. Since the genetic backgrounds of patients in various studies are different. For patients with wild-type *TP53*, they may carry other alterations, and effects of these alterations may be comparable with *TP53*, and the final effect is decided by multiple factors.

One of our main purposes was to investigate distinct resistant mechanisms in T790M-positive and T790M-

negative patients. We found ~25% T790M-positive patients had other acquired oncogenic mutations. Because these patients had a much shorter PFS than other T790M-positive patients, we are currently investigating whether they are primarily resistant to the third-generation TKIs and whether a more aggressive therapy or combinational target therapy is necessary. Conventional chemotherapy is often used in T790M-negative patients; however, several patients in our cohort acquired druggable mutations. Two patients acquired *IDH1* or *IDH2* oncogenic (or likely oncogenic) mutations that can be targeted by ivosidenib or enasidenib, and one patient had *EGFR* 20-exon insertion (targeted by poziotinib). Whether these patients can benefit from targeted therapy worths further investigations.

Some SCNAs were associated with TKI-resistant mechanisms, including *MET* amplification, *ERBB2* amplification, *PTEN* deletion, and *EGFR* amplification [19]. In our study, we found overall CIN may be a key resistant mechanism in T790M-negative patients. The increase of CIS in T790M-negative patients was significantly greater than that in T790M-positive patients. Acquired SCNAs of several genes that are involved in the maintenance of CIN, including *TP53* and *AURKA*, imposed more significant effects on T790M-negative patients. In accordance with the increase of CIS, there were also more SCNAs in T790M-negative patients, including *CDKN2A*, *PTEN*, and *SMAD2* deletion that only occurred in T790M-negative group. We found there was a nonlinear relationship between CIS change and PFS in T790M-negative patients. The worst PFS was observed in patients whose CIS increase was in the upper third quartile, whereas patients with most dramatic CIS increase had a better PFS. Our results were consistent with other studies [55] that excessive CIN induces cell-autonomous lethality. Interestingly, we found SNVs and SCNAs showed a complementary effect on acquired resistance. In T790M-negative patients who already had oncogenic mutations, the increase of CIS was similar to that of T790M-positive patients, while T790M-patients without definite oncogenic mutations had the most significant increase of CIS.

Several studies found that CIN is involved in the primary or acquired resistance of multiple anticancer drugs [56, 57]. Recently, activation of *AURKA*, a member of Aurora serine/threonine kinase family, which participates in the regulation of mitosis and maintenance of genome stability [58], is identified to be an important mechanism for acquired resistance to the third-generation TKIs [59]. *AURKA* amplification is a known oncogenic alteration occurred in a variety of cancers. In our cohort, acquired *AURKA* amplification (12%) was the second most frequent SCNAs, and patients with *AURKA* amplification had a significant increase in CIS, particularly in T790M-negative patients. Our study suggests that dysfunction of *AURKA* may
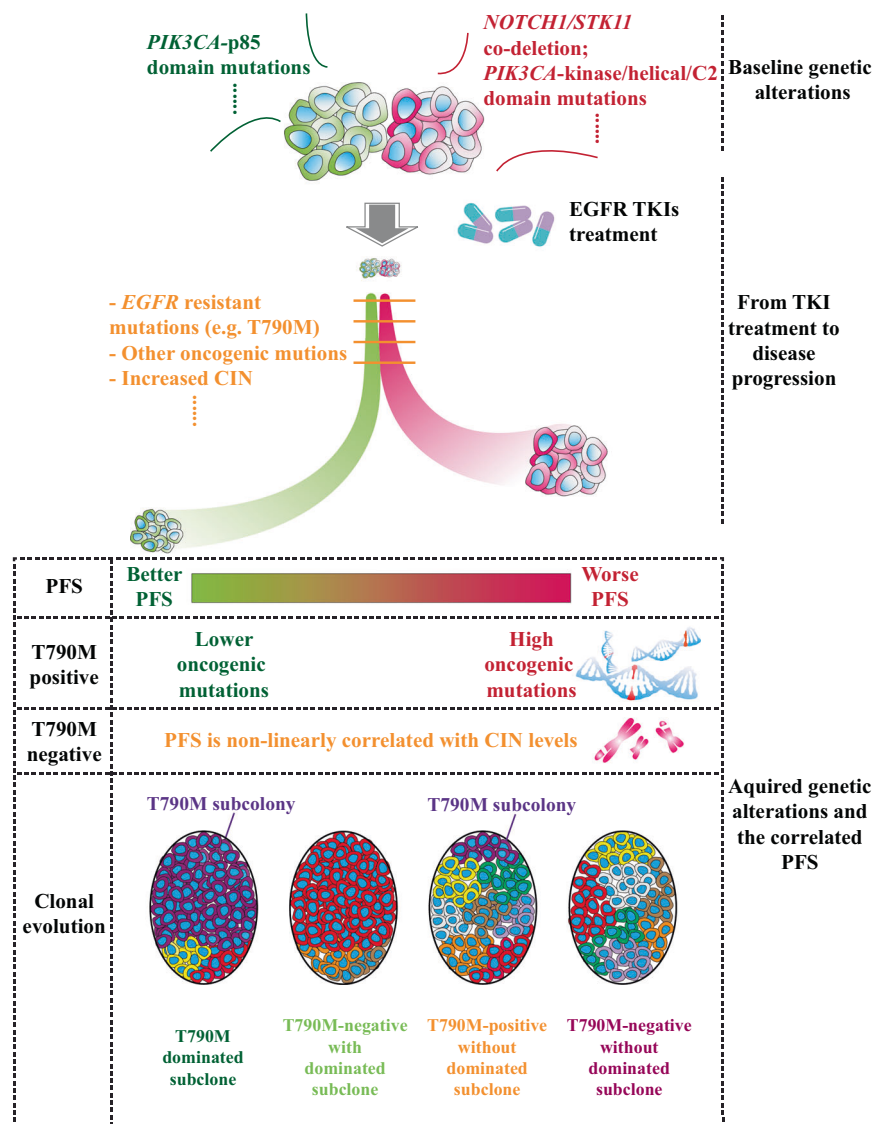
Fig. 7 Summary of key conclusions from this study

account for the resistance to the first-generation TKIs, and these patients can potentially benefit from Aurora kinase inhibitor treatment.

Finally, our subclonal evolution analyses suggest that the relationship between various resistant subclones is also important for treatment responses and patients' outcomes. We found a high competitive subclonal architecture (or high subclone heterogeneity) at PD was often associated with a worse PFS regardless of the T790M mutation status, whereas the existence of a dominant subclone, especially T790M subclone, was associated with attenuated progression. Multiple studies have shown that high subclonal diversity is associated with rapid progression of tumor or precancerous lesion in head and neck squamous cell carcinoma [60], chronic lymphocytic leukemia [61], Barrett's esophagus [62], or pan-cancers [63]. High subclonal diversity may provide a rich repertoire of alterations so that

subclones with highly competitive advantage can stand out [64]. Nevertheless, our findings are limited by the small sample size (10 cases) and need to be validated in large sample size studies. Moreover, further studies will elucidate how these evolutional patterns influence patient's response to subsequent therapies including the third-generation TKIs.

A diagram summarizing our findings was shown in Fig. 7. In summary, our study identified novel primary and acquired resistance mechanisms against the first-generation TKIs, which may improve the risk stratification, medical decision, and prognosis for NSCLC patients receiving TKI treatment.

Compliance with ethical standards

Conflict of interest HB, XF, YX, and XW are the employees of Geneseeq Technology Inc., JY, XW, YWS, and JH are the employees of Nanjing Geneseeq Technology Inc.; JZ reports personal fees from BMS, AstraZeneca, Geneplus, OrigMed, Innovent, grant from Merck, Johnson & Johnson, outside the current work.

Publisher's note Springer Nature remains neutral with regard to jurisdictional claims in published maps and institutional affiliations.

References

1. Boolell V, Alamgeer M, Watkins DN, Ganju V. The evolution of therapies in non-small cell lung cancer. Cancers (Basel). 2015;7:1815–46.
2. Rosell R, Carcereny E, Gervais R, Vergnenegre A, Massuti B, Felip E, et al. Erlotinib versus standard chemotherapy as first-line treatment for European patients with advanced EGFR mutation-positive non-small-cell lung cancer (EURTAC): a multicentre, open-label, randomised phase 3 trial. Lancet Oncol. 2012;13:239–46.
3. Mok TS, Wu YL, Thongprasert S, Yang CH, Chu DT, Saijo N, et al. Gefitinib or carboplatin-paclitaxel in pulmonary adenocarcinoma. N Engl J Med. 2009;361:947–57.
4. Wu YL, Zhou C, Hu CP, Feng J, Lu S, Huang Y, et al. Afatinib versus cisplatin plus gemcitabine for first-line treatment of Asian patients with advanced non-small-cell lung cancer harbouring EGFR mutations (LUX-Lung 6): an open-label, randomised phase 3 trial. Lancet Oncol. 2014;15:213–22.
5. Bivona TG, Doebele RC. A framework for understanding and targeting residual disease in oncogene-driven solid cancers. Nat Med. 2016;22:472–8.
6. Pao W, Miller VA, Politi KA, Riely GJ, Somwar R, Zakowski MF, et al. Acquired resistance of lung adenocarcinomas to gefitinib or erlotinib is associated with a second mutation in the EGFR kinase domain. PLoS Med. 2005;2:e73.
7. Rosell R, Moran T, Queralt C, Porta R, Cardenal F, Camps C, et al. Screening for epidermal growth factor receptor mutations in lung cancer. N Engl J Med. 2009;361:958–67.
8. Majem M, Remon J. Tumor heterogeneity: evolution through space and time in EGFR mutant non small cell lung cancer patients. Transl Lung Cancer Res. 2013;2:226–37.
9. Remon J, Moran T, Majem M, Reguart N, Dalmau E, Marquez-Medina D, et al. Acquired resistance to epidermal growth factor receptor tyrosine kinase inhibitors in EGFR-mutant non-small cell lung cancer: a new era begins. Cancer Treat Rev. 2014;40:93–101.
10. Nagano T, Tachihara M, Nishimura Y. Mechanism of resistance to epidermal growth factor receptor-tyrosine kinase inhibitors and a potential treatment strategy. Cells. 2018;7:212.
11. VanderLaan PA, Rangachari D, Mockus SM, Spotlow V, Reddi HV, Malcolm J, et al. Mutations in TP53, PIK3CA, PTEN and other genes in EGFR mutated lung cancers: correlation with clinical outcomes. Lung Cancer. 2017;106:17–21.
12. Jin Y, Shao Y, Shi X, Lou G, Zhang Y, Wu X, et al. Mutational profiling of non-small-cell lung cancer patients resistant to first-generation EGFR tyrosine kinase inhibitors using next generation sequencing. Oncotarget. 2016;7:61755–63.
13. Balak MN, Gong Y, Riely GJ, Somwar R, Li AR, Zakowski MF, et al. Novel D761Y and common secondary T790M mutations in epidermal growth factor receptor-mutant lung adenocarcinomas with acquired resistance to kinase inhibitors. Clin Cancer Res. 2006;12:6494–501.
14. Wang J, Wang B, Chu H, Yao Y. Intrinsic resistance to EGFR tyrosine kinase inhibitors in advanced non-small-cell lung cancer with activating EGFR mutations. OncoTargets Ther. 2016;9:3711–26.
15. de Bruin EC, McGranahan N, Mitter R, Salm M, Wedge DC, Yates L, et al. Spatial and temporal diversity in genomic instability processes defines lung cancer evolution. Science. 2014;346:251–6.
16. Zhang J, Fujimoto J, Zhang J, Wedge DC, Song X, Zhang J, et al. Intratumor heterogeneity in localized lung adenocarcinomas delineated by multiregion sequencing. Science. 2014;346:256–9.
17. Blakely CM, Watkins TBK, Wu W, Gini B, Chabon JJ, McCoach CE, et al. Evolution and clinical impact of co-occurring genetic alterations in advanced-stage EGFR-mutant lung cancers. Nat Genet. 2017;49:1693–704.
18. Ma G, Zhang J, Jiang H, Zhang N, Yin L, Li W, et al. Epidermal growth factor receptor T790M mutation as a prognostic factor in EGFR-mutant non-small cell lung cancer patients that acquired resistance to EGFR tyrosine kinase inhibitors. Oncotarget. 2017;8:99429–37.
19. Sequist LV, Waltman BA, Dias-Santagata D, Digumarthy S, Turke AB, Fidias P, et al. Genotypic and histological evolution of lung cancers acquiring resistance to EGFR inhibitors. Sci Transl Med. 2011;3:75ra26.
20. Yu HA, Arcila ME, Rekhtman N, Sima CS, Zakowski MF, Pao W, et al. Analysis of tumor specimens at the time of acquired resistance to EGFR-TKI therapy in 155 patients with EGFR-mutant lung cancers. Clin Cancer Res. 2013;19:2240–7.
21. Westover D, Zugazagoitia J, Cho BC, Lovly CM, Paz-Ares L. Mechanisms of acquired resistance to first- and second-generation EGFR tyrosine kinase inhibitors. Ann Oncol. 2018;29:i10–9.
22. Buermans HP, den Dunnen JT. Next generation sequencing technology: advances and applications. Biochim Biophys Acta. 2014;1842:1932–41.
23. Jackman D, Pao W, Riely GJ, Engelman JA, Kris MG, Janne PA, et al. Clinical definition of acquired resistance to epidermal growth factor receptor tyrosine kinase inhibitors in non-small-cell lung cancer. J Clin Oncol. 2010;28:357–60.
24. Li H, Durbin R. Fast and accurate short read alignment with Burrows-Wheeler transform. Bioinformatics. 2009;25:1754–60.
25. Cibulskis K, Lawrence MS, Carter SL, Sivachenko A, Jaffe D, Sougnez C, et al. Sensitive detection of somatic point mutations in impure and heterogeneous cancer samples. Nat Biotechnol. 2013;31:213–9.
26. Carter SL, Cibulskis K, Helman E, McKenna A, Shen H, Zack T, et al. Absolute quantification of somatic DNA alterations in human cancer. Nat Biotechnol. 2012;30:413–21.
27. Talevich E, Shain AH, Botton T, Bastian BC. CNVkit: genome-wide copy number detection and visualization from targeted DNA sequencing. PLoS Comput Biol. 2016;12:e1004873.
28. Mroz EA, Rocco JW. MATH, a novel measure of intratumor genetic heterogeneity, is high in poor-outcome classes of head and neck squamous cell carcinoma. Oral Oncol. 2013;49:211–5.
29. Roth A, Khattra J, Yap D, Wan A, Laks E, Biele J, et al. PyClone: statistical inference of clonal population structure in cancer. Nat Methods. 2014;11:396–8.
30. Niknafs N, Beleva-Guthrie V, Naiman DQ, Karchin R. SubClonal hierarchy inference from somatic mutations: automatic reconstruction of cancer evolutionary trees from multi-region next generation sequencing. PLoS Comput Biol. 2015;11:e1004416.
31. Ohgaki H, Kros JM, Okamoto Y, Gaspert A, Huang H, Kurrer MO. APC mutations are infrequent but present in human lung cancer. Cancer Lett. 2004;207:197–203.

32. Shigemitsu K, Sekido Y, Usami N, Mori S, Sato M, Horio Y, et al. Genetic alteration of the beta-catenin gene (CTNNB1) in human lung cancer and malignant mesothelioma and identification of a new 3p21.3 homozygous deletion. Oncogene. 2001;20:4249–57.

33. Kohno T, Yokota J. How many tumor suppressor genes are involved in human lung carcinogenesis? Carcinogenesis. 1999;20:1403–10.

34. Sanchez-Vega F, Mina M, Armenia J, Chatila WK, Luna A, La KC, et al. Oncogenic signaling pathways in the cancer genome atlas. Cell. 2018;173:321–37 e310.

35. Pfarr N, Penzel R, Klauschen F, Heim D, Brandt R, Kazdal D, et al. Copy number changes of clinically actionable genes in melanoma, non-small cell lung cancer and colorectal cancer-A survey across 822 routine diagnostic cases. Genes Chromosomes Cancer. 2016;55:821–33.

36. Rosell R, Bivona TG, Karachaliou N. Genetics and biomarkers in personalisation of lung cancer treatment. Lancet. 2013;382:720–31.

37. Liang H, Pan Z, Wang W, Guo C, Chen D, Zhang J, et al. The alteration of T790M between 19 del and L858R in NSCLC in the course of EGFR-TKIs therapy: a literature-based pooled analysis. J Thorac Dis. 2018;10:2311–20.

38. Toth LN, de Abreu FB, Tafe LJ. Non-small cell lung cancers with isocitrate dehydrogenase 1 or 2 (IDH1/2) mutations. Hum Pathol. 2018;78:138–43.

39. Zhao JJ, Liu Z, Wang L, Shin E, Loda MF, Roberts TM. The oncogenic properties of mutant p110alpha and p110beta phosphatidylinositol 3-kinases in human mammary epithelial cells. Proc Natl Acad Sci USA. 2005;102:18443–8.

40. Oda K, Okada J, Timmerman L, Rodriguez-Viciana P, Stokoe D, Shoji K, et al. PIK3CA cooperates with other phosphatidylinositol 3'-kinase pathway mutations to effect oncogenic transformation. Cancer Res. 2008;68:8127–36.

41. Ikenoue T, Kanai F, Hikiba Y, Obata T, Tanaka Y, Imamura J, et al. Functional analysis of PIK3CA gene mutations in human colorectal cancer. Cancer Res. 2005;65:4562–7.

42. Eng J, Woo KM, Sima CS, Plodkowski A, Hellmann MD, Chaft JE, et al. Impact of concurrent PIK3CA mutations on response to EGFR tyrosine kinase inhibition in EGFR-mutant lung cancers and on prognosis in oncogene-driven lung adenocarcinomas. J Thorac Oncol. 2015;10:1713–9.

43. Wu SG, Chang YL, Yu CJ, Yang PC, Shih JY. The role of PIK3CA mutations among lung adenocarcinoma patients with primary and acquired resistance to EGFR tyrosine kinase inhibition. Sci Rep. 2016;6:35249.

44. Yard BD, Adams DJ, Chie EK, Tamayo P, Battaglia JS, Gopal P, et al. A genetic basis for the variation in the vulnerability of cancer to DNA damage. Nat Commun. 2016;7:11428.

45. McNeill RS, Stroobant EE, Smithberger E, Canoutas DA, Butler MK, Shelton AK, et al. PIK3CA missense mutations promote glioblastoma pathogenesis, but do not enhance targeted PI3K inhibition. PLoS ONE. 2018;13:e0200014.

46. Gill RK, Yang SH, Meerzaman D, Mechanic LE, Bowman ED, Jeon HS, et al. Frequent homozygous deletion of the LKB1/STK11 gene in non-small cell lung cancer. Oncogene. 2011;30:3784–91.

47. Nowell CS, Radtke F. Notch as a tumour suppressor. Nat Rev Cancer. 2017;17:145–59.

48. Xie M, He CS, Wei SH, Zhang L. Notch-1 contributes to epidermal growth factor receptor tyrosine kinase inhibitor acquired resistance in non-small cell lung cancer in vitro and in vivo. Eur J Cancer. 2013;49:3559–72.

49. Guo L, Zhang T, Xiong Y, Yang Y. Roles of NOTCH1 as a therapeutic target and a biomarker for lung cancer: controversies and perspectives. Dis Markers. 2015;2015:520590.

50. Cancer Genome Atlas Research Network. Comprehensive molecular profiling of lung adenocarcinoma. Nature. 2014;511:543–50.

51. Kim HR, Cho BC, Shim HS, Lim SM, Kim SK, Chang J, et al. Prediction for response duration to epidermal growth factor receptor-tyrosine kinase inhibitors in EGFR mutated never smoker lung adenocarcinoma. Lung Cancer. 2014;83:374–82.

52. Skoulidis F, Goldberg ME, Greenawalt DM, Hellmann MD, Awad MM, Gainor JF, et al. STK11/LKB1 mutations and PD-1 inhibitor resistance in KRAS-mutant lung adenocarcinoma. Cancer Discov. 2018;8:822–35.

53. Zhao RX, Xu ZX. Targeting the LKB1 tumor suppressor. Curr Drug Targets. 2014;15:32–52.

54. Canale M, Petracci E, Delmonte A, Chiadini E, Dazzi C, Papi M, et al. Impact of TP53 mutations on outcome in EGFR-mutated patients treated with first-line tyrosine kinase inhibitors. Clin Cancer Res Off J Am Assoc Cancer Res. 2017;23:2195–202.

55. Birkbak NJ, Eklund AC, Li Q, McClelland SE, Endesfelder D, Tan P, et al. Paradoxical relationship between chromosomal instability and survival outcome in cancer. Cancer Res. 2011;71:3447–52.

56. Lee AJ, Endesfelder D, Rowan AJ, Walther A, Birkbak NJ, Futreal PA, et al. Chromosomal instability confers intrinsic multidrug resistance. Cancer Res. 2011;71:1858–70.

57. McGranahan N, Burrell RA, Endesfelder D, Novelli MR, Swanton C. Cancer chromosomal instability: therapeutic and diagnostic challenges. EMBO Rep. 2012;13:528–38.

58. Fu J, Bian M, Jiang Q, Zhang C. Roles of Aurora kinases in mitosis and tumorigenesis. Mol Cancer Res. 2007;5:1–10.

59. Shah KN, Bhatt R, Rotow J, Rohrberg J, Olivas V, Wang VE, et al. Aurora kinase A drives the evolution of resistance to third-generation EGFR inhibitors in lung cancer. Nat Med. 2019;25:111–8.

60. Mroz EA, Tward AD, Pickering CR, Myers JN, Ferris RL, Rocco JW. High intratumor genetic heterogeneity is related to worse outcome in patients with head and neck squamous cell carcinoma. Cancer. 2013;119:3034–42.

61. Nadeu F, Clot G, Delgado J, Martin-Garcia D, Baumann T, Salaverria I, et al. Clinical impact of the subclonal architecture and mutational complexity in chronic lymphocytic leukemia. Leukemia. 2018;32:645–53.

62. Maley CC, Galipeau PC, Finley JC, Wongsurawat VJ, Li X, Sanchez CA, et al. Genetic clonal diversity predicts progression to esophageal adenocarcinoma. Nat Genet. 2006;38:468–73.

63. Andor N, Graham TA, Jansen M, Xia LC, Aktipis CA, Petritsch C, et al. Pan-cancer analysis of the extent and consequences of intratumor heterogeneity. Nat Med. 2016;22:105–13.

64. Turajlic S, Sottoriva A, Graham T, Swanton C. Resolving genetic heterogeneity in cancer. Nat Rev Genet. 2019;20:404–16.

EDITORIAL

Patient-derived xenograft models—the future of personalised cancer treatment

For many tumours there is a lack of randomised data from which we can guide systemic treatments. Although gene expression profiling along with proteomics has led to advances in diagnosis, classification and prognosis, our ability to target many cancers has been further limited due to a lack of therapeutic options. The use of patient-derived xenograft (PDX) models in the setting of a rare malignancy is discussed here by Kamili et al, with the successful establishment of new model systems.

MAIN

There is almost always a discrepancy between preclinical efficacy in trials and actual clinical outcomes. This generates a demand for improving preclinical modelling. The rapidly evolving field of targeted personalised therapy is the future of oncological practice and sometimes this cannot be evaluated through traditional research methodology, such as randomised control trials (RCTs).[1] Biomarker-driven therapy has become integral to treatment of cancer patients, leading to the introduction of novel trial designs with populations of biomarker-identified patient groups.[2] A review of predictive and prognostic tumour biomarkers advocated that reliance on clinical judgement and expertise is vital in developing personalised cancer medicine, rather than utilisation of published clinical data.[3]

Despite the variability and heterogeneity of cancer types, most treatments remain 'generic' and usually involve chemotherapy as the mainstay.[4] Chemotherapy has often been shown to be only minimally beneficial to overall survival, and is often ineffective with intolerable side effects—though one could argue that this is the case with all treatments. The hidden costs of managing chemotherapy toxicities, with repeated admissions and discussions about side effects, are likely to be substantial. Targeted monoclonal antibodies, immune checkpoint inhibitors and CAR T-cell therapies have shown promising advances in individualised cancer treatment, however, only a few are available for standard clinical practice.[4] In Phase 1 clinical trials, both response rate and progression-free survival were greatly improved with personalised oncology therapy by using biomarker selection strategies compared with those undergoing generic treatment.[5] Currently, developments in the detection of cancer drug targets, comprehensive molecular profiling and personalised combined treatment regimens are all contributing to increasing availability of personalised oncology to a wider range of patients.[6]

Patient-derived xenograft (PDX) models have been increasingly used in translational research since their development.[7] Currently, cell-line xenografts are the standard for preclinical research, able to create a tumour microenvironment.[8] More often than not however, they do not accurately reflect the true behaviour of the host tumour and are able to adapt to in vitro growth, losing the original properties of the host tumour.[7] Other models for tumour graft strategies have previously had limited success.[8]

Trials examining PDX models have shown that they can produce samples that are authentic to the host tumour.[9] They are able to accurately replicate tumour growth, diversity of tumour cells and tumour progression, including metastatic potential.[7,9,10] PDX models have been shown to be used for prognostication: studies have shown that successful engraftment is associated with a poorer prognosis that can be correlated clinically.[10] Another study, by exploring heterogeneous sarcoma patients with a wide range of prognoses and tumour subtypes, demonstrated that PDX models aided therapeutic decision-making in the case of a collection of disparate tumours where each one is a rare subtype.[11]

While neuroblastomas are the most common extracranial solid tumour in children, they are generally rare, and have a wide variety of outcomes depending on the specific, albeit variable, biology of the tumour.[12–14] Children with high-risk neuroblastoma have a less than 50% chance of cure.[10] This has led to recognition of an increasing need for personalised treatment for patients with high-risk neuroblastomas.[15] This is especially relevant as current treatment regimens have a range of acute toxicities and long-term side effects.[15,16,17] RCTs effectively test new interventions, remove allocation bias, are ethically conducted and ensure that no subject receives less-than-baseline care; however, they are expensive and can take many years to complete. RCTs are also ultimately not appropriate for the requirement for rapid developments in any field, let alone a rare cancer[18]—where they are less valid, almost impossible to recruit adequate numbers for and are thus performed less frequently, leading to a dearth of evidence.[19] In children there is a scarcity of trials conducted, with issues relating to feasibility as well as ethics. This leads to an absence of evidence, and alternatives need to be sought.[20] Existing in vivo and in vitro data will always remain the preclinical vanguards of drug development, but the clinical use of patient-derived xenografts can enhance the robustness of preclinical studies.[14]

In this edition of the BJC, Kamili et al. investigated the reliability of establishing PDX models for high-risk neuroblastomas.[16] They examine different techniques including different engraftment sites and different biological sample types, such as metastatic and primary tumour samples. Previous papers have reported that PDX models are more informative than cell-line xenografts; however, they have demonstrated limited engraftment success rates, prolonged establishment of grafts and high costs.[12,13,21] This paper's key finding is that of successful engraftment via orthotopic implantation, a method leading to more rapid model development. This is in keeping with previous research in advanced sarcoma patients, which highlighted the need for time-efficient engraftment in order to see a benefit within a clinically appropriate timescale.[16]

Kamili et al. are able to address the lengthy establishment time that has been a limiting factor in previous studies.[16] All of the

orthotopically inoculated tumours were successfully engrafted and resulted in the quickest time to engraftment compared with subcutaneously and intramuscularly inoculated tumours. Indeed, PDX models were established for 4 of 9 of patients at diagnosis and all patients tested (5/5) at relapse.[16] These findings show that PDX can be established quickly, which is key in high-risk and rapidly developing tumours. Although the orthotopic model was found to be the most rapid engraftment approach, there were also subcutaneous and intramuscular xenografts that were found to be equally as representative of the donor tumour. This suggests that in future, the xenograft type can be selected depending on its clinical utility. It has also shown that PDX models can reliably be established from a diverse range of samples, depending on which is most accessible clinically.[16] This is going to be especially central to rare cancers, paediatric tumours or those with a range of subtypes, though one can argue that oncology is heading in that direction already. It is also recognised that tissue samples from tumours have often been inaccessible, and this has been a limiting factor.[21] This is significant for development of personalised models that can be used in future clinical trials and clinical practice. Another important aspect of this paper is the expansion of patient material for ex vivo and in vivo drug testing. Personalised PDX models would allow for prioritisation of therapeutic options and provide an evidence-based platform for decisions regarding personalised therapy.[16]

This research explores the challenges of developing PDX models, including xenogeneic graft versus host disease and proliferation of EBV-infected cells. It does, however, propose a strategy to overcome and limit using this T-lymphocyte depletion.[16] It emphasises the possibility that a personalised approach to cancer treatment and research can be developed with these models. With the development of reliable engraftment, this could lead to informative preclinical models for individual patients.[16,22] It also proposes the use of xenografts to expand the current limited basis for drug testing in cancer patients, minimising the need for expensive and prolonged randomised controlled trials.[7,9] Changes in research practice are needed to adapt to the current medical climate. Innovations, such as PDX models, have the ability to change what is considered standard practice and improve access to personalised treatment.

ACKNOWLEDGEMENTS
None

AUTHOR CONTRIBUTIONS
All authors contributed to the writing of the paper and approved the final submitted version.

ADDITIONAL INFORMATION
Ethics approval and consent to participate Not applicable

Consent to publish Not applicable.

Data availability Not applicable.

Competing interests In 2018—present Professor Stebbing, the Editor-in-Chief of Oncogene sat on SABs for Celltrion, Singapore Biotech, Vor Biopharma, TLC Biopharmaceuticals and Benevolent AI, has consulted with Lansdowne partners, Vitruvian and Social Impact Capital and he chairs the Board of Directors for BB Biotech Healthcare Trust and Xerion Healthcare. Jenna Bhimani and Katie Ball declare no competing interests.

Funding information This work is supported by the Imperial BRC and ECMC.

Note: This work is published under the standard license to publish agreement. After 12 months the work will become freely available and the license terms will switch to a Creative Commons Attribution 4.0 International (CC BY 4.0).

Jenna Bhimani[1], Katie Ball[1] and Justin Stebbing[1,2]
[1]Department of Oncology, Charing Cross Hospital, Imperial College and Imperial College Healthcare NHS Trust, Fulham Palace Road, London W6 8RF, UK and [2]Imperial College Centre for Translational and Experimental Medicine, Hammersmith Hospital, Du Cane Road, London W12 0NN, UK
Correspondence: Jenna Bhimani (j.bhimani@nhs.net)

REFERENCES
1. Jackson, S. E. & Chester, J. D. Personalised cancer medicine. *Int. J. Cancer* **137**, 262–266 (2015).
2. Janiaud, P., Serghiou, S. & Ioannidis, J. New Clinical trial designs in the era of precision medicine: an overview of definitions, strengths, weaknesses and current view in oncology. *Cancer Treat. Rev.* **73**, 20–30 (2019).
3. Kelley, R. K., Van Bebber, S. L., Phillips, K. A. & Venook, A. P. Personalized medicine and oncology practice guidelines: a case study of contemporary biomarkers in colorectal cancer. *J. Natl Compr. Canc. Netw.* **9**, 13–25 (2011).
4. Krzyszczyk, P., Acevedo, A., Davidoff, E. J., Timmins, L. M., Marrero-Berrios, I., Patel, M. et al. The growing role of precision and personalized medicine for cancer treatment. *Technology Singap. World Sci.* **6**, 79–100 (2018).
5. Schwaederle, M., Zhao, M., Lee, J., Lazar, V., Leyland-Jones, V., Schilsky, R. L. et al. Association of biomarker-based treatment strategies with response rates and progression-free survival in refractory malignant neoplasms: a meta-analysis. *JAMA Oncol.* **2**, 1452–1459 (2016).
6. Hannah, C., Wise & David, B. Solit, precision oncology: three small steps forward. *Cancer Cell* **35**, 825–826 (2019).
7. Hildago, M., Amant, F., Biankin, A. V., Budinska, E., Byrne, A. T., Caldas, C. et al. Patient derived xenograft models; an emerging platform for translational cancer research. *Cancer Discov.* **4**, 998–1013 (2014).
8. Yada, E., Wada, S., Yoshida, S. & Sasada T. Use of patient-derived xenograft mouse models in cancer research and treatment. *Future Sci. OA.* **4**, FSO271 (2017).
9. Tentler, J. J., Tan, A. C., Weekes, C. D., Jimeno, A., Leong, S., Pitts, T. M. et al. Patient derived tumour xenografts as models for oncology drug development. *Nat. Rev. Clin. Oncol.* **9**, 338–350 (2012).
10. DeRose, Y. S., Wang, G., Lin, Y. C., Bernard, P. S., Buys, S. S., Ebbert, M. T. et al. Tumor grafts derived from women with breast cancer authentically reflect tumor pathology, growth, metastasis and disease outcomes. *Nat. Med.* **17**, 1514–1520 (2011).
11. Stebbing, J., Paz, K., Schwartz, G. K., Wexler, L. H., Maki, R., Pollock, R. E. et al. Patient-derived xenografts for individualized care in advanced sarcoma. *Cancer.* **120**, 3588 (2014).
12. Van Arendonk, K. J. & Chung, D. H. Neuroblastoma: Tumor Biology and Its Implications for Staging and Treatment. *Children* **6**, 12 (2019).
13. Kaatsch, P. Epidemiology of childhood cancer. *Cancer Treat. Rev.* **36**, 277–285 (2010).
14. Matthay, K. K., Maris, J. M., Schleiermacher, G., Nakagawara, A., Mackall, C. L., Diller, L. et al. Neuroblastoma. *Nat. Rev. Dis. Primers* **2**, 16078 (2016).
15. Pinto, N. R., Applebaum, M. A., Volchenboum, S. L., Matthay, K. K., London, W. B., Ambros, B. F. et al. Advances in risk classification and treatment strategies for Neuroblastoma. *J. Clin. Oncol.* **33**, 3008–3017 (2015).
16. Kamili A., Gifford A., Li N., Mayoh C., Chow S. O., Failes T. W. et al. Accelerating development of high-risk neuroblastoma patient-derived xenograft models for pre-clinical testing and personalised therapy. *Br. J. Cancer* (2019); https://doi.org/10.1038/s41416-019-0682-4.
17. Cohen, L. E., Gordon, J. H., Popvsky, E. Y., Gunawardene, S., Duffey-Lind, E., Lehmann, L. E. et al. Late effects in children treated with multimodel therapy for high risk neuroblastoma: high incidence of endocrine and growth problems. *Bone Marrow Transplant.* **49**, 502–508 (2014).
18. Perez-Gomez, A., Mejia-Trujillo, J. & Mejia, A. How useful are randomized controlled trials in a rapidly changing world? *Glob. Ment. Health (Camb)*. **3**, e6 2016).
19. Behera, M., Kumar, A., Soares, H., Sokol, L. & Djulbegovic, B. Evidence Based medicine for rare diseases: implications for data interpretation and clinical trial design. *Cancer Control.* **14**, 160–166 (2017).
20. Joseph, P. D., Craig, J. C. & Caldwell, P. Clinical trials in children. *Bri. J.Clin. Pharmacol.* **79**, 357–369 (2015).
21. Applebaum, M. A. Second malignancies in patients with neuroblastoma: the effects of risk based therapy. *Paediatr. Blood Cancer.* **62**, 128–133 (2015).
22. Zarzosa, P., Navarro, N., Giralt, I., Molist, C., Almazán-Moga, A., Vidal, I. et al. Patient derived xenografts for childhood solid tumours; a valuable tool to test new drugs and personalize treatments. *Clin. Transl. Oncol.* **19**, 44–50 (2017).